Università degli Studi di Padova

Department of Information Engineering

Master thesis in ICT for Internet and Multimedia

Curriculum: Photonics

Nonlinear noise in WDM systems: study of classical and quantum channel interaction and capacity

Master candidate:
Francesco Lorenzi

Supervisor:
Prof.
Marco Santagiustina

Academic year 2021/2022
Graduation day: 5th September 2022

Francesco Lorenzi: Nonlinear noise in WDM systems: study of classical and quantum channel interaction and capacity.
Master Thesis in ICT for Internet and Multimedia, August 2022.

Alla mia famiglia, che mi ha insegnato la cura ed il lavoro.
Alla scienza, all'amore.

ABSTRACT

This thesis is a theoretical and numerical work that aims at expanding the knowledge of noise in broadband optical communication systems. The target phenomena to be addressed is the nonlinear interaction between channels that copropagate into the same physical medium. Since in recent times quantum communication schemes in optical fibers are gaining interest for QKD, an effort is done in the theoretical modeling of the interaction between quantum channels and "classical" channels – i.e. channels for which the detection scheme does not target the detection of a quantum state. Finally, special attention is devoted to deriving metrics of interest for realistic optical communication systems.

Wavelength Division Multiplexing (WDM) is a major enabling technology for wideband optical communications, however, aspects belonging to nonlinear effects are not yet completely understood and modeled. In the scenario of WDM systems, many intrinsic subtleties arise, such as the increased effort required to compensate for chromatic dispersion, channel-dependent Raman on-off gain in Raman fiber amplifiers, Four Wave Mixing (FWM) [157], and Cross Phase Modulation (XPM). In particular, a major nonlinear penalty is the Nonlinear Interference Noise (NLIN), originated from XPM-related pulse phase perturbation due to other channels which propagate in the same fiber medium. This is particularly interesting in the case of coherent optical transmission. The modeling of the NLIN phenomenon was approached in the fist place with a frequency-domain analysis [130, 83]. However, the frequency-domain approach predicts noise spectrum which is independent from the modulation format, in contrast with experiments [102]. A different approach is the one in the time-domain [115] which correctly accounts for modulation format dependence, and predicts also that a large part of NLIN is phase noise on the received symbol. Still, the time-domain approach fails to account for wavelength-dependent attenuation, intrinsic to silica, and gain, which is a characteristic of many components, especially Raman fiber amplifiers [19].

On a separate research track, quantum channels are gaining interest, as Quantum Key Distribution (QKD) is a possible disruptive technology in the secure communication field, and it is enabled by physical phenomena which can take place in optical fibers [15]. QKD over dark optical fibers is reaching its technological maturity [8] but models for interaction with classical channels are somehow still lacking. An experimental study has been done for On-Off Keying [84]. Existing models for interaction between classical and quantum channels focus on Raman scattering and optimal spectral placement for avoiding Stokes and anti-

Stokes bands [156, 152]. At the same time, technological circumvention of the interaction problem, such as time scheduling [20] is an interesting alternative.

The contribution of this thesis is to extend the previous NLIN model to wavelength and position-dependent attenuation and Raman gain, give numerical results for realistic WDM transmission scenarios, and connect the model to previous works in Raman amplification. In second place, another aspect will be to generalize the method and its results also for quantum channels, to study the feasibility of co-propagation of channels for various purposes inside the same fiber, linking it to key fiber and channel properties and parameters.

SOMMARIO

Questa tesi è uno studio teorico e di simulazione numerica con l'obiettivo di espandere la modellistica del rumore nei sistemi di comunicazione ottici a banda larga. Tra i vari fenomeni che concorrono all rumore complessivo, quello di interesse è l'interazione non lineare tra canali che si propagano all'interno dello stesso mezzo materiale di una data fibra, in particolare una fibra monomodale standard. Dato che recentemente le comunicazioni quantistiche in fibra ottica stanno guadagnando sempre più interesse, soprattutto per la distribuzione di chiavi crittografiche, si è valutata l'estensione del modello del rumore anche al caso di canali quantistici, che possono interagire e subire interferenze da parte di canali "classici", ovvero la cui ricezione non punta a misurare un stato quantistico. Per l'estensione del modello di rumore classico, speciale cura è stata dedicata a derivare delle metriche di interesse per sistemi realistici, basandosi su risultati delle simulazioni numeriche.

La multiplazione a lunghezza d'onda (WDM) è, tra tutte, la tecnologia che ha permesso lo sviluppo più notevole delle comunicazioni ottiche negli ultimi decenni, tuttavia alcuni aspetti legati all'interazione nonlineare non sono completamente compresi e considerati. Nello scenario di un sistema WDM, alcune sottigliezze rendono l'analisi difficoltosa, ad esempio la difficile compensazione della dispersione cromatica in modo uniforme per tutti i canali, la dipendenza del guadagno di Raman dalla lunghezza d'onda del canale, fenomeni di miscelazione a quattro onde, e modulazione di fase. In particolare, un fattore determinante per i sistemi moderni è il rumore dovuto all'interferenza non lineare, originato dalla modulazione di fase inter-canale. La modellistica sviluppata per questo fenomeno è stata incentrata dapprima su modelli nel dominio della frequenza [130, 83]. Tuttavia, questo approccio non consente di prevedere la dipendenza del rumore dal formato di modulazione, effetto recentemente sperimentato [102]. Un approccio diverso è quello di svolgere un'analisi nel dominio del tempo [115]: oltre a descri-

vere correttamente gli esperimenti sul formato di modulazione, questo modello indica che il rumore NLIN consiste in un rumore di fase. Tuttavia il modello proposto non fornisce un modo per considerare gli effetti dell'attenuazione e il guadagno di Raman dipendenti dalla lunghezza d'onda, che è una caratteristica determinante degli amplificatori di Raman.

Su un altro fronte di ricerca, i canali quantistici in fibra ottica stanno guadagnando interesse, infatti la distribuzione quantistica di chiavi crittografiche è una possibile tecnologia dirompente nel campo della sicurezza nelle telecomunicazioni [15]. Questa tecnologia, implementata su fibre "buie" – i.e. senza la presenza di altri canali – sta raggiungendo la sua maturità tecnologica [8]. Tuttavia sono ancora carenti dei modelli per considerare il rumore indotto dalla presenza di altri canali all'interno della stessa fibra. Alcuni esperimenti di compresenza di canali classici e quantistici sono stati realizzati per la modulazione On-Off [84]. I modelli già presenti per l'interazione tra canali si basano su effetti di conversione parametrica, e focalizzano l'attenzione sull'evitare le bande di Stokes e anti-Stokes [156, 152]. Allo stesso tempo, altre tecniche per evitare il problema sono state proposte, come la multiplazione di slot di tempo [20].

Il contributo del presente lavoro è quello di estendere il modello NLIN per il caso di reti amplificate Raman, estremamente utili nella pratica, ottenendo risultati numerici per sistemi WDM realistici. Verrà prospettata anche al possibilità di integrare questo modello di rumore in metodi di ottimizzazione per il posizionamento delle pompe di Raman. In un secondo momento, la generalizzazione del modello per interazione tra canali classici e quantistici viene studiata.

ACKNOWLEDGEMENTS

Un lavoro ben fatto, qualsiasi lavoro, fatto dall'uomo... che non si prefigge solo il guadagno, ma anche un arricchimento. [...] Un lavoro ben fatto è quello che appaga l'uomo.

Mario Rigoni Stern

This thesis would have been impossible without the enthusiastic cooperation of many people. I would like to deeply thank my supervisor Prof. Marco Santagiustina, which transmitted me the passion for nonlinear optics and stimulated me during these years of study, with constant precision and availability. With his help, the help of Dr. Gianluca Marcon, and of the members of the Photonics and Electromagnetics Group at the Department of Information Engineering, I started moving the first steps in research.

A special thought goes to my university friends Marco, Federico, and Giacomo, who taught me computer programming. All the shared days of study, with all their joys and preoccupations, will stay in my heart in the future, so thanks for the lively discussions, the curiosity and the enthusiasm of these years. I wish to express my gratitude to Andrea Lanaro, the DEI librarian, and the university library staff, for their help in getting books and resources.

Finally, I heartily thank my family, for their constant support, and especially my father, who taught me the meaning of work.

CONTENTS

LIST OF FIGURES

LIST OF ABBREVIATIONS

APD	Avalanche Photodiode
ASE	Amplified Stimulated Emission
BER	Bit Error Rate
BPSK	Binary Phase Shift Keying
CSCO	Complete Set of Commuting Observables
CV-	Continuous Variable [prefix]
CW	Continuous Wave
DCF	Dispersion Compensating Fiber
DSP	Digital Signal Processing
DV-	Discrete Variable [prefix]
EVM	Error Vector Measure
FWM	Four Wave Mixing
GKSL	Gorini-Kossakowski-Lindblad-Sudarshan quantum master equation
GVD	Group Velocity Dispersion
IM/DD	Intensity Modulation / Direct Detection
ISI	Inter Symbol Interference
LCT	Linear Canonical Transform
LP	Linearly Polarized (mode)
M-PSK	M-ary Phase Shift Keying
M-QAM	M-ary Quadrature Amplitude Modulation
MSE	Mean Square Error
NLIN	NonLinear Interference Noise
NLSE	NonLinear Schrodinger Equation
NZDSF	Non-Zero Dispersion Shifted Fiber
OOK	On-Off Keying

OSNR	Optical Signal to Noise Ratio
PMD	Polarization Mode Dispersion
POVM	Positive Operator Valued Measurement
QFT	Quantum Field Theory
QKD	Quantum Key Distribution
RAL	Raman amplified link
RMSE	Root Mean Square Error
SBS	Stimulated Brillouin Scattering
SLA	SuperLarge effective Area fiber
SNR	Quantum NonDemolition (measurement)
SNR	Signal to Noise Ratio
SPM	Self Phase Modulation
SRS	Stimulated Raman Scattering
SVEA	Slowly Varying Envelope Approximation
WDM	Wavelength Division Multiplexing (prefix C: Coarse, D: Dense)
XPM	Cross Phase Modulation

LIST OF MATHEMATICAL SYMBOLS

$\mathbb{C}$	Field of complex numbers
$\mathbb{R}$	Field of real numbers
A	Classical field amplitude, normalized as $[\lvert A\rvert^2] = W$
ω	Angular frequency, or frequency for brevity, when unambiguous
β	Propagation constant
θ	Absolute temperature
$\hat{a}$	Annihilation operator
$\hat{a}^\dagger$	Creation operator
Π	Projection operator
$\langle\cdot\rangle$	Expectation operator, probabilistic or quantum definition is clarified by the context
Tr	Trace operator
$\otimes$	Tensor product
$:\hat{O}:$	Normal ordering for a given operator $\hat{O}$
$\delta(\cdot)$	Dirac delta distribution

1 INTRODUCTION

In this chapter we will start by reviewing current state of the art in optical communication systems, describing WDM, Raman amplification, coherent detection, and also optical quantum technologies.

First of all, a brief mathematical introduction about classical physical principles of nonlinear interactions occurring in the fiber will be given. After that, the description of the technologies of our interest, together with the review of past literature, are presented. Finally, we will give an outline of the thesis, highlighting original aspects, and connections to previous works.

1.1 OPTICAL FIELD PROPAGATION MODEL

This section will be devoted to a presentation of the main mathematical model of interest in this study, and its physical significance. Its generalizations will be the main topic of chapters 2 and 3.

1.1.1 *Single-mode fibers*

Currently used fibers in wideband systems are single-mode: this allows the avoidance of modal dispersion, which can easily cause disruptive modal Inter-Symbol Interference (ISI). However in the single-mode fiber two propagating modes are present, which are the orthogonal axis of polarizations. In this work we will consider only light polarized in one direction, supposing that the polarization is unperturbed along the fiber, ignoring polarization random walks and other related effects, like Polarization Mode Dispersion (PMD) [51]. This is a strong assumption, since realistic fibers suffer heavily from polarization non-idealities. Many phenomena of our interest, as Stimulated Raman Scattering (SRS) and interference in coherent detection are sensitive to polarization, however, this effect can be addressed within model without polarization via the introduction of correction factors in the interaction coefficients. The main propagation equation we are focusing on is called Nonlinear Schrödinger Equation (NLSE). Since this

is the main equation we are considering in this work, an extended description is useful. The equation reads

$$\frac{\partial A}{\partial z} = -\frac{\alpha}{2}A - \beta_1\frac{\partial A}{\partial t} - i\frac{\beta_2}{2}\frac{\partial^2 A}{\partial t^2} + i\gamma|A|^2A. \tag{1.1}$$

This equation derives from the separation of Helmholtz equation in cylindrical coordinates, which model the evolution of a field with fixed polarization along a transverse direction $\hat{\mathbf{e}}_\tau$, i.e. $\mathbf{E} = E\hat{\mathbf{e}}_\tau$. If z is the longitudinal direction of the fiber, using the usual cylindrical coordinate systems (ρ, ϕ, z), the separation ansatz can be written as

$$E(\rho, \phi, z, t) = G(\rho, \phi)A(z, t)\exp(i\beta_0 z), \tag{1.2}$$

β_0 being a propagation constant to be determined by the separated equations – more precisely, by the resulting dispersion relations. The function G, obeying the transverse part of the separated Helmholtz equation, satisfy a Sturm-Liouville problem whose solution is the mode transverse distribution, expressed as combination of Bessel functions. For single mode fibers, the transverse distribution is well approximated by the so-called LP_{01} mode, which is well approximated itself by a Gaussian transverse profile [142]. With exception of extremely powerful and broadband pulses, the transverse distribution remains constant. Eq. (1.1), for the function A describes the longitudinal evolution of the field. All propagation properties of pulses are summarized by the evolution of the complex envelope A. By choosing adequately the separation physical units, one can define A in such a way that $|A(z, t)|^2$ represents power flowing through the fiber cross section at time t and position z. As for the other terms, the NLSE describes dispersion to the second order approximation. The phenomenon of nonlinear dependence of the propagation constant by the frequency is called also Group Velocity Dispersion (GVD). The dispersion profile of the fiber is represented by $\beta(\omega)$, the frequency dependent wave number, obtained from models of electric susceptibility of the material and waveguide properties. By expanding around the central frequency ω_0, that is the frequency of the optical carrier, and truncating the expansion to the second order,

$$\beta(\omega) \approx \beta_0 + \beta_1(\omega - \omega_0) + \frac{\beta_2}{2}(\omega - \omega_0), \tag{1.3}$$

it is possible to obtain the definition of the coefficients β_1 and β_2. The inverse of β_1 is called v_g, the group velocity, which depends on the central frequency ω_0. An interesting analogy can be done with the Schrödinger equation from quantum

mechanics [134]. By considering that equation for a free particle in the direction z

$$\frac{\partial \psi}{\partial t} = -i\frac{\hbar}{2m}\frac{\partial^2 \psi}{\partial z^2}, \tag{1.4}$$

we see a clear analogy between the term containing the mass and the GVD term, with the exception of having inverted time and space coordinates. A more precise quantum-mechanical formulation of this fact, addressed in chapter 3, will introduce the concept of *dressed photon*, which justify the statement that *GVD gives "mass" property to the photon*.

The truncation to the second order of the propagation constant is justified only as far as the field A has a narrow spectrum, i.e. it is slowly varying. This assumption is called Slowly Varying Envelope Approximation (SVEA). SVEA validity is a topic of theoretical interest, studied for example in [93].

Finally, the Kerr effect is represented by the coefficient γ, and it is due to silica cubic nonlinear susceptibility. In the NLSE model it is considered as instantaneous. This is a reasonable assumption since the relaxation time is many orders of magnitude lower than common pulse periods, being < 1ps for common telecommunication fibers [47]. The finite relaxation time of the Kerr medium needs to be included in the model only when pulses which are to be analyzed have duration comparable to the relaxation time [67].

Recalling that the NLSE model does not take into account light polarization effects, we point out a more complete model which is able to describe also polarization effects, and is called Manakov model [2]. It uses a system of coupled NLSE with polarization coupling terms.

For the communication purposes, the signal launched into the fiber is physically represented by a complex amplitude, and encodes symbols in a space of in-phase and quadrature components. Moreover, since the optical frequencies are as high as 193THz at 1550nm, the SVEA is acceptable even for relatively high modulation bandwidth, which means the possibility of modeling multiple channels, as in the case of Wavelength Division Multiplexing (WDM), without substantial changes to the NLSE. However, if the physical scenario includes only the interaction between multiple narrowband fields at spaced center frequencies, an useful alternative model is the one with coupled NLSEs, one for each narrowband field, equipped with adequate coupling coefficients which encode nonlinearity [2]. Of course this model is unable to account for wave mixing, but it is sufficient for modeling Cross Phase Modulation (XPM), which is the main phenomenon of interest for NLIN. This will be the starting point of the analysis in chapter 2.

Let us now relate the propagation model with useful telecommunication metrics, in particular with a frequency response formalism for linear propagation. First of all, a common model for IM/DD transmission is the magnitude of the frequency response of the fiber, intended as the ratio of the optical power spectrum at the output and at the input. This makes sense as long as the propagation is considered to be linear. In fact, if we consider a fiber in which pulses undergo high dispersion, and then the initial shapes are recovered just before the receiver by using dispersion compensation, it is possible to neglect, at the zero-order approximation, the nonlinearity. This setup is often called pseudolinear [115, 30]. By neglecting effects of nonlinearity, we can write such frequency response as [13]

$$H_F(\omega) = A_F(\omega) \exp\left[-\frac{(\omega\sigma_F)^2}{2}\right] \exp[-i\omega t_F] \tag{1.5}$$

where A_F is the link attenuation, σ_F the overall dispersion accumulated along the link, and t_F the link propagation delay. If z is the link length, and if the attenuation coefficient α in dB km^{-1} and the dispersion coefficient D in ps nm^{-1}km^{-1} are available, then

$$\begin{aligned} A_F &= 10^{-\alpha z} \\ \sigma_F &= zD\Delta\lambda. \end{aligned} \tag{1.6}$$

Despite being a commonly used frequency response, Eq. (1.5) can be misleading. In fact, this is an equation which relates frequency response of the signal, which is intended to be the electrical signal feeded into the light modulator at the transmitter, and recovered from the photodetector and amplifier at the receiver, with ideal electronic transceivers. Equivalently, dropping the assumption of ideal transceivers, the frequency response is, as said before, the ratio between the spectra of output optical power and input one, since it is the optical power which is proportional to electrical amplitudes. The frequency response can be derived, with some passages, from Eq. (1.1), by assuming Gaussian input pulses.

As for coherent systems, in which phase properties of the light are used to encode information, this kind of frequency response in unsatisfactory. In a more detailed way, accounting for fiber phase characteristics, the Quadratic Phase Filter (QPF) model [124] is a useful tool for computing linear field evolution. Let us start from a linear NLSE, from which we remove, for simplicity, the term due

to group velocity. This accounts for a delay that can be considered in a separate moment. Such equation reads

$$\frac{\partial A}{\partial z} = -i\frac{\beta_2}{2}\frac{\partial^2 A}{\partial t^2}. \tag{1.7}$$

Using the shift theorem [149], it is possible to introduce the propagation operator

$$\mathbf{U}(z) = \exp\left[-i\frac{\beta_2}{2}z\frac{\partial^2}{\partial t^2}\right]. \tag{1.8}$$

Considering this operator as an $\mathcal{L}^2$ operator, when written in reciprocal domain, reads

$$\hat{\mathbf{U}}(z) = \exp\left[i\frac{\beta_2}{2}z\omega^2\right], \tag{1.9}$$

so, for example $\hat{U}(L)$ corresponds to the frequency response of a linear dispersive link of length L, with respect to the *optical complex amplitude*, and not the *optical power*. It is possible to relate this frequency response to the impulse response of the fiber. In fact, by using the Gaussian transform property

$$\exp\left[-st^2\right] \xrightarrow{\mathcal{F}} \sqrt{\frac{\pi}{s}}\exp\left[-\frac{\omega^2}{4s}\right] \tag{1.10}$$

where $\mathcal{F}$ indicates Fourier transform, it is possible to find a convolution kernel

$$\hat{\mathbf{U}}(z) = \exp\left[i\frac{\beta_2}{2}z\omega^2\right] \xrightarrow{\mathcal{F}^{-1}} \mathbf{U}(z,t) = \sqrt{\frac{-i}{2\beta_2 z\pi}}\exp\left[-i\frac{t^2}{2\beta_2 z}\right] \tag{1.11}$$

The linear propagation corresponds to a convolution operation by this kernel. Since the frequency response denotes a *quadratic phase term*, the corresponding filter assume the name of QPF. The convolution assumes a well-known expression, as it coincides with the expression of a Fresnel transform:

$$\bar{f}(t) = \sqrt{\frac{\xi}{i\pi}}\int_{\mathbb{R}} d\tau f(\tau)\exp\left[-i\xi(t-\tau)^2\right], \tag{1.12}$$

in this case the coefficient is $\xi = 1/(2\beta_2 z)$. It is interesting to point out that this transformation is analogous to the one occuring in paraxial optics, which lead to Fourier optics in far field [124, 18]. In optical fibers, it can describe pulse spreading and chirping, with precise phase information. This fact will allow to develop an

approximation of the propagated amplitude with its Fourier transform, useful to model NLIN in pseudolinear systems [30], which will be discussed in chapter 2.

As a last remark on the transfer properties of the optical fiber, from a mathematical point of view, the amplitude signal propagating into the fiber undergoes a particular form of Linear Canonical Transform (LCT). LCT is a unifying formalism which includes Fourier, Laplace, Fresnel, pulse chirping and others; with inverses. A generic transform $X(u)$, $u \in \mathbf{C}$ of the function $x(t)$, with parameters (a, b, c, d) is defined as

$$X_{(a,b,c,d)}(u) = \begin{cases} \sqrt{\frac{1}{ib}} \exp\left[i\pi \frac{d}{b} u^2\right] \int_{\mathbb{R}} dt \exp\left[-i2\pi \frac{1}{b} ut\right] \exp\left[i\pi \frac{a}{b} t^2\right] x(t), & \text{when } b \neq 0, \\ \sqrt{d} \exp\left[i\pi c d u^2\right] x(du), & \text{when } b = 0. \end{cases} \tag{1.13}$$

in which it is possible to identify, in order, a chirping term, a Laplace transform term, and a quadratic phase one. Such transform is characterized by the matrix

$$T = \begin{bmatrix} a & b \\ c & d \end{bmatrix} \tag{1.14}$$

This formalism is particularly useful as it naturally gives a composition property. The cascade of linear optical devices, represented by LCT, turns out to be described with a LCT whose matrix is the product of the LCT matrices [73].

1.2 TECHNOLOGIES FOR OPTICAL COMMUNICATIONS

In this section we will discuss technologies and physical effects that are important for framing the discussion on nonlinear noise, by reviewing relevant literature.

1.2.1 *Detection and noise*

Optical detection is based on optoelectronic devices that are grouped in a pair of different technological families: photodiodes and avalanche devices [1, 98]. Photodiodes are characterized by a large area of the semiconductor device which is exposed to incoming radiation, and in which electron-hole pairs are simply generated by photoabsorption. Typically te region exposed to incoming radiation is the intrinsic region of a PIN diode. Since the rate of electron-hole generation is proportional to the incoming photon flux, the electrical signal is proportional to the incoming optical power. As for avalanche devices, a typical avalanche

device used in the past is the photomultiplier tube, which consists on a first photocatode plate and a sequence of "dynode" plates inserted in a potential, and designed in a way that a single electron emission in the photocathode triggers a series of emissions, that eventually turn out to be a macroscopically detectable charge at the output of the vacuum tube. In a similar way, a more recent device, the Avalanche Photodiode (APD) consists in amplification of charge carriers generated by photoabsorption in a semiconductor region. The process, that would proceed up to reach energies capable of destroying the device, is quenched shortly after the event, by supply electronics, so that the increase in total event charge is stopped. A key parameter for evaluating system performance of a photodetector is the quantum efficiency η defined as the ratio between the average emitted charge rate and the incoming photon rate. Moreover, especially if multiple charges are generated from a single incoming photon, as in avalanche devices, another useful parameter is the responsivity R defined as the average current generated per unit of incoming optical power [1]. In a typical scenario, the photodetection current is feeded inside a transimpedance amplifier, from which the output voltage is used for decision or further processing. We will call *ideal photodetector* a detector which provides a current which is exactly proportional to the incoming photon flux, in a deterministic way, for some positive proportionality constant, and does not introduce additional noise. For the present study, optical detection is considered only as far as total system noise performance needs to be estimated, or fundamental quantum mechanical measurement aspects have to be considered. Optoelectronic design and device non-idealities are out of the scope of the present work, and are not addressed.

Shot noise

Shot noise is a noise model that derives from the discreteness of photons inside an optical signal. While the classical description of the incoming radiation field is deterministic, a more accurate model for radiation is the semiclassical one, which describes the arrival photon flux of a typically used laser radiation as a inhomogeneous Poisson process [70]. Since the average power must correspond in the two models, the photon rate Λ must be such that $\Lambda(t) = |A(t, L)|^2/(\hbar\omega)$ for a field of carrier frequency ω. If we consider the task of detecting a symbol by using an ideal photodetector, if the symbol is transmitted in a symbol time T, the average number of detected photons will be ΛT, with variance ΛT. Of course in the limit of high average photon number, the random variable degenerates into a number, since for a Poisson random variable of mean ΛT the variance is ΛT. This additional fluctuations, with respect to average photon flux integrated in the time T, is considered as noise.

This simple model allows to introduce a fundamental limit on amplitude detection. Consider a binary transmission, in the form of a simple On-Off Keying (OOK), in which symbols are transmitted by zero optical power and a generic high optical power. Let the transmitted symbol be random variable a, assuming values a_0 or a_1 respectively for low and high transmitted power. Let the voltage after the transimpedance amplifier, integrated and measured after the k_{th} symbol period, be v_k. Since the photon arrival is inhomogeneous Poisson distributed, and we assume ideal photodetection and neglecting thermal noise, we expect v_k to be Poisson distributed too, with parameter $N_R(k) > 0$, the average number of received photons in the symbol period k. If N'_R is the expected number of photons for a transmission of symbol a_1, for every detection rule, there is a fundamental indistinguishability between the two symbols at the detector. In fact, by using Poisson statistics,

$$P[v_k = 0|a = a_1] = \exp\left[-N'_R\right]. \tag{1.15}$$

The fundamental limit on the probability of error, for uniform symbol distribution, is obtained using the law of total probability,

$$P_e > \frac{1}{2}\exp\left[-N'_R\right]. \tag{1.16}$$

This semiclassical result is usually called the *quantum limit* for OOK communications.

Thermal noise, interaction with reservoirs at thermal equilibrium

Thermal noise occurs when information-carrying physical quantities are coupled to thermally excited system components. An example is the perturbation in the motion of the electrons by the thermal fluctuation of the position of nuclei in the lattice structure of a conductor: that was the first case of thermal noise called Johnson-Nyquist noise [70, 13]. Any case of interaction with a thermally excited medium is a source of thermal noise. For example, when a guided wave interacts with a guiding medium at finite temperature, by assuming thermal equilibrium, statistical mechanics predict that every degree of freedom of every mode of the radiation field must have an energy of $k_B\theta/2$ where k_B is the Boltzmann constant and θ is the absolute temperature [70]. This is a consequence of the equipartition theorem [79]. The thermal noise of a guided field, which turns out to be approximately Gaussian by the Central Limit Theorem [70], can impact noise performances as an additive noise. This contribution is more important at radiofrequencies and microwaves than in optical frequencies, because of the lower

value of the energy quanta. In fact, at optical frequencies, at room temperature, $\hbar\omega \sim 1\text{eV}$, whereas $k_B\theta \sim 10^{-2}\text{eV}$. In order to shed light onto analogies between quantum-theoretical and classical treatment of noise, in section 3.3.4, we discuss this aspect in more detail.

1.2.2 *Amplification: Erbium doping and Raman techniques*

Optical amplification is a technique which allow to increase the number of photons of an incoming signal via coupling to an excited reservoir, which undergoes stimulated emission. Historically speaking, even if Raman amplification principle was known before, the first efficiently implemented method to obtain optical amplification was Erbium doping [55], in which one of the energy transitions of Erbium dopant falls into the infrared telecommunication band. The process is dependent on the absolute wavelength, because of Erbium energy levels properties. Moreover, such amplifiers, called Erbium Doped Fiber Amplifiers (EDFAs) are lumped, as the lenght of the doped fiber in which pumping and amplification is realized is much less than the link length.

Another method to obtain optical amplification is the exploitation of Stimulated Raman Scattering (SRS) [19]. This phenomenon is the frequency conversion of pump photons due to interaction with a phonon reservoir, which is due to molecular resonance excitation in the silica medium. A representation is given in Fig. 1.1. In the most elementary application scheme, shown in Fig. 1.2, a pumping wave is injected in the fiber (a standard fiber), consisting in a high-power Continuous Wave (CW) radiation propagating in the direction of the signal (copropagating), or in the opposite direction (counterpropagating), or from both ends. Interaction with molecular resonances triggers the frequency conversion of the pump wave into signal wave, due to stimulated emission, and emission of a phonon of the corresponding energy difference. A simple semiclassical model to understand the phenomenon, in the simplified case of a s, -ingle wavelength pump, is the following. Let P_p^+ represent the copropagating wave power, P_p^- the (same wavelength) counterpropagating one, and P_s the signal power. They obey the following system of differential equations:

$$\begin{aligned}
\frac{dP_s}{dz} &= -\alpha_s P_s + C_R(\lambda_s,\lambda_p)\left[P_p^+ + P_p^-\right]P_s \\
-\frac{dP_p^-}{dz} &= -\alpha_p P_p^- - \left(\frac{\lambda_s}{\lambda_p}\right) C_R(\lambda_s,\lambda_p)\, P_s P_p^- \\
+\frac{dP_p^+}{dz} &= -\alpha_p P_p^+ - \left(\frac{\lambda_s}{\lambda_p}\right) C_R(\lambda_s,\lambda_p)\, P_s P_p^+
\end{aligned} \tag{1.17}$$

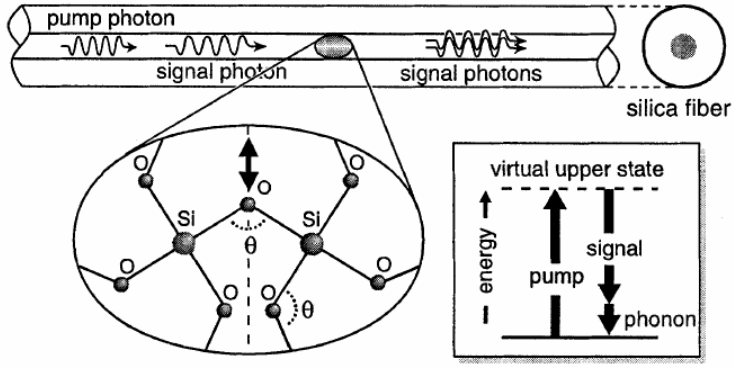

Figure 1.1: Pictorial representation of the stimulated Raman scattering [19].

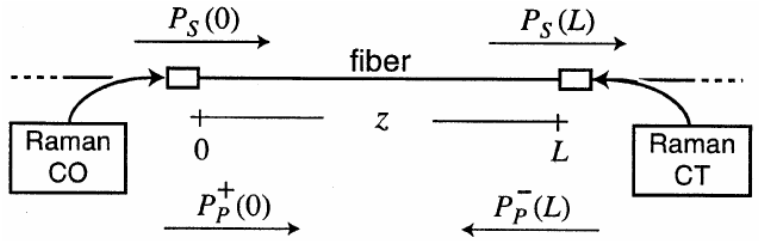

Figure 1.2: Copumping and counterpumping of a Raman amplifier [19].

where α_s, α_p are the attenuation coefficients at the signal and pump wavelengths, and the coupling coefficient C_R is a phenomenological Raman gain coefficient. This last coefficient has the important property to be only dependent on *wavelength difference* and not to absolute wavelength. This is in fact the effect of interaction with phonon reservoirs, which allows a conversion to a frequency offset from the exciting wave. Notice that the frequency shifting could be positive or negative, following the elastic process of creation or annihilation of a phonon, respectively. In the negative case, the resulting down-converted wave is called Stokes wave, whereas in the positive one the up-converted wave is called anti-Stokes wave. The Raman gain coefficient's spectrum is plotted in Fig. 1.3a, exibiting a peak at about 12THz spectral distance from the excitation wave, which is fundamentally different to the pumping and lasing of a fixed-energy transition. In the figure, represented fibers are: Dispersion Compensating Fiber (DCF), Non-zero Dispersion Shifted Fiber (NZDSF) and SuperLarge effective Area fiber (SLA). Eq. (1.17) can predict the complete exchange of power, including the pump depletion phenomenon. Notice how the wavelength ratio term λ_s/λ_p is justified as, in absence of attenuation, by combining the three equation and substituting power product terms like $P_s P_p^{\pm}$, we obtain a Manley-Rowe equation for photon flux [121]. Fig. 1.3b shows how the polarization or the signal impact the magnitude of the gain. SRS is strongly sensitive on polarization. If one among

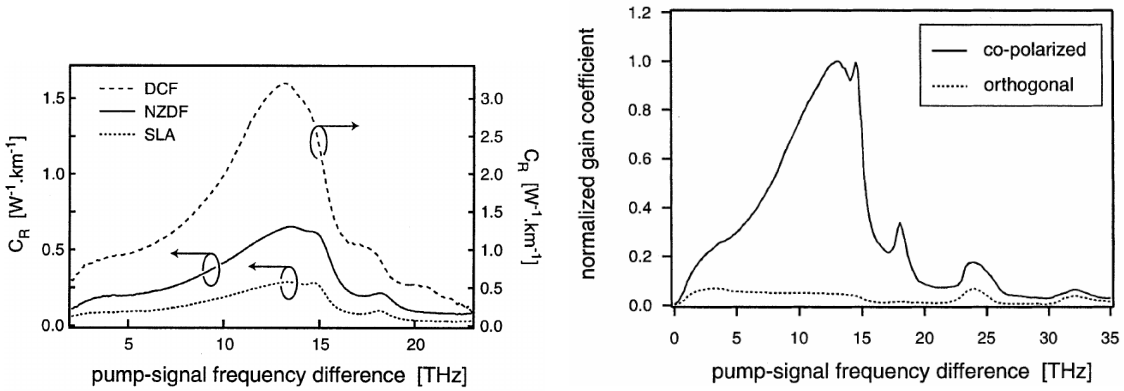

(a) Raman gain coefficients for common fiber types. Pump wavelength is 1450nm

(b) Polarization dependence of Raman gain.

Figure 1.3: Raman gain spectrum properties [19]

.

signal or pump radiation is completely depolarized, the effect of polarization mismatch can be approximately addressed by dividing by 2 the gain coefficient [19].

By going beyond this simple model which explains the physical features of SRS, the presence of multiple pumps can be addressed in a generalized model. Treating indistinctly signal and power wavelengths using the indices i, j, for a fiber with N wavelengths, there are 2N equations, a counterpropagating and a copropagating equation for each wavelength:

$$\pm \frac{dP_i^{\pm}}{dz} = -\alpha_s P_i^{\pm} + \left[\sum_{j \neq i} C'_{R\,i,j} \left[P_j^{+} + P_j^{-} \right] \right] P_i^{\pm}, \tag{1.18}$$

where the $+$ sign is for copropagating and $-$ sign for the counterpropagating. $C_{R\,i,j}$ includes also the wavelength ratios discussed before, in the following way

$$C'_{R\,i,j} = \begin{cases} C_R(\lambda_i, \lambda_j) & \text{if } \lambda_i > \lambda_j, \\ \dfrac{\lambda_i}{\lambda_j} C_R(\lambda_j, \lambda_i) & \text{if } \lambda_i < \lambda_j. \end{cases} \tag{1.19}$$

From a technological point of view, Raman pumping scheme can leverage the presence of multiple pumps as a bonus feature. The adoption of such scheme is justified by the need of having flat gain spectra over a wide bandwidth, occupied for example by WDM channels. In this scenario, Raman amplification is ideal, as gives an unprecedented flexibility of placing pump wavelengths and powers. By superimposing the gain spectra, it is possible to tune a total gain of the link, as shown in Fig. 1.4a. Simple superposition of gain spectra may not be correct if

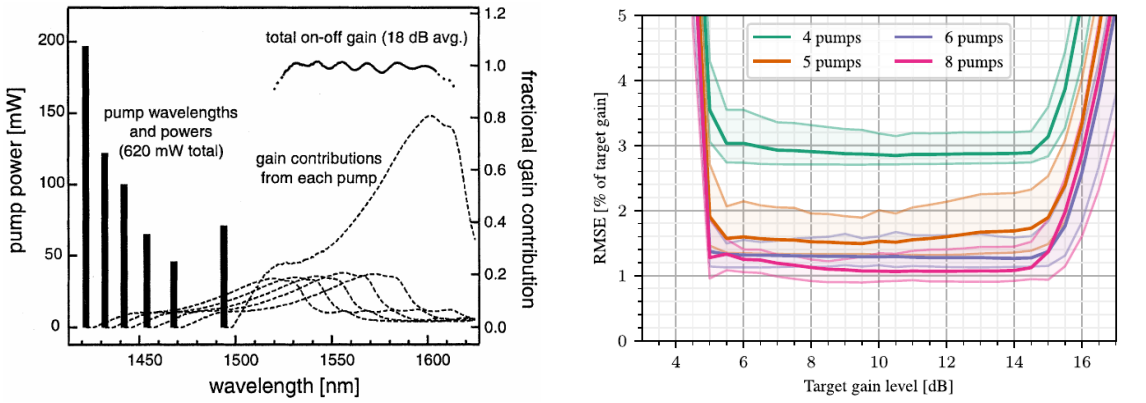

(a) Example of optimized pump placement, using only marginally high-order techniques [19].

(b) Performance of pump placement optimizer with deep learning in a few mode fiber setup [111].

Figure 1.4: Optimization of pump wavelength and power.

one or many pumps are affected by amplification or attenuation due to scattering from and toward other pumps. In this case, the resulting scenario is called *higher-order pumping*. These interactions, may be exploited in order to obtain a desired pump evolution over the link length.

Optimization procedures for pump placement have been studied, some of them using also deep learning techniques [111]. By using optimization it is possible to obtain unprecedented wideband amplification. As an example, considering a flat target gain profile over the C+L band, with 50 equally spaced wavelengths, the result for a 4-mode fiber are shown in Fig. 1.4b, in which the shaded area is the RMSE variation over the modes, and the solid line is the mean RMSE loss. This result considers a 70km amplifier.

ASE noise

The conversion process described above may also happen in a spontaneous way. In this case, emitted photons in the signal band are to be considered as noise, as they are independent on the signal. Furthermore, those photons may trigger stimulated emissions, thus being amplified. The overall phenomenon is known as Amplified Stimulated Emission (ASE), and is a major impairment in optical amplified systems. In order to predict the amount of ASE in a given amplifier, power equations similar to Eq. (1.18) are used. The main difference consists in the introduction of a noise source representing the process of spontaneous emission.

The number of equations for ASE should be equal to the number of signals we are interested in, as every signal has to be decoded along with its in-band ASE component. It is often possible to use a reasonable simplifying assumption in the coupled power equations: since ASE power is usually small with respect to

pumps and signals, it is reasonable to assume that ASE does not deplete pumps or signals, and ASE does not pump other waves. In this way, ASE equations can be solved in a separate moment with respect to signal and pump equations as ASE power do not influence their evolution.

A useful parameter for evaluating link noise performance with respect to ASE is the Optical Signal to Noise Ratio (OSNR), which is defined as the optical power ratio between signal and noise. This definition is often referred to a single channel bandwidth, or, as an alternative, referred to a reference bandwidth, usually chosen to be 0.1nm for signals in C+L band [19]. We will use the symbols $OSNR_s$ for the ratio referred to signal s bandwidth, and $OSNR_{REF}$ for the one referred to the 0.1nm bandwidth

$$\begin{aligned} OSNR_s &= \frac{P_s}{P_n} \qquad \text{powers referred to signal } s \text{ bandwidth} \\ OSNR_{REF} &= \frac{P_s}{P_n} \qquad \text{powers referred to 0.1nm reference bandwidth} \end{aligned} \tag{1.20}$$

From the statistical point of view, it has been shown that ASE can be treated as additive Gaussian noise [44, 19]. Typically, the noise performance of an amplifier is indicated by its *noise figure*. For optical amplifiers, the overall noise performance is obtained not just by the OSNR, but by the electrical SNR, which is the standard signal to noise ratio measured after photodetection, in the electrical domain. The electrical signal power is proportional to the photocurrent squared, which in turn is proportional to the optical *power* squared. The same notation for bandwidth reference is used in SNR and OSNR. Noise figure F is defined as the ratio between SNR at the input and at the output of an amplifier, assuming an ideal detector for SNR_{out}. In narrow-band approximation the dependence on bandwidth reference is no more relevant for the computation of noise figure.

$$F = \frac{SNR_{s,in}}{SNR_{s,out}} = \frac{SNR_{REF,in}}{SNR_{REF,out}} \tag{1.21}$$

The minimum noise figure for a high gain amplifier is dictated by quantum limitations, and it is 3dB [19, 68].

1.2.3 *Coherent fiber communications*

All kind of optical communications rely on detection, however notice that simple photodetectors as those described before are not able to measure phase properties of the incoming field. Moreover, unlike in radiofrequency and microwave communications, in optical communications there are not practical nonlinear

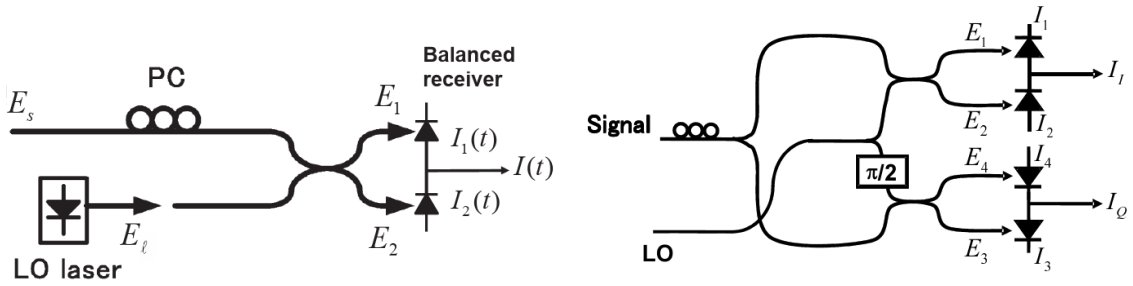

(a) Balanced detector. (b) Phase-diversity detector.

Figure 1.5: Homodyne detection schemes [92]

devices that would realize a mixer, able to do frequency conversion in the baseband by interaction with a local oscillator. So, by using only linear effects, the detection of optical coherent transmission leverage on interference properties and measurement using a couple of "slow" photodetectors. Starting from the 2000s, some technological advancements started to open the possibility to exploit also phase degree of freedom of the light for encode information, as it was the case in radio communications. Those techniques involved mainly carrier estimation and recovery, laser stabilization, and digital signal processing.

First studies on coherent optical communications have been carried out in the 1980s, for enhancing unrepeated transmission distance, but the advent of WDM and EDFAs in the 1990s shifted the research attention back to Intensity Modulation / Direct Detection (IM/DD) technique [1], that, in connection with these novel technologies, became very appealing for high-capacity systems. In 2005, interest in coherent receivers sparkled again from the demonstration of digital carrier-phase estimation [92, 145]. This technique enable a low Bit Error Rate (BER) regime of use for more spectrally efficient codes such as M-ary Phase Shift Keying (M-PSK), or M-ary Quadrature Amplitude Modulation (M-QAM). Futhermore, the recovery of the phase information allows to reconstruct and equalize linear propagation impairments, like GVD and PMD, all via DSP in post-processing [90].

Considering the optical part of the receiver, typical detectors are shown in Fig. 1.5. Usually these setups are called *homodyne* detectors, because they interfere the incoming field with a local oscillator with the same wavelength of the carrier. Nomenclature is similar with respect to radiofrequency receivers, in which homodyne refers to the technique of mixing an incoming signal with a same-frequency local oscillator, which converts the signal to baseband [131]. In Fig. 1.5a, the interference is performed in two different fiber branches, which contain fields E_1 and E_2, which have an offset component due to the local oscillator field which typically is much larger than the incoming signal, and an interference term

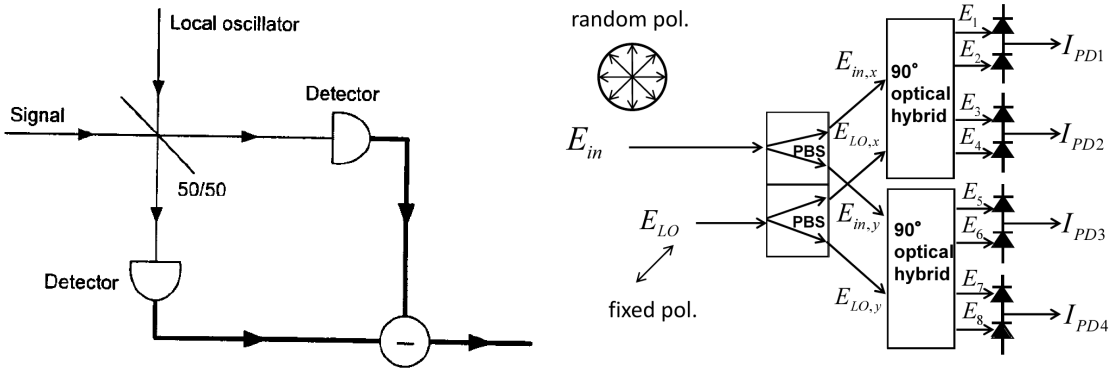

(a) Balanced detector using beam splitter [70] (b) Polarization-diversity detector [92]

Figure 1.6: Variations on the coherent detection schemes

phase-shifted by π. By detecting both fields and take the difference, the offset component is canceled and the only remaining field represents amplitude of the interference. This is the operational meaning of the composition operation between I_1, I_2 and I in the figure, after the photodiodes. This operation is shown more clearly in the alternative schematic in Fig. 1.6a. The setup just shown is able to measure one quadrature of the field. Instead, the *phase diversity* setup in Fig. 1.5b, by interfering, in a second balanced photodetector, the incoming field with a $\pi/2$ shifted local oscillator field, measures both the in-phase *and* quadrature components [92].

Finally an issue we have not taken into account is the polarization dependence of optical interference inside the fiber. If the fields do not share the same polarization states, photocurrent will not be proportional to the amplitude interference term. This problem is mitigated by the usage of Polarization Controllers (PC), that may eventually be automatized. Another solution is the usage of the *polarization diversity* detector, shown in Fig. 1.6b, in which two orthogonal polarization are processed independently by using a polarization beam splitter.

In recent times, 100-Gbit/s transmission systems, which employ quadrature PSK (QPSK) modulation, polarization-division multiplexing, and phase-diversity homodyne detection assisted with high-speed DSP at a symbol rate of 25 Gbaud, have been developed and introduced into commercial networks [90]. Using this example, by placing WDM channels at 50-GHz-spaced grids, it is possible to transmit up to 8.8 Tbit/s through a single fiber [92].

1.2.4 *NLIN effect*

Starting from Eq. 1.1, it is possible to describe effects of nonlinearity in terms of phase modulation of the complex amplitude [2]. Phase modulation effects,

for what regards telecommunications influence *pulse dynamics*: the local field amplitude modulates the refractive index, and a propagating field in the same medium experiences additional phase shifts with respect to the linear propagation. This effect is encoded in the coefficient γ in the following way

$$\gamma = \frac{n_2 \omega_0}{c A_{eff}} \tag{1.22}$$

where ω_0 is the carrier frequency, c the speed of light, n_2 is the coefficient that models intensity dependence of refractive index,

$$n = n_L + n_2 |E|^2 \tag{1.23}$$

where n_L is the linear part deriving from linear part of susceptibilty. As instantaneous Kerr effect is considered, n_2 is independent on frequency, unlike n_L. Finally, A_{eff} is the effective modal area calculated as:

$$A_{eff} = \frac{\left(\int_S ds |F|^2\right)^2}{\int_S ds |F|^4}, \tag{1.24}$$

S being the cross-section of the fiber.

By describing the field as a superposition of pulses at different carrier frequencies, as for example in a WDM system, the effect of phase modulation of a pulse on itself is called Self Phase Modulation (SPM), whereas modulation on a pulse induced by other channels pulses is called Cross Phase Modulation (XPM). From a system perspective, assuming to have coherent detection, phase imbalance due to nonlinear effects affects symbol detection. For example, SPM induces constellation rotation proportional to constellation point amplitude squared. This impairment can be easily equalized in post-processing by analysis of backpropagation. As for XPM, the effect is very much dependent on other channels, so it is more difficult to equalize. Recognizing that the influence of XPM constitutes noise, the effect is called Nonlinear Interference Noise (NLIN). Because of dispersion, pulses from different channels travels at different group velocities. Considering a train of interfering pulses, and a single pulse from the channel of interest, the spatial region in which the XPM interaction takes place is the collision region between the pulse of interest and each one of the interfering pulses, which have different launching times at the input. The outcome of this interference process can be visualized in Fig. 1.7. Details of the computation will be furnished in Chapter 2.

A proposed model to tackle NLIN is that by Dar and Mecozzi [30]. It consists in writing a single NLSE equation, encode into the field a couple of channels' train of pulses: one for the channel of interest and one for an interferent channel.

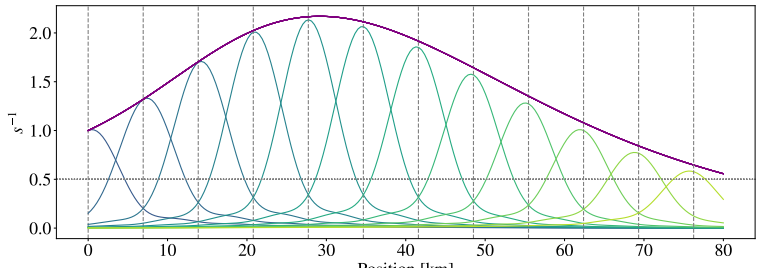

Figure 1.7: Overlap integral between power of an interfering channel and amplitude of the channel of interest (arbitrary units), in the case of 80km Raman co-pumping scheme, versus position. Green shades curves are collision for different symbols (Nyquist pulses), purple line is proportional to cumulative Raman amplification squared.

The main result is to obtain perturbative coefficients using normalized pulse shapes, with which it is possible to evaluate the total impact of pulse collision. The average total NLIN in this case is shown to be a phase noise term, and it is dependent on the interfering channel modulation format. However, Dar and Mecozzi model considers only a perfect amplification scenario, in which the overall attenuation coefficient α in Eq.(1.1), that could be substituted with a coefficient that jointly encode the effect of Raman gain and attenuation, is null. The full model will be reviewed in Chapter 2, and will be the starting point of a generalized version able to tackle also realistic attenuation and gain scenarios.

1.2.5 *Quantum detection*

Usually, when speaking about optical detection, we consider the measurement of some variables, like field power, which have classical meaning, and can be easily described in the quantum domain as *observables*. So the distinction between classical and quantum detection is inessential in this setup: if we treat properly the non-commutativity of observables, for example in in-phase *and* quadrature detection, the outcomes are completely analogous. In fact, the experimental detection setup may not even change from classical to quantum treatment. The only aspect changing is, obviously, the prediction of noise performance, as shown for the semiclassical model of shot noise in 1.2.1.

However, in the 1970s some studies [75, 76] started to tackle the problem of detecting a quantum state using the formalism of projection in Hilbert spaces. This opened up the possibility of understanding how to design optimized receivers for sets of transmitted quantum states, instead of relying on the measurement of the same observables as in classical detection. This framework developed later to be the concept of a quantum channel. In this most general scenario of communication, the transmitter chooses symbols from an alphabet of quantum

states to be transmitted $\{|\psi_k\rangle\}_k$, and the receiver, using measurement of some observables, detect the state. Every signal at the receiver can be characterized by its density matrix, which is used to model an ensemble of quantum states, that is analogous to the random variable considered in classical telecommunications. An ensemble in which the state $|\psi_i\rangle$ is associated with probability p_i has density matrix

$$\rho = \sum_i p_i |\psi_i\rangle \langle\psi_i| . \tag{1.25}$$

which is an operator. Density operators take the place of the probability density functions of probability theory, generalizing the statistical theory to a quantum statistical theory. In fact, it can be shown that quantum statistical theory includes the classical as a special case [76], as classical theory is represented by so-called *incoherent* ensembles, whereas also *coherent* ensembles can be represented in quantum statistical theory [159], [134, p. 178], [79, p. 183-185]. The diagonal elements of a density matrix are often called "populations", whereas the off-diagonal terms are called "coherences". The time evolution of the density matrix can be described through master equations of various forms, and in general is a branch of open quantum systems theory. Often times, it happens that, by interacting with a large environment, the time evolution of the density matrix exibit vanishing coherences. This process is called quantum decoherence, and it corresponds to the loss of quantum statistical properties [159, 94, 49, 139]. The measurement operation is done by projecting the density matrix by using projector - Positive Operator Valued Measurements (POVM), which are sets of projection operators $\{\Pi_0, ..., \Pi_n\}$ satisfying the requirements

$$\begin{aligned} &\Pi_i \Pi_j = \Pi_i \delta_{i,j}, \\ &\sum_i \Pi_i = \mathbf{I}. \end{aligned} \tag{1.26}$$

where $\mathbf{I}$ is the identity operator. The measurement is intended in a probabilistic sense, so product of the density matrix by a certain projector gives the probability of obtaining the corresponding decoded symbol. The framework is as follows: the transmitted state in a quantum channel is $|\psi\rangle_i$, but, by the presence of noise in the channel, the corresponding received quantum state is described, in general, by the density matrix ρ_i. Finally, a set of projector-POVM detects the density matrix and reconstruct the symbol, including additional conditional probability. The last step is easy to model, as it is a posteriori with respect to the physical channel noise evaluation. The transition probability of this step is obtained in the formalism of density matrix by taking the trace over the product of the received

density matrix related to the transmitted symbol i, ρ_i and the operator Π_j, which encodes the transition from state i to state j. In this setup, the correct decision probability is

$$P_c = \sum_i q_i Tr[\rho_i \Pi_i] \tag{1.27}$$

where q_i is the transmission probability of state i. The trace has the property to be independent on the basis in which the computation is carried out.

So the novel perspective with respect to classical channel is the possibility to design the projection operators in an optimized way to recover the transmitted state. In general this is an hard task, corresponding to function optimization in a eventually very large Hilbert space. We will refer to this problem as the *quantum detection* problem. Nonetheless, an important optimization bound result was obtained by Helstrom, in the case of binary quantum detection. Let $\{|\psi_0\rangle, |\psi_1\rangle\}$ be the alphabet of transmitted states, and let ρ_0, ρ_1 the corresponding noise-corrupted density matrices at the receiver. The receiver, being designed for binary reception, employs two projectors Π_0, Π_1, with the property that $\Pi_0 + \Pi_1 = \mathbf{I}$. By calculating the probability of correct decision, we can factorize [21]

$$\begin{aligned} P_c &= q_0 Tr[\rho_0 \Pi_0] + q_1 Tr[\rho_1 \Pi_1] && (1.28)\\ &= Tr[q_0 \rho_0] + Tr[(q_1 \rho_1 - q_0 \rho_0)\Pi_1] && (1.29)\\ &= q_0 + Tr[\mathcal{D}\Pi_1] && (1.30) \end{aligned}$$

where the $\mathcal{D} = q_1\rho_1 - q_0\rho_0$ is called the difference operator. The problem is cast into a maximization problem:

$$\Pi_i^* = \arg\max_{\Pi_1} Tr[\mathcal{D}\Pi_1]. \tag{1.31}$$

By finding the eigendecomposition of $\mathcal{D}$,

$$\mathcal{D} = \sum_k \eta_k |\eta_k\rangle \langle\eta_k|, \tag{1.32}$$

we notice that quantities $\varepsilon_k := \langle\eta_k|\Pi_1|\eta_k\rangle$ are probabilities of detection of $|\gamma_1\rangle$ if the received state is in $|\eta_k\rangle$, so they must be in the interval $[0, 1]$. Now, building the projector as

$$\tilde{\Pi}_1 = \sum |\eta_k\rangle \langle\eta_k|, \tag{1.33}$$

we maximize the value of every ε_k, and have a simultaneous diagonalization of operators $\mathcal{D}$ and Π_1. Computing the trace:

$$\mathrm{Tr}[\mathcal{D}\tilde{\Pi}_1] = \sum_{\eta_k>0} \eta_k. \tag{1.34}$$

by generality of the eigendecomposition of $\mathcal{D}$, we can state that $\tilde{\Pi}_i = \Pi_i^*$. So by finding a diagonalization of the difference operator we can build the optimal set of projectors that maximize the probability of correct decision. The explicit calculation for the probability of error is available in the simple hypotesis of pure states at the receiver. Consider the normalized received states to be $|\gamma_0\rangle$ and $|\gamma_1\rangle$. The diagonalization procedure of the difference operator gives the eingenstates that can be expressed in the basis of the received states, which are assumed to be independent.

$$\begin{aligned} |\eta_0\rangle &= a_{00}\,|\gamma_0\rangle + a_{01}\,|\gamma_1\rangle\,, \\ |\eta_1\rangle &= a_{10}\,|\gamma_0\rangle + a_{11}\,|\gamma_1\rangle\,, \end{aligned} \tag{1.35}$$

we obtain, by simple extension of the eigenvalue equations $\mathcal{D}\,|\eta_0\rangle = \eta_0\,|\eta_0\rangle$ and $\mathcal{D}\,|\eta_1\rangle = \eta_1\,|\eta_1\rangle$, a couple of equations

$$q_1(a_{0i}\,\langle\gamma_0|\gamma_1\rangle + a_{1i})\,|\gamma_1\rangle - q_0(a_{0i} + a_{1i}\,\langle\gamma_1|\gamma_0\rangle)\,|\gamma_0\rangle = \eta_i(a_{0i}\,|\gamma_0\rangle + a_{1i}\,|\gamma_1\rangle) \qquad i = 0,\ 1 \tag{1.36}$$

which in turn, by independence, can be separated in

$$q_1(a_{0i}\,\langle\gamma_0|\gamma_1\rangle + a_{1i}) - \eta_i a_{0i}\,|\gamma_0\rangle = 0, \tag{1.37}$$

$$q_0(a_{0i} + a_{1i}\,\langle\gamma_1|\gamma_0\rangle) - \eta_i a_{1i}\,|\gamma_1\rangle = 0, \tag{1.38}$$

finally, by solving the system with respect to η_i,

$$\eta_i^2 - (q_1 - q_0)\eta_i - q_0 q_1(1 - |\,\langle\gamma_0|\gamma_1\rangle\,|^2) = 0, \tag{1.39}$$

whose solution is

$$\eta_{0,1} = \frac{1}{2}\left(q_1 - q_0 \mp \left(1 - 4q_0 q_1 |\,\langle\gamma_0|\gamma_1\rangle\,|^2\right)^{\frac{1}{2}}\right). \tag{1.40}$$

so, only η_1 is positive, and by expressing the probability of error using 1.34,

$$P_e = \frac{1}{2}\left(1 - \left(1 - 4q_0 q_1 |\,\langle\gamma_0|\gamma_1\rangle\,|^2\right)^{\frac{1}{2}}\right) \tag{1.41}$$

The exposed treatment regards a theoretical lower bound, which is the quantum limit to binary detection of states, a much more powerful result with respect to the quantum limit for OOK direct detection. The bound is in fact better in terms of error probability than semiclassical detection theory in the same scenario. The fact that full quantum detection performs better than semiclassical one is justified by the fact that quantum detection exploit interference, which is encoded in the density matrices [118, 117]. Some receivers designs have been ideated to get close to the bound. Those optimized detector designs have been proposed by Kennedy [87] and Dolinar [33], and are often based on feedback techniques in the optical domain. The physical implementation of such devices is difficult, and it is an active research topic [101, 41, 21, 122].

So far we have described the detection task into a well defined Hilbert space of the received symbols. In general, the interaction with the external environment is described in the framework of a much bigger space, of which the signal Hilbert space is a small subspace. A phenomenon of great interest is present in this setup. The interaction with the measurement apparatus induces intrinsic perturbations to the quantum state, in an unavoidable way. The effect of measurement interaction can be described in many ways. If we consider a strong division between microscopic and macroscopic world, i.e. if we consider the measurement apparatus to be completely out of the quantum-mechanical description of the system, it is possible to encode the effect using the von Neumann postulate. The postulate states that a measurement operation collapse the observable into one of its eigenstates, and the quantum state, will be projected by the measurement operation onto the eigenspace of this eigenvalue. This postulate is justified by consistency of a sequence of immediately realized measures, as explained in Dirac [32]. However, the correct interpretation of such postulate cannot be literal, since the framework of quantum theory give only probabilistic predictions about measurements [70, p. 473]. So in this work we will rely on another theory of quantum measurements, which is the *theory of decoherence* [159, 158]. This theory includes into the quantum treatment not only the system under study, but also the measurment apparatus. The interaction with the apparatus is usually modeled by an interaction Hamiltonian. In this framework, the measurement operation has a precise mathematical representation: it corresponds to taking *partial traces* on the density matrix [49, 94]. In the framework of fiber optics, the theory of decoherence allow to model some of the so-called Quantum Nondemolition measurements (QND). These measurements allow to obtain a measurement of a physical phenomenon with the minimum perturbation to it. An excellent example is the XPM coupling of a signal with a probe, which furnish a way to measure the photon number of the signal [85, 61].

In conclusion, the main difference between classical detection theory is the inclusion of *density matrices*: during the propagation in the fiber the signal incurs in disturbances, and the quantum state, that most frequently is a coherent state, gets perturbed by states of disturbances factors, as phonons, polaritons and in general reservoirs. In a full quantum treatment, this would be perfectly modeled using many-body theory, however for practical purposes, the noise sources may be encoded in the post-propagation (partial) density matrix. By using projections of the density matrix, it is possible to obtain the probability of error of the transmission over the quantum channel. Physical realization of the optimized and near-optimized devices are a topic of active research. A key note is necessary: the channel we are considering are designed to convey classical information using quantum states. Transmitted sequences are classical information.

From the point of view of this work, the full quantum reception will not be addressed, but the channel impairments will be related to this kind of framework in order to facilitate further investigations.

1.2.6 *Quantum Key Distribution*

The measurement properties of quantum channels are particularly interesting from the point of view of information security. Even in the absence of optimized quantum receivers, since measurement of a quantum state has fundamental physical limits on the perturbation of the state itself, as we have anticipated introducing decoherence, it is possible to exploit this physical bound to prevent sensible signals to be detected in an unnoticed manner. This allows to develop Quantum Key Distribution (QKD) systems [21]. This allow to reach unprecedented levels of security with relatively simple procedures, when compared to current techniques such as RSA system. The effective distribution of keys can follow one of two paradigms: the prepare and measure scheme, represented in Fig. 1.8a, the key information is generated by the transmitter and sent into a quantum channel for reception. After correct reception, and eventual additional passages like security amplification [105], a classical channel is used for encrypted information. Alternatively, the entanglement-based paradigm, represented in Fig. 1.8b show how a third party can generate entangled states to both the transmitter and the receiver, which obtain in such a way the key, and then encode the message sent through the classical channel. The presence of quantum channels in Fig. 1.8b is encoded into the source-measurement links in the top part. We will consider the entanglement based paradigm, as it is mostly used in fiber optics applications.

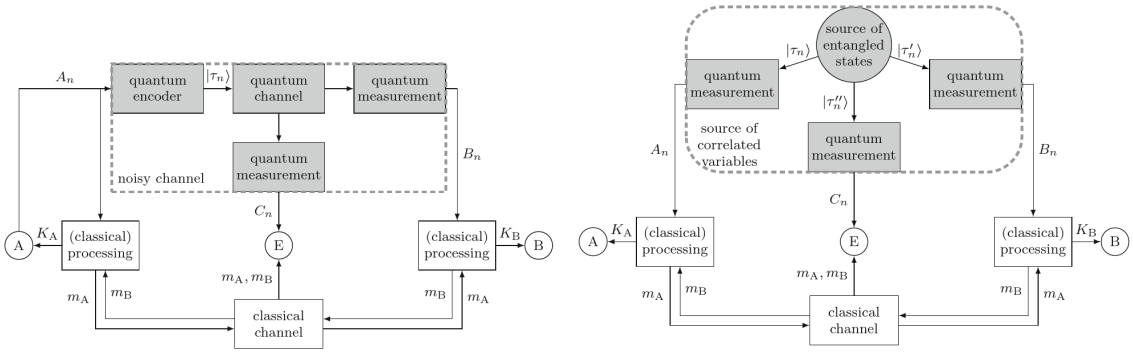

(a) Prepare and measure QKD.

(b) Entanglement-based QKD.

Figure 1.8: Quantum Key Distribution information schemes[21]

Without entering the implementation details and security of those protocols, we formulate the main fiber propagation problem pertaining to these technologies. The problem is to model how other channels, along with fiber non idealities, affect the *entanglement* properties of the quantum signal. So it is a decoherence problem. The usual approach to QKD is to use the so-called Discrete Variable-QKD (DV-QKD), in which the quantum state is encoded in discrete quantum variables of the transmitted signal, typically polarization. This is done using a laser source of entangled photons (for example using spontaneous parametric down conversion in nonlinear crystals) as coherent states attenuated to the single-photon level, and single photon detection using Single Photon Avalanche Photodiodes (SPAD). This is the case of the famous BB84 protocol. Another more recent approach is to encode quantum states in continuous variables of the signal, for example amplitude and phase of a coherent field, thus using the approach of Continuous Variable-QKD (CV-QKD) This is the basis of the GG02 protocol [63, 65].

Coexistence experiments and models

So far, some experiments of coexistence between WDM channels and QKD channels have been carried out. Recent results show how QKD is a mature technology, as deployment ready systems have been developed [8, 9]. In particular, an experiment show how transmission is available using common telecommunication equipment, integrated with a quantum state generation and detection inserted into a DWDM slot, which implements a version of the BB84 DV-QKD protocol. In this scenario, a single 1Gb/s OOK modulated classical channel is sent at at the minimum power for reception of -31dBm at the receiver, over a 13km long standard fiber already deployed. Secret key rate of 1.7kb/s was achieved in a relatively simple setup.

Experiments targeting coexistence of quantum and classical channels can be divided in scenarios with WDM channels along with CV-QKD, or, alternatively, along with DV-QKD. Experiment show how DV-QKD channels suffer most from the presence of other DWDM channels, as they use signal levels at the single photons. A interesting circumvention of the problem of high sensibility of DV-QKD with respect to nonlinear effects is the usage of Hollow Core-Nested Antiresonant Nodeless Fibers (HC-NANF), experimented recently [3, 4]. Interesting results show how 8×200Gb/s 16-QAM modulated, 50GHz spaced WDM channels, at −9dBm/channel launch power can coexist with DV-QKD in a 2km long HC-NANF [3]. The quantum channel was placed 75GHz out of the DWDM spectrum. With the same experimental setup, a Single Mode Fiber (SMF) with the same length was tested for comparison, showing that to reach the same QKD performance (targeted around 2kb/s secret key rate using Coherent One Way protocol) WDM launch power must be reduced by ~ 24dB [4]. Major experiments in SMFs consider CV-QKD, as it is more robust due to higher power level [42, 43]. In one experiment, 10km fiber was used, populated with 18x24.5Gbaud Polarization Multiplexed-16QAM (PM-16QAM) with launch power up to 1.4dBm. Secret key rate was shown to be stable around 24kb/s. The main investigated impairment has been in-band ASE, injected from a noise loading source at the transmitter [43]. The result showed how how in-band ASE spectral power as low as −68dBm/0.1nm significatively affects the quantum channel, and for power higher than −59.5dBm/0.1nm no secure communication is possible. Numerical simulations have been addressed in [156].

Mathematical modeling of the impact of classical channel driven XPM in CV-QKD has been addressed in a simple way, using a power spectral density argument, in [25]. However this approach lacks to account for dispersion, and do not take into account high order correlations of the interference process, as stated in [30], addressing methods using power spectral density. The original approach showed how in Gaussian-Modulated Coherent State (GMCS) CV-QKD protocol the influence of XPM is negligible assuming a single OOK modulated signal at 2dBm launch power.

1.3 OUTLINE OF THE THESIS

This thesis is articulated in two main chapters, which have different methodology and purpose.

Chapter 2 deals with the original result of extending the NLIN model to Raman amplified systems. This is the main novel result of the thesis. By starting from previous mathematical formulation of the Dar and Mecozzi model, we extend

its validity to Raman amplified links. Several results of numerical simulations for realistic scenarios complement the treatment, and show peculiar properties of NLIN connected to Raman amplifiers. Finally, we comment how NLIN performance can be taken into account into Raman amplifier design. The purpose of chapter 2 is to contribute to the known models for nonlinear impairments in classical optical communication systems, and to give almost readily-usable prompts and suggestions for design of amplified links.

Chapter 3 is devoted to explore and survey the available methods for modeling of quantum communication systems in optical fibers, with particular focus on the description of field propagation. The main outcome of this chapter is a model of NLIN based on stochastic equations, mutuated from previously used noise models for Raman scattering and absorption. This model may represent a starting point for further investigations aiming to link methods from different branches of telecommunications. Some final notes are given about the phenomena of quantum decoherence and quantum nondemolition measurements, and related to the propagation description. The purpose of chapter 3 is to carry out a preliminary study on quantum models for field propagation inside fibers, and try to individuate, and prepare for future investigations, the relevant connections between adjacent fields of physics of matter, information theory and classical and quantum telecommunication system design.

2 NLIN MODEL FOR RAMAN AMPLIFIED WDM LINKS

> [...] *der Traum vom "Gras wachsen hören" stellte sich wieder einmal recht greifbar der Menschheit dar.*[†]
>
> W.H. Schottky [137]

The aim of the chapter is to generalize the time domain model by Dar and Mecozzi [30], in the case of a fiber with imperfect amplification, i.e. more specifically, a fiber with silica attenuation and Raman gain. A crucial property of attenuation and Raman gain is the dependence on frequency. As explained in 1.2.2, the Raman effect is strongly dependent on frequency, and, even if the attenuation does not exibit such a strong dependence, its variation is not negligible over a sufficiently broad WDM spectrum. As explained in the section 1.2.4, the phenomenon of NLIN is characterized by the presence of overlap region between pulses from different channels. The model by Dar and Mecozzi utilizes the evaluation of a noise metric for each of the collisions, called $X_{0,m,m}$ [30, eq. 7]. The goal of this chapter is to derive a convenient expression for the coefficient $X_{0,m,m}$ in the generalized scenario, studying the similarities and the differences of the two approaches. The method outlined in [30], and further developed in [28, 29, 31, 115], consists in the computation of NLIN through the definition of the coefficient $X_{0,m,m}$, which is evaluated via a double time and space integral. The separation between the integrals allows a two-steps computation of NLIN: the time step calculates the spatial collision shapes of the interferences, and the space step integrates the contribution of the collision over space. This method allows for efficient evaluation of XPM interaction that would otherwise involve, for every choice of parameters, full computation of collisions, that typically involve several thousands pulses. The possibility of computing the interference properties opens up many technological possibilities, one of them being the online computation and mitigation of NLIN, as outlined by Dar et al. [31]. In fact, by using long

[†][...] *the dream of "hearing the grass grow" appeared achievable to mankind.* Translation by H.A. Haus [70].

temporal autocorrelation of the NLIN process, a filter can be tailored to eliminate part of the noise. However this method is out of the scope of this thesis.

In order to compute the coefficient of interest, we will start by reviewing the main steps of the original derivation by Dar and Mecozzi in 2.1, commenting the utilized approximations. In the following section, 2.2, the generalization is derived, and in section 2.3 the connections between the two models, that may seem not straightforward, are clarified by a simple calculation. The actual computation of $X_{0,m,m}$ in the Dar and Mecozzi model was performed through an approximation called *high-dispersion appproximation*: under reasonable assumptions the double integral is approximated with an elementary function of the parameters. In section 2.4, we comment this approximation by referring it to the Fresnel transform, and assess the possibility of applying it also in the generalized scenario. Since this is not possible in general, we explore some analytical simplifications assuming Gaussian pulse shape. The computation of ASE noise is described in section 2.5. Numerical simulation setup and results are reviewed in section 2.6, where we will answer some questions of interest for the design of systems. Finally, in section 2.7, the evaluation of system performance, using the noise characterization of this chapter, is commented.

2.1 EQUATIONS FOR THE FIELD AND ASSUMPTIONS

In the model developed in [30], a single NLSE is adopted to model the field inside the fiber. Let us examine the structure of the equation. First of all, let us define the Raman amplification profile $r(z)$. Starting from power equations (1.18), considering the wave corresponding to the signal wave, of subscript s, we identify the coefficient for the amplitude gain to be the sum of all the contribution from the pumps and signals different from s:

$$r(z) = \sum_{i \neq s} C'_{R\,s,i} \left[P_i^+ + P_i^- \right]. \tag{2.1}$$

By using the definition of $r(z)$, we can insert the effect of Raman gain into the usual NLSE (Eq. (1.1)), dividing it by 2 in order to have an amplitude coefficient:

$$\frac{\partial}{\partial z} A = -\frac{\alpha - r(z)}{2} A - \beta_1 \frac{\partial}{\partial \tau} A - i \frac{\beta_2}{2} \frac{\partial^2}{\partial \tau^2} A + i\gamma |A|^2 A \tag{2.2}$$

where τ is the physical time. Recall that A is proportional to the electric field inside the fiber, in a way such that the dimension of A is $[|A|^2] = W$.

2.1.1 *Narrowband approximation*

Equation (2.2) holds for a narrowband field, in other words, for the complex amplitude $A(z,t)$, the SVEA holds true. In a WDM system, this approximation is still assumed to be valid, even if the usual channel spectral spacing is greater than 12.5GHz in third window (see Appendix 4 for frequency standards). In the presence of tens of channels, the total field may still be assumed as narrowband, when compared to the hundreds of THz optical carrier frequency.
However, while this assumption can be used for modeling dispersion in a simple way, using β_2, it is not sufficient for assuming constant attenuation-gain terms along all the wavelengths. In fact, a constant attenuation and Raman gain over the signal bandwidth may be an assumption too strong to be made, especially when interested in multiple pump Raman amplification. So the model with a single NLSE equation holds for *perfect amplification* scenarios, but needs to be modified in the generalization, to different situations.

Let us comment now about a common mathematical procedure that simplifies the notation in the NLSE, in presence of attenuation.

2.1.2 *Rescaling of fields*

Let $\psi(z)$ be defined as a solution of the following differential equation

$$\frac{d}{dz}\psi(z) = -\frac{\alpha - r(z)}{2}\psi(z), \tag{2.3}$$

using such function, let $u(z,t)$ be defined as the *normalized field* in the following way. By assuming a moving reference frame such that time is defined as $t = \tau - v_g z$, $u(z,t)$ is defined by

$$A(z,t) = \psi(z)u(z,t). \tag{2.4}$$

The above definition, when substituted in Eq. (2.2), in the scaled time t, gives the following equation:

$$\frac{\partial}{\partial z}u = -i\frac{\beta_2}{2}\frac{\partial^2}{\partial t^2}u + i\gamma f(z)|u|^2 u \tag{2.5}$$

where $f(z) = \psi(z)^2$. The advantage in using the Eq. (2.5) is that the amplitude dynamics can be described with a space-dependent nonlinear term: $\gamma f(z)$.
The model by Dar and Mecozzi uses the *perfect amplification* assumption, i.e. $\gamma f(z) = \gamma$, since $f(z) \equiv 1$.

2.1.3 *Overview of the perturbation analysis*

Let us now review the main steps of the derivation of the NLIN model in [30], under the assumption of perfect amplification. In order to clarify the following treatment, we summarize the steps as follows.

1. Write the field $u(0,t)$ as a superposition of a train of modulated symbols from the channel of interest $\{a_k\}$ and the interfering channel $\{b_k\}$.
2. Obtain a 0^{th} order solution of the normalized NLSE (Eq. (2.5)), $u^{(0)}(z,t)$.
3. Compute the first order perturbation of this solution, $u^{(1)}(z,t)$. This will include collision integrals between pulses, from which $X_{0,m,m}$ is defined.
4. Assuming perfectly matched filter at reception, compute the first order error induced on the first received symbol of the channel of interest: $\Delta\tilde{a}_0$. A single symbol is sufficient as it entails all the statistics of interest.
5. Utilize the expression of $u^{(1)}(z,t)$ to separate the interference integrals from the modulation format dependence of $\Delta\tilde{a}_0$, thus expressing it via $X_{0,m,m}$.
6. Obtain a final expression for the phase noise of the received symbol.

all these steps were done assuming perfect amplification in Eq. (2.5).

2.2 GENERALIZATION OF NLIN MODEL

The generalization is straightforward, first of all let us recall fundamental assumption used in the model. By including attenuation and gain it is required to drop the narrowband approximation: in doing so, a useful well-known model is the one of the coupled NLSEs.
Consider two WDM channels named A and B. The following hypotesis are made:

- channels A and B have a spectral separation of Ω (a multiple of the WDM spectral spacing), let A be the channel of interest, and B the interfering one,
- both channels have the same nonlinear coefficient, since it depends from modal field distribution in the core which is assumed to be the same for all channels: $\gamma_A = \gamma_B = \gamma$,
- the group velocity profile is approximately linear in the frequency (β_2 is constant) in the whole band of interest: in this way $\beta_{1B} = \beta_{1A} + \beta_2\Omega$

- attenuation and Raman gain depend on the channel choice, but are approximately constant within the band of a given channel, so it is justified to define α_A, α_B, $r_A(z)$, $r_B(z)$ for channels A and B.

2.2.1 *Coupled NLS equations*

Following Agrawal [2, p.263], a system of *coupled NLSE*, including Raman gain, is given by

$$\left(\frac{\partial}{\partial z}A_A + \beta_{1A}\frac{\partial}{\partial \tau}A_A\right) = -\frac{\alpha_A - r_A(z)}{2}A_A - i\frac{\beta_2}{2}\frac{\partial^2}{\partial \tau^2}A_A + \\ + i\gamma(|A_A|^2 + 2|A_B|^2)A_A \tag{2.6}$$

$$\left(\frac{\partial}{\partial z}A_B + \beta_{1B}\frac{\partial}{\partial \tau}A_B\right) = -\frac{\alpha_B - r_B(z)}{2}A_B - i\frac{\beta_2}{2}\frac{\partial^2}{\partial \tau^2}A_B + \\ + i\gamma(|A_B|^2 + 2|A_A|^2)A_B, \tag{2.7}$$

As discussed, subscripts denotes complex amplitude, and propagation variables, of the channels A and B. Let us proceed in normalizing the fields A_A, A_B with the respective normalization functions ψ_A, ψ_B, as described in the rescaling method Eq. (2.3), and using the scaled time $t = \tau - v_{gA}z$, with respect to channel A group velocity $v_{gA} = \beta_{1A}^{-1}$. These passages lead to:

$$\frac{\partial}{\partial z}u_A = -i\frac{\beta_2}{2}\frac{\partial^2}{\partial t^2}u_A + i\gamma\left(f_A(z)|u_A|^2 + 2f_B(z)|u_B|^2\right)u_A \tag{2.8}$$

$$\frac{\partial}{\partial z}u_B = -\Delta\beta_1\frac{\partial}{\partial t}u_B - i\frac{\beta_2}{2}\frac{\partial^2}{\partial t^2}u_B + i\gamma\left(f_B(z)|u_B|^2 + 2f_A(z)|u_A|^2\right)u_B, \tag{2.9}$$

where $\Delta\beta_1 = \beta_{1B} - \beta_{1A} = \beta_2\Omega$.
Following [30], a first order perturbation analysis is proposed for these equations. Let us start from the linear propagation, i.e. the 0^{th} order approximation.

2.2.2 *Generalization of the 0^{th} order term*

Since the attenuation and gain only affect the nonlinear term, the normalized field of the 0^{th} order must be identical to the one derived in [30, eq. 1]. The only exception is due to the notation used: the total field in this case can not be expressed by a simple sum of terms $u_A^{(0)} + u_B^{(0)}$. There are in fact two notational caveats:

- $u_A^{(0)}$ and $u_B^{(0)}$ functions represent normalized fields with different normalization functions ψ_A, ψ_B,

- $u_A^{(0)}$ and $u_B^{(0)}$ are *complex amplitudes* ([142, pp. 523-525]) referred to *different* carrier frequency signals, and their evolution is described by different propagators.

These aspects are addressed in section 2.3.

Consider the initial fields as sums of shifted impulses which encode a given message. Let T be the symbol period:

$$\begin{aligned} u_A(0,t) &= \sum_k a_k g(0, t - kT) \\ u_B(0,t) &= \sum_k b_k g(0, t - kT) \end{aligned} \tag{2.10}$$

The pulses $g(0,t)$ are assumed to be normalized, so

$$\int_{-\infty}^{+\infty} dt |g(0,t)|^2 = 1 \tag{2.11}$$

Let $g^{(0)}(z,t)$ be the linearly propagated field in channel A. The solution for the 0^{th} order field is:

$$u_A^{(0)}(z,t) = \sum_k a_k g^{(0)}(z, t - kT) \tag{2.12}$$

$$u_B^{(0)}(z,t) = \sum_k b_k g^{(0)}(z, t - kT - \beta_2 \Omega z) \tag{2.13}$$

because of linearity and definition of $g^{(0)}$.

As in [30][‡], we define the operator of linear propagation for channel A:

$$\mathbf{U}_A(z) = \exp\left[-i\frac{\beta_2}{2} z \frac{\partial^2}{\partial t^2}\right]. \tag{2.14}$$

in fact, the propagator for channel B is not required for further first order perturbation analysis.

2.2.3 *First order perturbation*

The splitting in two of the equation allow us to analyze separately the effects of SPM and XPM in a natural way, as they compare inside the nonlinear term

[‡]We report equations by Dar and Mecozzi with slightly changed signs, arguing that this is a consequence of conventions in the writing of the NLSE. Keeping the NLSE with the sign chosen in this thesis, the signs are consistent.

in additive fashion. Let us apply the perturbation method to equation (2.8) for channel A:

$$\frac{\partial}{\partial z}u_A^{(1)} = -i\frac{\beta_2}{2}\frac{\partial^2}{\partial t^2}u_A^{(1)} + i\gamma\left(f_A(z)|u_A^{(0)}|^2 + 2f_B(z)|u_B^{(0)}|^2\right)u_A^{(0)} \tag{2.15}$$

Notice that the normalized fields $u_A^{(0)}$ and $u_B^{(0)}$ can not be summed together because they are complex amplitudes with respect to different carriers. However, their squared absolute value, multiplied by f_A or f_B, respectively, corresponds to the power of the wave, so the summation of these terms makes physical sense. Writing the integral solution to the inhomogeneous linear equation above gives

$$u_A^{(1)}(L,t) = i\gamma\int_0^L dz\mathbf{U}_A(L-z)\left(f_A(z)|u_A^{(0)}|^2 + 2f_B(z)|u_B^{(0)}|^2\right)u_A^{(0)}. \tag{2.16}$$

where L is the fiber length. Using this result it is possible to obtain the estimation of the error of a receiver.

2.2.4 *Generalization of estimation error*

Consider now the reception of the first symbol of the sequence of the channel of interest. Let the received symbol be $\tilde{a}_0$. The computation of the effect of NLIN on this symbol will provide all the statistical information about noise. The choice of the first symbol is of little effect and will be justified at the end of the section. Using a matched filter receiver, with matching to the linearly propagated initial pulse waveform $g^{(0)}(L,T)$, we obtain the following equation for the estimation error Δa_0

$$\Delta\tilde{a_0} = \int_{-\infty}^{+\infty} dt u_A^{(1)}(L,t)g^{(0)*}(L,t). \tag{2.17}$$

Recall that $\mathbf{U}_A$ is unitary, so it holds

$$\mathbf{U}_A(L-z)g^{(0)*}(L,t) = g^{(0)*}(z,t) \tag{2.18}$$

Using this identity, the expression for the error can be written as[3]:

$$\Delta\tilde{a_0} = i\gamma\int_{z_0}^L dz\int_{-\infty}^{\infty} dt g^{(0)*}(z,t)\left(f_A(z)|u_A^{(0)}|^2 + 2f_B(z)|u_B^{(0)}|^2\right)u_A^{(0)} \tag{2.19}$$

[3]Notice that, being that the two fibers linear propagation terms are different, the substitution described in Eq. (2.18) is only valid because filter matching is done considering the propagated symbol waveform over channel A.

By substituting the modulation of choice for the symbols inside the fields $u_A^{(0)}, u_B^{(0)}$, we get an expression ready to be computed with respect to a given modulation format. Finally, substituting the modulation and using the same notation as [30, eq. 5, 6, 7], the resulting expression is

$$\Delta\tilde{a}_0 = i\gamma \sum_{h,k,m} (a_h a_k^* a_m S_{h,k,m} + 2a_h b_k^* b_m X_{h,k,m}) \tag{2.20}$$

where

$$\begin{aligned} S_{h,k,m} = \int_0^L dz\, f_A(z) \int_{-\infty}^{\infty} dt\, g^{(0)*}(z,t) g^{(0)}(z,t-hT) \times \\ \times\, g^{(0)*}(z,t-kT) g^{(0)}(z,t-mT) \end{aligned} \tag{2.21}$$

for the SPM, and

$$\begin{aligned} X_{h,k,m} = \int_0^L dz\, f_B(z) \int_{-\infty}^{\infty} dt\, g^{(0)*}(z,t) g^{(0)}(z,t-hT) \times \\ \times\, g^{(0)*}(z,t-kT-\beta_2\Omega z) g^{(0)}(z,t-mT-\beta_2\Omega z) \end{aligned} \tag{2.22}$$

for the XPM.
These are the terms of major interest in the model, since they only include the normalized pulse shapes. In their generalization, they include attenuation and gain. This argument proves that the only modification to the original model is to include the terms $f_A(z)$, $f_B(z)$, which represent the power exchanged with the medium, into nonlinear interaction terms $S_{h,k,m}$, $X_{h,k,m}$.

It is possible, using Eq. (2.20), and Eq. (2.22), to write the expression for the NLIN. Some approximating assumptions are useful. Since the disturbance is greatly enhanced when interfering pulse amplitude are considered from the same pulse, with $k = m$, we will concentrate on terms like $X_{h,m,m}$. In addition, we are not interested in SPM, as it can be filtered using digital signal processing techniques (for an example, see Tan et al. [143]). Moreover, for the same argument, we may neglect contributions from $h \neq 0$, since $h = 0$ greatly enhances the product. So terms with $h = 0$, $k = m$ dominate the sum, and the others will be neglected. In this case, the coefficient in Eq. (2.22) can be expressed as

$$X_{0,m,m} = \int_0^L dz\, f_B(z) \int_{-\infty}^{+\infty} dt\, |g^{(0)}(z,t)|^2 |g^{(0)}(z,t-mT-\beta_2\Omega)|^2 \tag{2.23}$$

Let us justify the choice of the first symbol of the sequence. If the product $\beta_2\Omega$ is negative, we expect to have many collisions in a sufficiently long fiber, as many

pulses interact. In practical terms, if the dispersion is normal, which is often the case, a red-shifted channel ($\Omega < 0$) propagates with higher group velocity, and reaches the pulses of the channel of interest. By choosing the first symbol to be transmitted, we maximize the number of collisions inside the fiber span. This is a matter of convenience, and will turn out to be useful in numerical simulations, however it is a minor assumption for the general model: in fact, in the long transmission run, all the symbols will experience the same number of collisions, equal to the one experienced by the first pulse. Moreover, not all the integer m are of interest, as, for some limiting $\bar{m}$, for every $m > \bar{m}$, most of the collision would take part outside the fiber span, and may be totally neglected. The choice of $\bar{m}$ can be simply done by inspecting the maximum of the collision, located at $z_m = -\frac{mT}{\beta_2\Omega}$, and imposing $z_m < L$. In this case $\bar{m} \approx -\frac{\beta_2\Omega L}{T}$. A more refined analysis, which includes *partial collisions* will be addressed later.

Finally, we can write the total noise as

$$\Delta\tilde{a_0} = i2\gamma a_0 \sum_m |b_m|^2 X_{0,m,m} = i a_0 \Delta\phi, \tag{2.24}$$

which show a phase noise term to the first order:

$$\tilde{a_0} = a_0 + \Delta\tilde{a_0} = a_0(1 + i\Delta\phi) \approx a_0 \exp[i\Delta\phi]. \tag{2.25}$$

We are interested in writing the variance of phase noise, so we average over the distribution of interfering symbols, arbitrarily selecting b_0 because of the stationarity of the process

$$\left\langle (\Delta\phi)^2 \right\rangle = 4\gamma^2 \underbrace{\left(\left\langle |b_0|^4 \right\rangle - \left\langle |b_0|^2 \right\rangle^2 \right)}_{\text{modulation format}} \underbrace{\sum_m X_{0,m,m}^2}_{\text{pulse overlap}}, \tag{2.26}$$

this last formula shows how the computation of phase noise can be subdivided in the – numerically heavy – computation of $X_{0,m,m}$ for $m = 0, 1, ..., \bar{m}$, and the lightweight computation of constellation energy variance. In fact, the constellation energy variance can be decomposed further into a term proportional to the average transmitted power, and a constellation form factor. If P_B is the average launch power of channel B, it holds

$$\left\langle |b_0|^2 \right\rangle = P_B T, \tag{2.27}$$

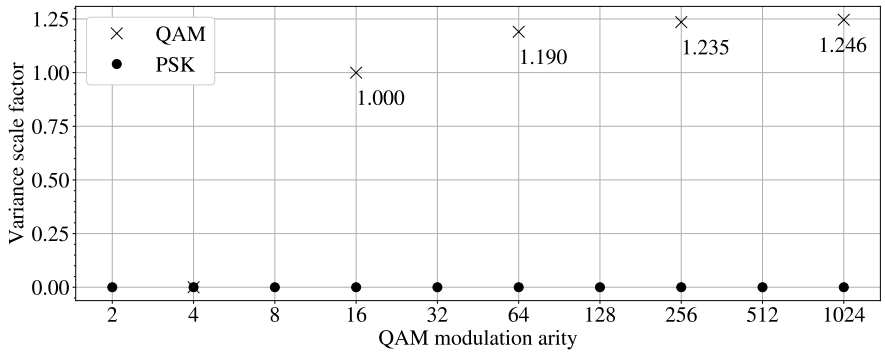

Figure 2.1: Constellation factor Eq. (2.28), normalized to 16-QAM case.

so the energy variance can be written as

$$\left(\left\langle |b_0|^4 \right\rangle - \left\langle |b_0|^2 \right\rangle^2\right) = (P_B T)^2 \left(\frac{\left\langle |b_0|^4 \right\rangle}{\left\langle |b_0|^2 \right\rangle^2} - 1\right), \tag{2.28}$$

the ratio term $\frac{\left\langle |b_0|^4 \right\rangle}{\left\langle |b_0|^2 \right\rangle^2}$ is actually a well known shape factor for the constellations. Examples of values of the factor $\left(\frac{\left\langle |b_0|^4 \right\rangle}{\left\langle |b_0|^2 \right\rangle^2} - 1\right)$ are plotted in Fig. 2.1. A very important point is that all PSK constellations have null variance, as all the symbols have the same energy. This imply that PSK transmissions, which include 4-QAM, are immune to NLIN. Intuitively, this can be explained as the fact that the phase shift, in the case of interference with a PSK channel, is deterministic, so the noise induced by random phase shifts is zero.

2.3 CONNECTION BETWEEN MODELS

In order to check that generalized model properly describes all the scenarios that can be described with the original model, let us relate the total linear propagated field for the single NLSE model by Dar and Mecozzi, to the separated fields u_A, u_B, computed without gain and attenuation. If the generalized model is correct, the solutions should correspond.

The fields in the original model are represented as complex amplitudes with respect to the channel A center frequency. So the function corresponding to channel B field in the generalized model, at the initial position, needs to multiply the complex amplitude of channel B by $\exp[-i\Omega t]$ in order to obtain the corresponding complex amplitude with respect to channel A carrier frequency. Moreover, the propagated field for the interacting channel are no more corresponding. In

fact, while the linear propagator operator for the interfering field in Dar and Mecozzi [30], called $\mathbf{U}'$, is

$$\mathbf{U}'(z) = \exp\left[-i\frac{\beta_2}{2}z\frac{\partial^2}{\partial t^2}\right] \tag{2.29}$$

with no walkoff term, the propagator in the coupled equations model is

$$\mathbf{U}_B(z) = \exp\left[-i\frac{\beta_2}{2}z\frac{\partial^2}{\partial t^2} - \Delta\beta_1 z\frac{\partial}{\partial t}\right] \tag{2.30}$$

so, the propagated field notation $g^{(0)}(z, t-\beta_2\Omega z)$ for channel B in the coupled equations model, and the corresponding notation with corrected phasor term $\exp[-i\Omega t]g^{(0)}(z, t-\beta_2\Omega z)$ in the original model, are not coincident. This is the reason behind the apparent discrepancy of Eq. (2.13) with respect to [30, eq. 1], which is

$$\begin{aligned} u^{(0)}(z,t) = &\sum_k a_k g^{(0)}(z, t-kT) + \\ &+ \exp\left[-i\Omega t - \underbrace{i\frac{\beta_2\Omega^2}{2}z}_{\text{discrepancy}}\right]\sum_k b_k g^{(0)}(z, t-kT-\beta_2\Omega z) \end{aligned} \tag{2.31}$$

where $u^{(0)}(z,t)$ is the linearly propagated field corresponding to the channel superposition. In order to clarify the meaning of the additional term, let us introduce the following notation. Functions appearing in the original Dar and Mecozzi model will be referred to using the subscript C, to mean comprehensive, whereas functions in the coupled equations model will have the subscript notation introduced before.

In the new notation, the task is to show that

$$\exp\left[-i\Omega t - i\frac{\beta_2\Omega^2}{2}z\right] g_C^{(0)}(z, t-\beta_2\Omega z) = g^{(0)}(z, t-\beta_2\Omega z) \tag{2.32}$$

where,

$$g^{(0)}(z, t-\beta_2\Omega z) = \mathbf{U}_B(z)g^{(0)}(0,t). \tag{2.33}$$

At the fiber input, it holds

$$\exp\left[-i\Omega t\right] g_C^{(0)}(0,t) = g^{(0)}(0,t) \tag{2.34}$$

So now, substituting in the left term of Eq. (2.33) the left hand side of Eq. (2.34), we can compute the propagation

$$g^{(0)}(z, t - \beta_2 \Omega z) = \mathbf{U}_B(z) \exp[-i\Omega t]\, g_C^{(0)}(0, t). \tag{2.35}$$

Let us do the calculation in frequency domain: indicating the transformed right hand side of Eq. (2.35) as

$$\hat{\mathbf{U}}_B(z) \hat{g}_C^{(0)}(0, \omega - \Omega), \tag{2.36}$$

and taking the inverse transform, using square completion,

$$\frac{1}{2\pi} \int_{-\infty}^{+\infty} d\omega \exp\left[i \frac{\beta_2}{2} z \omega^2 - i \beta_2 \Omega z \omega \right] \hat{g}_C(0, \omega - \Omega) \exp[i\omega t] = \tag{2.37}$$

$$= \frac{1}{2\pi} \int_{-\infty}^{+\infty} d\omega \exp\left[i \frac{\beta_2}{2} z (\omega - \Omega)^2 \right] \hat{g}_C(0, \omega - \Omega) \exp[i(\omega - \Omega) t] \times$$

$$\times \underbrace{\exp[i\Omega t]}_{\text{frequency shifting}} \underbrace{\exp\left[-i \frac{\beta_2 \Omega^2}{2} z \right]}_{\text{constant}}. \tag{2.38}$$

The first two factor of the integrand show the application of $\hat{\mathbf{U}}(z)$, the propagator from Dar and Mecozzi. By applying the inverse transform, using the definition of the propagated field $g_C^{(0)}(z, t)$, the expression in Eq. (2.32) is found. In this way we have shown that, despite the diversity in the notation, the apparent discrepancy in the results is encoded exactly in the difference between the definition of propagated pulses.

2.4 COMPUTATION OF $X_{0,m,m}$

In order to evaluate the noise due to nonlinear interference in different realistic scenarios, we may analyze the expression (2.23), and identify the parameter of interest. As discussed before, the channel power and constellation can be inserted separately in the expression of the phase noise, so the remaining part is related to linear propagation of normalized pulses and interaction with gain-attenuation term $f_B(z)$.

2.4.1 *Gain-attenuation profile choice*

The choice of the gain-attenuation profile, especially for what regards Raman pumping, is crucial in this thesis. As anticipated in the introduction, studies have

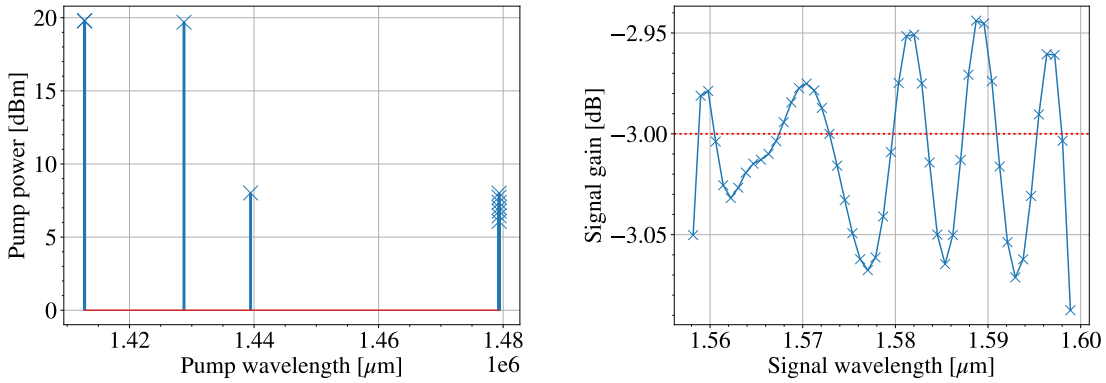

(a) Pump wavelength placement and power at the input.

(b) Overall link spectral gain. −3dB target gain in red.

Figure 2.2: Optimized Raman pumping scheme. −20dBm signal launch power.

been carried out on methods to obtain spectrally flat link amplification. This is obtained involving higher order pumping, with eventually numerous co- and counterpropagating pumps. In order to obtain interesting and realistic results, we use pump placement optimizer directly derived from the one developed by Marcon et al. [111], which uses automatic differentiation and model-aware learning. The input variables of the optimizer, other than the fiber span characteristics, are the WDM channels spectral arrangement and their average power, along with the number of pumps and an initial condition of pump wavelengths and powers – to be optimized – and a (flat) target gain, usually set to −3dB.

Illustrative results have been obtained for a common scenario of 80km amplified link, with 50 channels in the C+L band, with 4 copropagating and 8 counterpropagating pumps. The solver obtains the following performances. In Fig. 2.2a, an example of the optimized spectral placement of pumps is shown along with their power. The highest power pumps are the one at shorter wavelengths. This suggests that those pumps are indeed pumping the longer wavelengths pumps, that in turn pump the signal. Notice that the peak of the Raman gain, occuring at $\approx$ 12THz, corresponds, in the band of 1550nm, to $\approx$ 90nm. In Fig. 2.2b, the overall gain of the link is shown for each channel of the WDM comb. The target gain of −3dB is approximated with reasonable flatness. The values which are of most interest for this study are the *spatial evolution* functions of signal and pump waves. In Fig. 2.3a, three of the 50 channels are plotted in their evolution. Notice how the power value at the end of the fiber approaches the desired target gain. Fig. 2.3b displays the pump power evolution along the fiber, pumps are color-coded according to their wavelength. The role of copropagating and counterpropagating

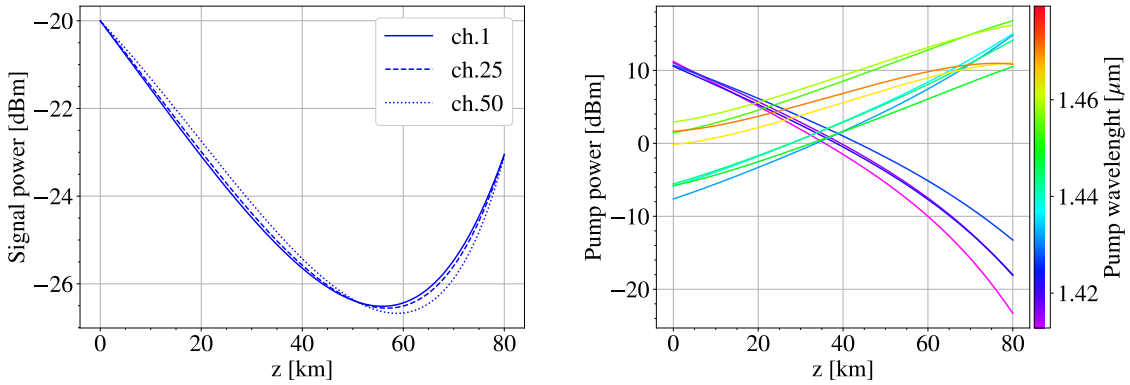

(a) Signal power for 3 equally spaced channels of the 50 channels.

(b) Power for the 4 copropagating and 8 counterpropagating pumps.

Figure 2.3: Evolution of signal and pump power along the bidirectionally pumped link link, −20dBm signal input level.

pumps is clear from the direction of decay. Depletion of the short wavelength copropagating pumps starts to happen around the end of the fiber.

In the previous section we described the derivation of f_B from Raman gain term $r(z)$ and the corresponding power equation. In fact, the value of f_B, for every interfering channel of choice, can be readily computed from the solution of the ordinary differential equation system integrated in the optimizer model. If $P_B(z)$ is the power evolution of the choosen B channel, then f_B represents a normalized amplification measure corresponding to

$$f_B(z) = \frac{P_B(z)}{P_B(0)}. \tag{2.39}$$

Since the problem is essentially nonlinear, Raman amplified pump placement optimization gives different results for different input channel launch power. So this component of the $X_{0,m,m}$ term must be computed for all the desired pumping schemes, and for all the desired input power.

As for the time integrals, let us review some analytical approximations.

2.4.2 *Analytical approximations: high dispersion*

This approximation, presented in [30, 115], is valid for pseudolinear systems, and allow to reduce the integrals to a simple evaluation of elementary function. The approximation relies on the model obtained in Eq. (1.12) for fiber propagation

using a QPF. By using this model, the linear propagation of the normalized pulse $g^{(0)}(z,t)$ is expressed by the convolution [4]:

$$g^{(0)}(z,t) = \sqrt{-\frac{i}{2\pi\beta_2 z}} \int_{-\infty}^{+\infty} d\tau\, g(0,\tau) \exp\left[-i\frac{1}{2\beta_2 z}(t-\tau)^2\right]. \tag{2.40}$$

By expanding the square at the exponential, and reorganizing the terms,

$$g^{(0)}(z,t) = \sqrt{-\frac{i}{2\pi\beta_2 z}} \exp\left[-\frac{it^2}{2\beta_2 z}\right] \int_{-\infty}^{+\infty} d\tau\, g(0,\tau) \exp\left[i\frac{t}{\beta_2 z}\tau\right] \exp\left[-i\frac{\tau^2}{\beta_2 z}\right]. \tag{2.41}$$

When the pulse propagates through many dispersion lengths $z >> L_D = \frac{T^2}{|\beta_2|}$ [2], the rightmost, chirping, term inside the integral becomes approximately 1 over the relevant span in which the signal is significatively larger than zero, that is of the order of T. This is called the highly-dispersed pulse approximation, and, recognizing the form of a Fourier integral at the resulting integrand, the propagated pulse is

$$g^{(0)}(z,t) \approx \sqrt{-\frac{i}{2\pi\beta_2 z}} \exp\left[-\frac{it^2}{2\beta_2 z}\right] \hat{g}\left(0, -\frac{t}{\beta_2 z}\right) \tag{2.42}$$

where $\hat{g}$ is the Fourier transform of the input signal. Notice that $-\frac{t}{\beta_2 z}$ has the dimension of a frequency. By using the last equation, corresponding to [30, eq. 10], it is possible to compute the coefficient $X_{0,m,m}$ through energy integral in Fourier space by defining $\nu = t/\beta_2 z$ [30, 31]. If the fiber is very long, we expect that all the relevant collisions happen in a regime of large dispersion. Let the regime of high dispersion be considered valid for $z > z_0$. In such case, for a sufficiently small z_0 compared to L, we can approximate $X_{0,m,m}$ with

$$X_{0,m,m} = \int_{z_0}^{L} dz\, f_B(z) \int_{-\infty}^{+\infty} \frac{d\nu}{4\pi^2\beta_2 z} |\hat{g}(0,\nu)|^2 \left|\hat{g}\left(0, \nu - \Omega - \frac{mT}{\beta_2 z}\right)\right|^2, \tag{2.43}$$

by doing a change of variable of the time integral. Moreover, the strongest overlap occurs at $z_m = -\frac{mT}{\beta_2\Omega}$, so in the spatial integral it may be possible to write $f_B(z) \approx f_B(z_m)$. This means that the integrand is non negligible only when $z_m/z \approx 1$, so, if z_m is inside the span $[z_0, L]$ we can extend the spatial integration

[4] Notice that the time delay induced by group velocity is neglected by the choice of the scaled time t instead of the physical time.

to infinity with negligible error. By inverting the two integration signs and using the approximations, it is found:

$$X_{0,m,m} = \int_{-\infty}^{+\infty} \frac{d\nu}{2\pi} |\hat{g}(0,\nu)|^2 \int_{-\infty}^{+\infty} dz \frac{z_m f_B(z_m)}{2\pi\beta_2 z^2} \left| \hat{g}\left(0, \nu - \Omega - \frac{mT}{\beta_2 z}\right) \right|^2. \quad (2.44)$$

Notice that the integration along space allow us to use an important property of the pulses at the input: they are of unit energy. Using Parseval identity it is possible to eliminate the impulse waveform in the following way. Let us adopt this change of variables:

$$y := -\frac{mT}{\beta_2 z} \quad (2.45)$$

Recalling $z_m = -\frac{mT}{\beta_2 \Omega}$, we readily obtain the change of variables

$$X_{0,m,m} = \int_{-\infty}^{+\infty} \frac{d\nu}{2\pi} |\hat{g}(0,\nu)|^2 \int_{-\infty}^{+\infty} \frac{f_B(z_m)}{2\pi\beta_2\Omega} \Big(-\underbrace{\frac{mT}{\beta_2 z^2} dz}_{dy} \Big) \left| \hat{g}\left(0, \nu - \Omega - \frac{mT}{\beta_2 z}\right) \right|^2 \quad (2.46)$$

$$= \frac{f_B(z_m)}{\beta_2\Omega} \int_{-\infty}^{+\infty} \frac{d\nu}{2\pi} |\hat{g}(0,\nu)|^2 \int_{-\infty}^{+\infty} -\frac{dy}{2\pi} |\hat{g}(0, \nu - \Omega + y)|^2, \quad (2.47)$$

the integrals simplify to

$$= \frac{f_B(z_m)}{\beta_2\Omega} \int_{-\infty}^{+\infty} \frac{d\nu}{2\pi} |\hat{g}(0,\nu)|^2 \int_{-\infty}^{+\infty} \frac{dy}{2\pi} |\hat{g}(0, \nu - \Omega + y)|^2 \quad (2.48)$$

finally, both integrals, by Parseval theorem, are 1, so

$$X_{0,m,m} = \frac{f_B(z_m)}{\beta_2\Omega}, \quad (2.49)$$

in the assumption that z_m falls inside the fiber and in the region of high dispersion, and 0 otherwise. This approximation is astonishingly powerful, since it works for every kind of pulse, is readily available with attenuation-gain term f_B, and it avoids the heavy computation of the integrals, that with current desktop machine capability would take a computation time in the order of several hours to few days per every interfering channel.

2.4.3 *High dispersion approximation is unfit for Raman amplification scenario*

Unfortunately, the assumption of high dispersion do not hold true in general for the commonly used Raman Amplified Links (RALs) under study. Usual RALs have lengths in the order of $\sim 10^2$km, and for a SMF with $\beta_2 = 20\text{ps}^2\text{km}^{-1}$, and a baud rate of $B = 10$GHz, which corresponds to symbol time $T = 100$ps, the dispersion length is $L_D = 500$km. It is reasonable to choose the term z_0 at least equal to one dispersion length, so the approximation (2.43) is not utilizable. In order to find another analytical approximation, and a significant simplification of the computation, let us assume that the pulses are Gaussian.

2.4.4 *Gaussian pulses*

The effect of linear propagation for Gaussian pulses has a closed form expression:

$$g^{(0)}(z,t) = \frac{U_0 \exp\left[\frac{i}{2}\arctan(D(z))\right]}{(1+D^2(z))^{1/4}} \exp\left[-\frac{t^2}{2T_0^2}\frac{1+iD(z)}{1+D^2(z)}\right] \tag{2.50}$$

where $D(z) = z\beta_2/T_0^2$, U_0 is the initial pulse amplitude at maximum.

Assuming pulse energy normalization to 1, amplitude and width parameters need to satisfy the following equation

$$U_0^2 T_0 \sqrt{\pi} = 1. \tag{2.51}$$

Substituting the shape (2.50) in (2.23), after some passages, the following expression is obtained

$$X_{0,m,m} = \int_0^L dz f_B(z) \int_{-\infty}^{+\infty} \frac{d\eta}{\sqrt{2}} \frac{U_0^4}{1+D^2(z)} \exp\left[-\frac{\eta^2}{T_0^2(1+D^2(z))}\right] \exp\left[-\frac{s^2}{2T_0^2(1+D^2(z))}\right] \tag{2.52}$$

where $\eta := \sqrt{2}t - \frac{mT+\beta_2\Omega z}{\sqrt{2}}$ is a scaled temporal variable, and $s := mT + \beta_2\Omega z$. It is possible to carry out the time integral, as it turns out to be a Gaussian integral

$$X_{0,m,m} = \sqrt{\frac{\pi}{2}} U_0^4 T_0 \int_0^L dz \frac{f_B(z)}{(1+D^2(z))^{\frac{1}{2}}} \exp\left[-\frac{s^2}{2T_0^2(1+D^2(z))}\right] \tag{2.53}$$

this represents a major simplification, obtained simply by assuming Gaussian pulse shapes: the inner temporal integral vanishes, under perfectly reasonable assumptions for RALs.

2.4.5 *Local interaction approximation*

The last step in the simplification procedure above is the assumption of local interaction for $z = z_m = -mT/\beta_2\Omega$. This assumption is a little bit stronger than the one before. This means that the functions $D(z)$, $f_B(z)$ can be substituted with constants $D(z_m)$, $f_B(z_m)$. By comparing the integral (2.53) result and this approximation, using common values for RALs, we found that the approximation is valid within a few percent of the numerically integrated value, and it increases in precision as dispersion gets higher. The offset value can be referred to the effect of partial collision at the borders of the fiber. This allow also to extend integration to infinity, for every m such that $z_m \in [0, L]$. Within these considerations, it is possible to simplify the integral

$$X_{0,m,m} = \sqrt{\frac{\pi}{2}} \frac{U_0^4 T_0 f_B(z_m)}{(1 + D^2(z_m))^{\frac{1}{2}}} \int_{-\infty}^{+\infty} dz \exp\left[-\frac{s^2}{2T_0^2(1 + D^2(z_m))} \right]. \tag{2.54}$$

Using s instead of z as the integration variable, this turn out to be a Gaussian integral, and it is possible to solve it as

$$X_{0,m,m} = \sqrt{\frac{\pi}{2}} \frac{U_0^4 T_0 f_B(z_m)}{(1 + D^2(z_m))^{\frac{1}{2}}} \int_{-\infty}^{+\infty} \frac{ds}{\beta_2\Omega} \exp\left[-\frac{s^2}{2T_0^2(1 + D^2(z_m))} \right] \tag{2.55}$$

$$= \frac{f_B(z_m)}{\beta_2\Omega} U_0^4 T_0^2 \pi. \tag{2.56}$$

Recall the normalization condition for the pulse energy in (2.51): the substitution cancels both parameters U_0 and T_0 from the final expression, so

$$X_{0,m,m} = \frac{f_B(z_m)}{\beta_2\Omega} \underbrace{U_0^4 T_0^2 \pi}_{=1} = \frac{f_B(z_m)}{\beta_2\Omega}. \tag{2.57}$$

The expression is found to coincide with the one derived in high dispersion approximation. This is not surprising, as Gaussian pulses have Gaussian Fourier transform, (Eq. (2.42)).

For application in which fast computation of the coefficients is needed, the above approximation may be useful. Moreover, if the local approximation for the dispersion is not sufficient, we developed a simple second order correction, given in the appendix 4, and a refined method for including border effects in

the approximated scenario 4. However, due to the imprecision to tackle border effects, the approximation is not used in the following analysis.

In order to conclude the analytical part of the generalization of the NLIN model, let us give a brief summary for clarity. A coupled NLSE model was adopted [2], by redefining the signal and the disturbing fields in a adequate way. This formulation, when applied to the analysis of noise on a symbol, predicts SPM and XPM effects which are formally similar to the one in the original model [30], and in case of perfect amplification it is shown to give compatible description with respect to the original model. Even in the generalized case, the coefficient of interest $X_{0,m,m}$ consists in a nested time integral inside a space integral, and it is computationally expensive. In order to simplify the computation of the coefficient, the high dispersion approximation, already presented in [30] was studied, but it has been shown to be unfit for the case of RALs, that are usually much shorter than the dispersion length. So, another suitable simplification was proposed, for Gaussian pulses, using which the time integral can be expressed analytically. Finally, we have shown how, joining the Gaussian pulse assumption with local interaction approximation, the resulting coefficient coincides with the one obtained through the high dispersion approximation. Comparing the approximations with numerical integration results, it has be seen that, for Gaussian pulses, the approximation is within a few percent of the $X_{0,m,m}$ value, however it fails to account for partial collisions at the fiber start and end. Since the most interesting results in literature are derived using Nyquist pulse (sinc shaped), the approximation is dropped and numerical integration is carried out directly for both integrals.

2.5 COMPUTATION OF ASE NOISE

ASE noise model is usually formulated in terms of coupled differential equations on steady-state noise power, which encode the interaction of ASE with pumps and signals, analogous to Eq. (1.18). Those equations introduce the average effect of spontaneous emission, thus taking into account the joint effect of *spontaneous emission* and *amplification* of photons. Some approximations need to be pointed out. First of all, since in realistic RALs, ASE power is much less than pump power, the effect of pump photons on ASE photons is neglected. In a similar way, the same is done for the signal and ASE interaction, so ASE is assumed to be unable to pump the signal in a significant way. By these assumption, the evolution of pump and signals turn out to be approximately independent from the evolution of the ASE, and the corresponding equations are decoupled. Within this assumption

one can, in principle, solve the pump and signal equations, and then compute the ASE in a separate moment by integrating the corresponding equation with the precomputed power profiles. As for the model itself, the spectrum of the ASE is considered to be subdivided with the same subdivision as the channel spectrum. This allow us to evaluate the amount of in-band noise power for each channel, which is the needed information to compute the OSNR. Lastly, as anticipated in 1.2.2, recall that ASE can be modeled as additive Gaussian noise.

A simple model uses Eq. (1.18) for the pump and signal waves, and in addition defines $\{N_i\}$ as the ASE power relative to the channel i. If there are n channels, the resulting additional n equations for the ASE are [148]:

$$\begin{aligned}\pm\frac{dN_i^{\pm}}{dz} = -\alpha_i N_i^{\pm} + \left[\sum_j C'_{R\,i,j}\left[P_j^{+} + P_j^{-}\right]\right] N_i^{\pm} \\ + \left[\sum_j \eta_{i,j} C'_{R\,i,j}\left[P_j^{+} + P_j^{-}\right]\right] 2h\nu_i B_{ref}\end{aligned} \tag{2.58}$$

the last term represents the coupling to a reservoir of phonons at thermal equilibrium. It is possible to tune the Raman gain factors by the phonon occupancy factor [19], by assuming thermal equilibrium of phonons and Bose-Einstein statistics [79], the factor is

$$\eta_{i,j} = \frac{1}{\exp\left[h(\nu_i - \nu_j)/k_B\theta\right] - 1} \tag{2.59}$$

for the energy difference $h(\nu_i - \nu_j)$, which corresponds to the difference in energy between the pump – or signal – and ASE photon. Since the energy of the phonon corresponds to the energy difference, this process is elastic. Finally, B_{ref} is the reference bandwidth, which in this case is equal to the signal bandwidth, which can be expressed as the WDM spectral spacing minus the guard width.

By integrating equations (2.58), with previously computed pump and signal powers, we obtain the noise at the end of the fiber considering the forward propagating noise terms $\{N_i^{+}\}$.

2.6 NUMERICAL RESULTS

In this section we will describe the numerical simulation software and the noise predictions for NLIN and ASE. Finally, we will answer some questions of interest for the design of systems. In order to frame the limitations of this investigation, let us describe the fixed simulation parameters that will be common to all the

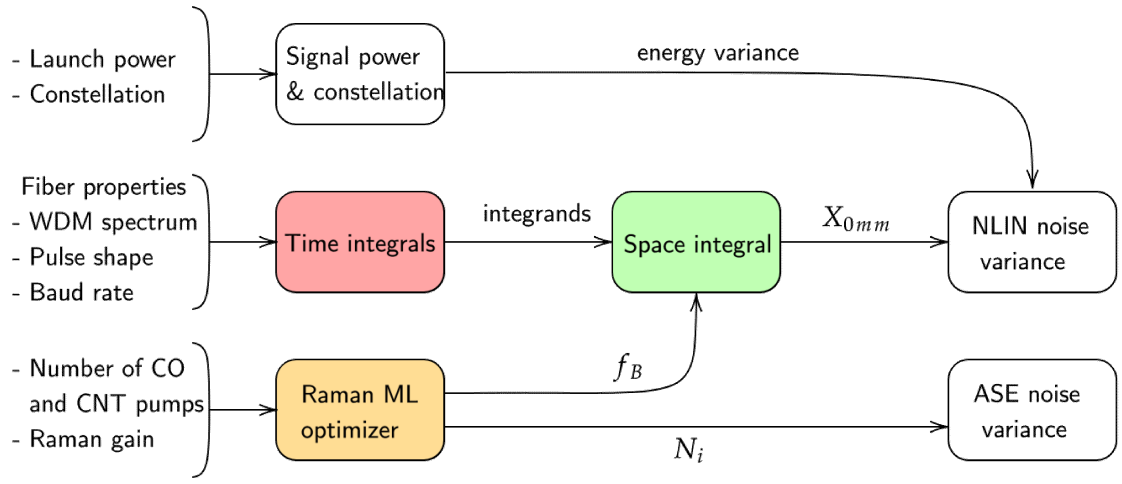

Figure 2.4: Simplified computational scheme to highlight the dependences. Computational times on desktop computer - without graphics hardware acceleration - are encoded in colors. Red: some hours to few days. Orange: tens of minutes to hours. Green: few minutes. No color: under one second.

computations. The RAL under consideration is characterized by a fiber of 80km length. The fiber has coefficients $\beta_2 = -23\text{ps}^2\text{km}^{-1}$, $\gamma = 1.3\text{Wkm}^{-1}$ and the WDM channels are disposed in a wavelength grid from 187.5THz to 192.4THz, for a total of 50 channels with 100GHz spacing. The baud rate is fixed at 10GHz. Since the modulation format can be easily integrated in the calculations, as discussed in 2.2.4 the modulation will be fixed to 16-QAM. By using the ratios shown in Fig. 2.1 in Eq. (2.28), the noise for every other modulation can be computed.

2.6.1 *Software and structure of routines*

Let us comment the structure of the numerical computation. The utilized code is available at the GitHub repository [110]. A simplified input-output scheme, with the subdivision of the various routines, is represented in Fig. 2.4. Notice how the computationally intensive part, that is the calculation of time integrals of Eq. (2.23), indicated with the red color, depends only on fiber properties, WDM spectrum, and pulse shape with baud rate. Other parameters such as the gain-attenuation factor f_B are irrelevant for this step of computation, so the optimization procedure can be run in a disjoint setting, and many different pumping schemes can be used with the same collision results. Finally, the computation of NLIN includes the results for $X_{0,m,m}$ from the space integration, and joins them with constellation average energy and energy variance. On the other hand, ASE computation depends only on average power and can be addressed separately.

2.6.2 *Systematic review of results*

Let us review the results in a systematic way. We will start by describing the Raman optimization results, then the computation of $X_{0,m,m}$, and finally the evaluation of ASE noise and NLIN, and the total link noise and OSNR. We will concentrate only on optical measures in this section, whereas in a following section we will discuss the adoption of metrics for the overall (electrical) link noise.

The optimization procedure for obtaining Raman pump placement is constrained by the choice of the copropagating and counterpropagating pumps. For simplicity, when referring to a pumping setup with n copropagating and m counterpropagating pumps, we will call it a $(n, m)-$bidirectional pumping. If the pumping is one-directional, one of the numbers is dropped. Moreover, in figures, the abbreviations CO, CNT, BI, perf., will be used to indicate, respectively, copumping, counterpumping, bidirectional pumping and perfect amplification. The choice of these numbers is crucial, especially for what regards bidirectional pumping. In fact, when choosing pump numbers and powers in an unbalanced way, the optimizer may give solution very similar to the optimized co- or counter-pumped case. In order to highlight the difference between the three setups, we

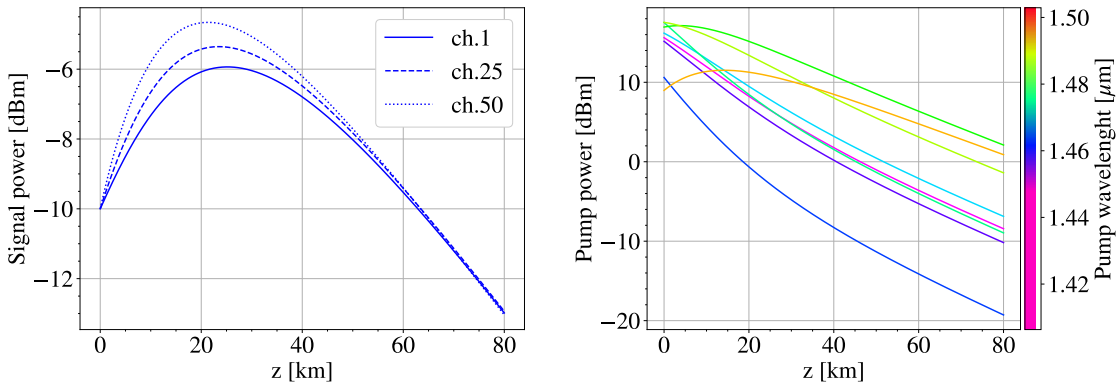

(a) First, last and middle channels of the WDM comb.

(b) Pumps (8 waves).

Figure 2.5: Signal and pump evolution in copropagating scheme.

selected a (8, 2)-bidirectional, a (8)-copropagating, and a (10)-counterpropagating for comparison. Signals and pumps power evolutions resulting from the optimized setup are shown for a signal power level of −10dB in Figures 2.5 (CO),2.6 (CNT), 2.7 (BI).

We then show, in Fig. 2.8, the profile of f_B for the two extremal channels. Recall that the amplification function was obtained directly from signal power as the

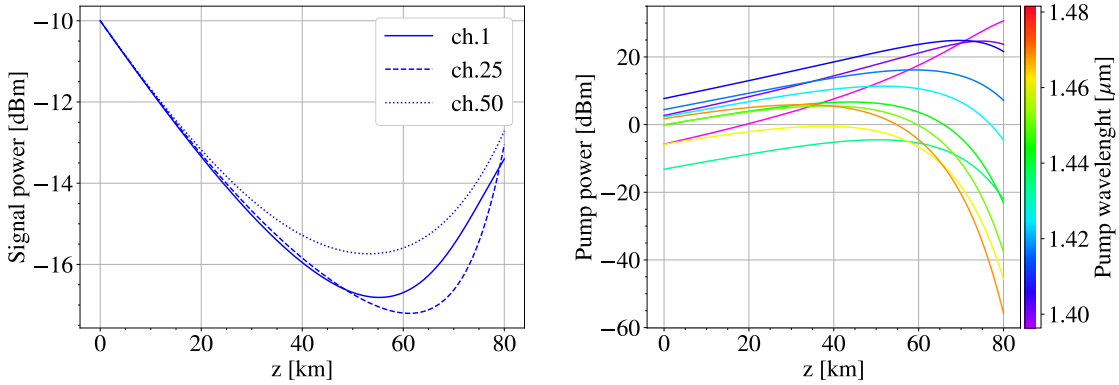

(a) First, last and middle channels of the WDM comb.

(b) Pumps (10 waves).

Figure 2.6: Signal and pump evolution in counterpropagating scheme.

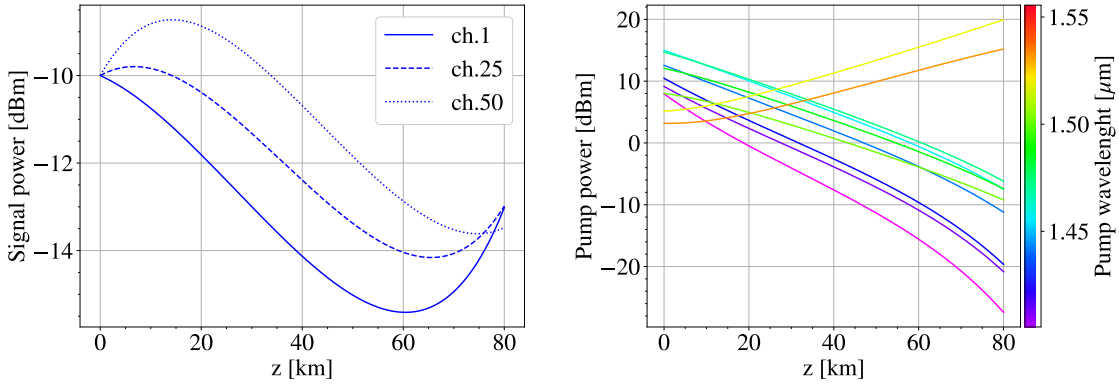

(a) First, last and middle channels of the WDM comb.

(b) Pumps (8 copropagating and 2 counterpropagating waves).

Figure 2.7: Signal and pump evolution in bidirectional pumping scheme.

ratio $f_B(z) = P_B(z)/P_B(0)$. In the figure, it appears that the general shape of the amplification function stays qualitatively constant for each pumping scheme. Copumping f_B show a prominent peak near the input, and then a decay that asymptotically reaches the intrinsic attenuation rate, due to pump depletion. Counterpumping f_B show an initial decay and then a recovery near the pump input at the fiber end; in the bidirectional case a mixture of the two behaviors takes place.

In order to visualize the spatial integrand, consider the set of all the collision (time integral) curve for each m, modulated by the f_B function. The evaluation of collisions, for all the m of interest, is shown in Fig. 2.9. In particular, in Fig. 2.9b the chosen couple of channels is the [49, 50] pair, of which chan. 49 is the channel of interest. In fact, the collision curves of interfering channel 50 exibit great

sensitivity to the pumping scheme, as suggested in Fig. 2.8b. Furthermore, by comparing the two plots in Fig. 2.8, we deduce that collision curves are strongly dependent from interfering channel position in the WDM comb. This imples that the magnitude of $X_{0,m,m}$ depends on the interfering channel position, and suggest that the total noise will vary with the choice of the set of interfering channels. This difference is clear comparing 2.9a and Fig. 2.9b.

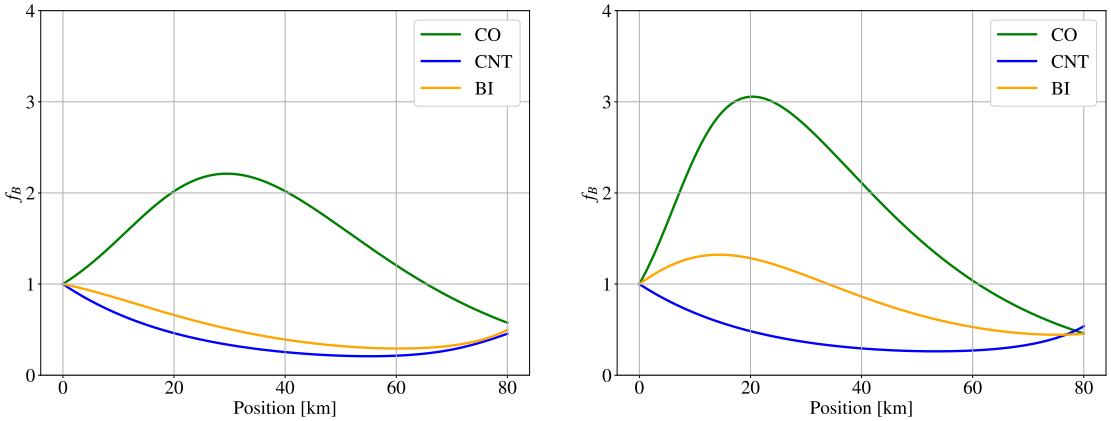

(a) Profile of f_B function for ch.1

(b) Profile of f_B function for ch.50

Figure 2.8: f_B function for the 80km, −20dBm launch power case.

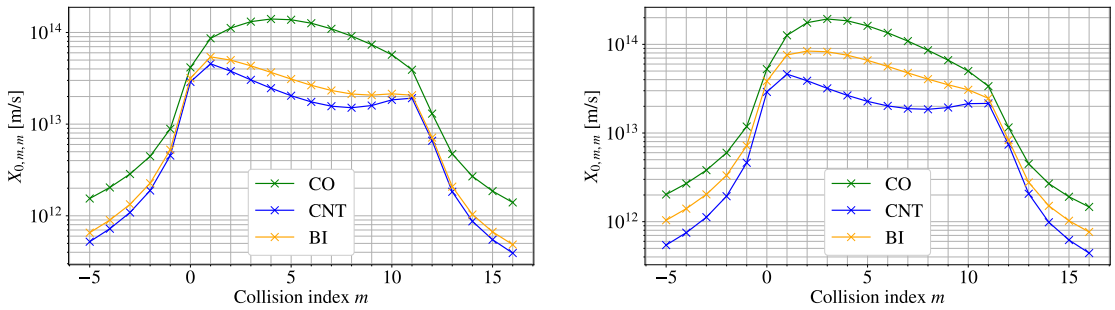

(a) Evaluation of $X_{0,m,m}$ for ch.1 and ch.2 interference.

(b) Evaluation of $X_{0,m,m}$ for ch.49 and ch.50 interference.

Figure 2.9: $X_{0,m,m}$ at various m. −20dBm launch power.

In order to describe the impact of the variability of total noise due to interfering channel position, a particularly interesting measure is the integral of f_B, for various B channels. In fact, neglecting the dependence of time integrals from spectral spacing, the only factor accounting for the noise due to B channel is

$$\int_0^L dz f_B(z). \tag{2.60}$$

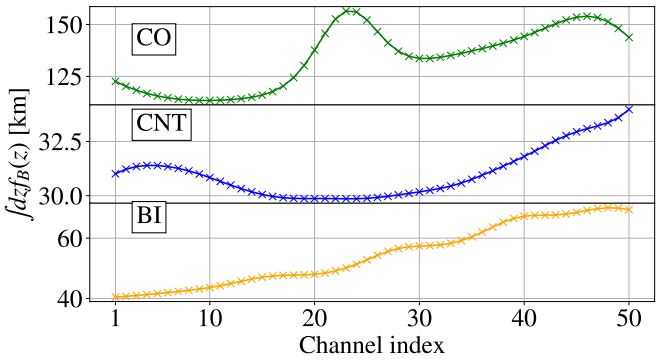

Figure 2.10: Evaluation of integral of f_B for all the WDM channels.

This is the value plotted in Fig. 2.10, for all the pumping schemes. It is clear that, to the first order, the channels that are most influent on NLIN, looking at their Raman amplification function, are the highest frequency ones. This asymmetry is observed in Fig. 2.11. In the perfect amplification case, the grey bottom-right plot, the distribution is symmetric, and the only variations are due to the diverse effect of different collision numbers. All the other plots show an asymmetry which is encoded in the respective amplification function, and reflects what shown in the integral computation in Fig. 2.10. In order to show the dependence of the time integrals on the choice of the interfering channel, let us neglect the influence of f_B, by considering the perfect amplification scenario. The total noise due to a single interfering channel, placed at spacing Ω, is proportional to

$$\mathrm{NLIN}_\Omega := P\left\langle \Delta\phi^2 \right\rangle \propto \sum_m X^2_{0,m,m}, \tag{2.61}$$

and by expressing the computation of $X_{0,m,m}$, as per Eq. (2.23), we notice how the only dependence on the interfering channel choice is encoded in the spectral spacing spacing Ω:

$$\int_0^L dz\, I_{\Omega,m}(z), \tag{2.62}$$

where

$$I_{\Omega,m}(z) = \int_{-\infty}^{+\infty} dt |g^{(0)}(z,t)|^2 |g^{(0)}(z, t - mT - \beta_2 \Omega z)|^2. \tag{2.63}$$

The total integral, for all the collisions that fall sufficiently inside $[0, L]$, is approximately the same for every m. By assuming absence of dispersion, which is $g^{(0)}(z,t) = g(0,t)$, it can be shown that the Ω has the role of a z-axis scaling

factor on $I_{\Omega,m}(z)$. So the integral (2.62) turns out to be inversely proportional to the scaling factor $|\beta_2\Omega|$, and the total $X_{0,m,m}$ in the sum (2.61) is

$$\sum_m X_{0,m,m}^2 \propto \sum_m \frac{1}{|\beta_2\Omega|^2}. \tag{2.64}$$

The total number of collision N_Ω to be counted are approximately the total length divided by the collision spacing, so recalling the collision position $z_m = -\frac{mT}{\beta_2\Omega}$, the number is

$$N_\Omega \approx \frac{L|\beta_2\Omega|}{T} \tag{2.65}$$

so the total noise in the Eq. (2.64) is roughly proportional to

$$\mathrm{NLIN}_\Omega \propto \frac{L}{T|\beta_2\Omega|} \tag{2.66}$$

similarly to what predicted in Eq. (2.49). In order to evaluate the impact of the interaction of all the other channels in the WDM spectrum, called NLIN without subscript, we sum over all the interfering channels each of the contributions NLIN_Ω. The spectral spacing, for an equally spaced WDM system, can be decomposed in $\Omega = \Omega_0 M$, where M is the index difference between the channel of interest and its interfering one in the WDM channel list. If we call J the index of the channel of interest, the sum reads

$$\mathrm{NLIN} \propto \sum_{M=1}^{J-1} \frac{2}{|\beta_2\Omega_0 M|} + \sum_{M=2J}^{50} \frac{1}{|\beta_2\Omega_0 M|} \tag{2.67}$$

$$= \frac{1}{|\beta_2\Omega_0|}\left(2\mathcal{H}(J-1) + \mathcal{H}(50) - \mathcal{H}(2J)\right) \tag{2.68}$$

where $\mathcal{H}$ are the harmonic numbers. In particular, this approximation is reported in the bottom-right plot of Fig. 2.11, where a least square fit is carried out using an offset term and a proportional term. This shows how, in perfect amplification, the most impactful collision are the ones with fewer, less frequent overlaps, i.e. the ones with lower $|\Omega|$, nearby channels, and than the overall effect is obtained evaluating how many of those channels are available for collisions, summing over all the channels. Fig. 2.11 show the OSNR obtained by considering only NLIN, and neglecting ASE. This can be viewed as the optical link performance measure in the case of absence of post processing of NLIN using autocorrelation [44, 115, 31].

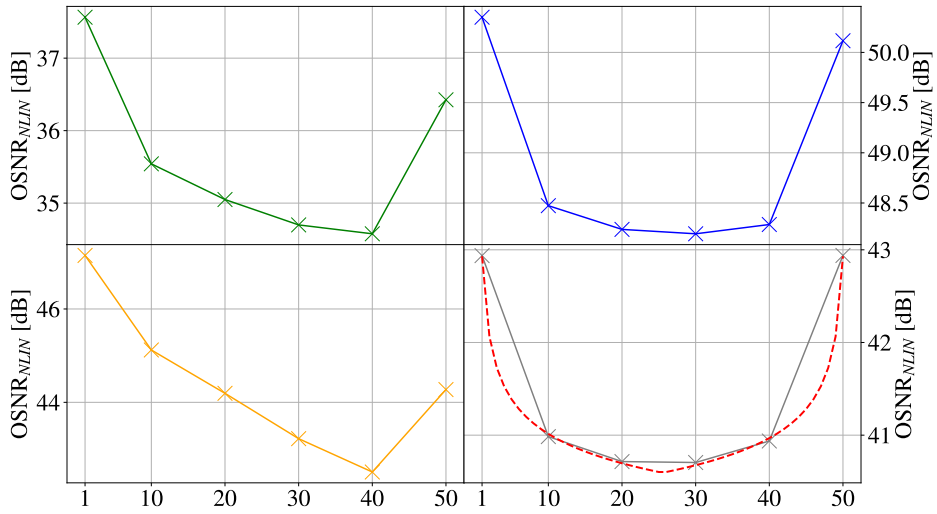

Figure 2.11: OSNR due to NLIN for various channels. Launch power −10dBm. In the bottom right plot, the dotted red curve is the fit of the analytical approximation in Eq. (2.68)

2.6.3 *Comparison of ASE noise and NLIN*

Let us now concentrate on the results of ASE computations. The following results highlight how the choice of the pumping scheme influence ASE: the evolution of the pumps and signals is critical, as the distribution of the amplification for the ASE along the fiber, give rise to effects totally similar to the cascade of noisy lumped amplifiers. In other words, supposing to have two interchangeable spans of a Raman link, with comparable excess noise and much different gains. Interchanging high and low gain sections, while keeping the total gain constant, alters the noise performance. It can be shown that putting the high gain part at the input of the link is more advantageous. This is the reason why links with copropagating Raman pumps perform better from the point of view of ASE.

In Fig. 2.12, this comparison is carried out for the case of input power. The difference between copumping and counterpumping is remarkable, and bidirectional pumping is shown to perform at an intermediate level. This phenomenon, when compared to the performance of NLIN, is shown to entail a *tradeoff*: the choice of the pumping scheme must balance between ASE noise and NLIN performance. Special attention may be given to the bidirectional pumping scheme, that can eventually be optimized for both metrics.

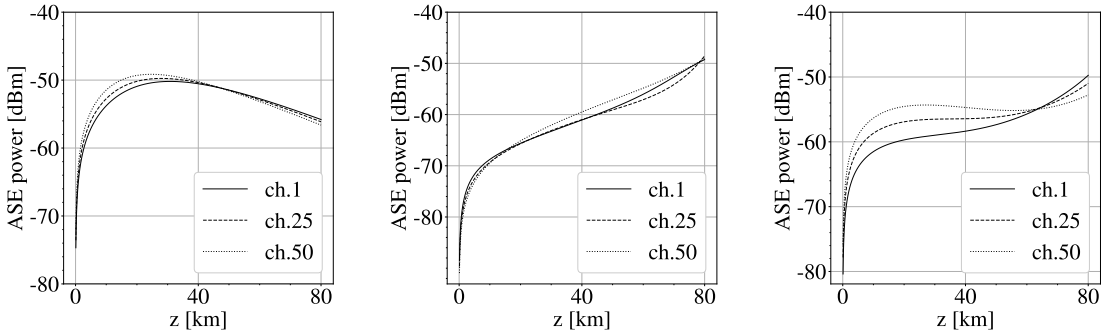

(a) Copumping (b) Counterpumping (c) Bidirectional pumping

Figure 2.12: ASE power evolution (for channels 1, 25, 50) along the fiber pumping scheme comparison. −10dBm signal power.

2.6.4 *Noise evaluation and answers to design questions*

The numerical study allow us to answer some questions regarding the design of systems. Those questions can be summarized in the following points.

1. How NLIN varies when varying the channel of interest in the WDM comb.
2. In terms of NLIN performance, which pumping scheme is more effective in mitigating noise.
3. By comparing NLIN and ASE, which one is the most impactful for RALs similar to the one studied.
4. Among the pumping schemes, is there an unconditional optimal in term of joint NLIN and ASE noise performance?

For this set of questions, there are no quantitative answer from the analysis part, and the previous exposition of numerical results will be of interest. Let us start from the first question.

The variation of the NLIN with the channel of interest reflects how impactful is composed by the channel dependence of Raman pumping profile, shown in Fig. 2.8, and the impact of the shape of the collisions, which is roughly proportional to $|\Omega|^{-1}$. The resulting noise performance, summarized in Fig. 2.11, show how the mosty affected channels are the central ones, and pumping induces an asymmetry in the profile, which is shown in the amplification profiles in Fig. 2.8, and in a more comprehensive way, in their integral for each channel in Fig. 2.10.

The second question is answered by Fig. 2.13, in which the noise power is shown versus input power. It is shown that, in a way that is almost uniform across the channels, the NLIN performance of the counterpumping scheme is

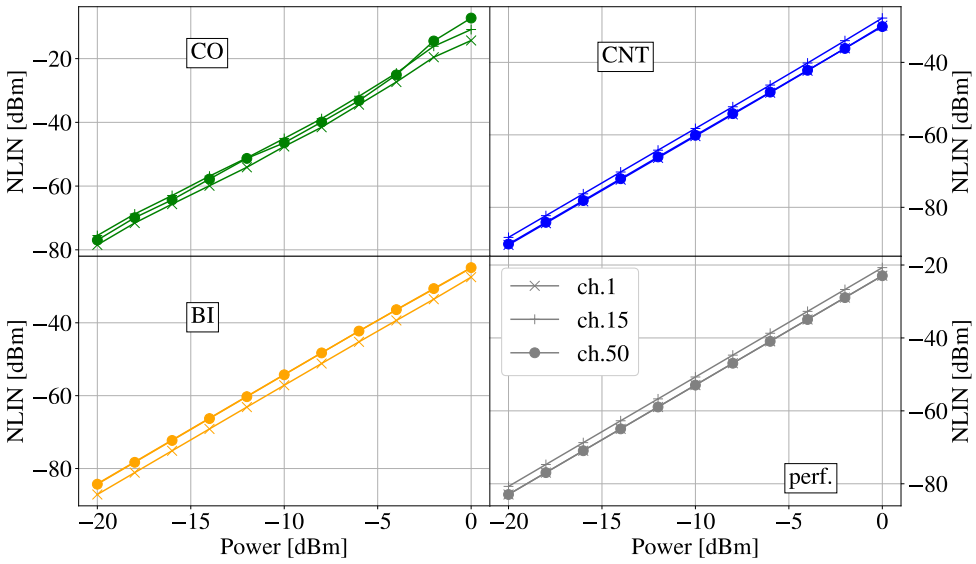

Figure 2.13: Noise versus launch power for different pumping schemes.

better than the other approaches. The bidirectional pumping scheme assume an intermediate position between counterpumping and copumping. For comparison, the perfect amplification turns out to have intermediate performance.

The third and fourth questions are answered by Fig. 2.14. As for the most important effect, it depends on the signal power at the input. NLIN varies in a significant way with signal power, whereas ASE is approximately constant with varying power. For signal launch powers below −17dBm for the copumping scheme, −7dBm for the counterpumping scheme, and −8.5dBm for the bidirectional pumping scheme, the dominating noise is ASE.

Analyzing Fig. 2.12, we see that better performing systems are the ones strongly using copropagating pumps. Instead, from Fig. 2.11 and Fig. 2.13, it is clear that systems amplifying at the end of the fiber suffer less from NLIN. So there is a tradeoff, and no preference can be assessed in terms of joint NLIN and ASE noise.

2.7 EVALUATION OF PERFORMANCES

The ultimate metric for considering the performance of an optical link is the EVM. It is a measurement of the bit probability of error P_b. While there are other more refined techniques for evaluate the performance of the system, such as information theoretical mutual information estimation, the EVM metric is highly practical. For example, it can be measured directly with a BER analyzer if the complete system is offline and available for measures, by sending a random stream of symbols and comparing the decoded stream counting errors. Alternatively, it can be induced by other measures as Error Vector Measure EVM, Q-factor, which do

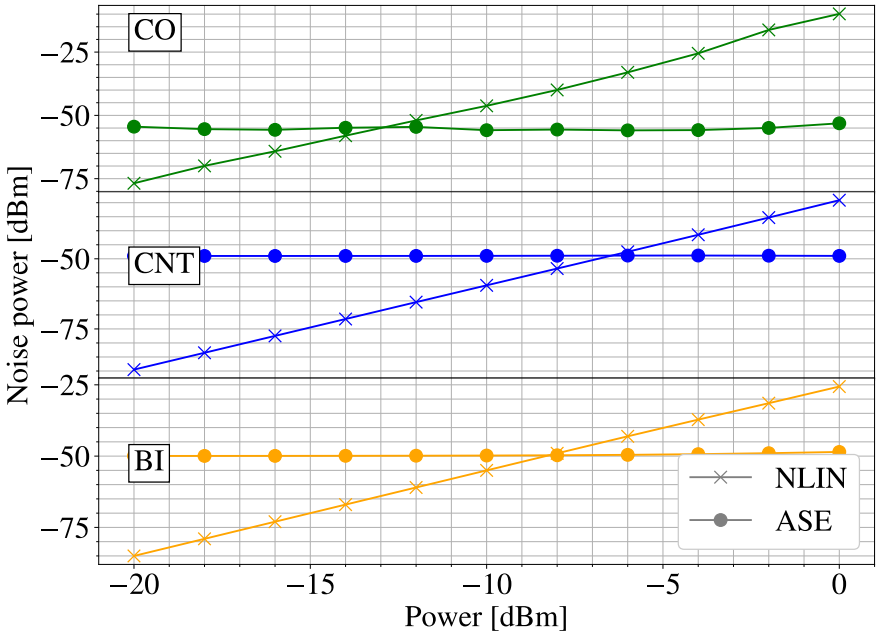

Figure 2.14: Comparison of ASE and NLIN contribution to total noise.

not require knowledge of the transmitted sequence [138, 136]. In the present case, being interested in coherent transmission, the usual scenario is an amplitude and phase modulated constellation, typically a QAM or PSK modulation. Additive circular white Gaussian noise, i.e. uncorrelated Gaussian with quadrature and in-phase components with the same variance, can be easily tackled using error functions for every QAM constellation. In this case, it is convenient to define the metric of EVM. Let $|E_i|$ the i-th received symbol amplitude of a sequence of I symbols (can be viewed as proportional to integrated photocurrent). Let $|E_a|^2$ be the average amplitude squared of the sequence, and $|E_{err,i}|^2$ be the magnitude of error squared with respect to the nearest symbol of the constellation. The nearest symbol is supposed to coincide with the transmitted symbol for low noise levels [50, 136].

$$\mathrm{EVM} = \frac{\left[\frac{1}{I}\sum_{i=1}^{I}|E_{err,i}|^2\right]^{1/2}}{|E_a|} \tag{2.69}$$

this is called also the RMS EVM. Let the constellation be M-ary with L identical signal levels within each dimension of the constellation (that is symmetric). Since the overall results of the previous study are based on OSNR, let us recall useful relations connecting it to BER and EVM. They are derived from a set of analytical

and experimental works about connection between measures [138, 136, 106, 50]. The

$$\mathrm{EVM} = \left[\frac{1}{\mathrm{OSNR}} - \sqrt{\frac{96/\pi}{(M-1)\mathrm{OSNR}}} \sum_{i=1}^{\sqrt{M}-1} \gamma_i e^{-\alpha_i} + \sum_{i=1}^{\sqrt{M}-1} \gamma_i \beta_i \Phi\left(\sqrt{\alpha_i}\right) \right]^{1/2} \tag{2.70}$$

where Φ is the Gaussian error function, and the auxiliary variables are defined as

$$\alpha_i = \frac{3\beta_i^2 \mathrm{OSNR}}{2(M-1)} \tag{2.71}$$

$$\beta_i = 2i - 1 \tag{2.72}$$

$$\gamma_i = 1 - \frac{i}{\sqrt{M}} \tag{2.73}$$

and the BER can be related to this EVM measure as [50]

$$\mathrm{BER} \approx \frac{(1 - L^{-1})}{\log_2 L} \Phi \left[\sqrt{\frac{3 \log_2 L}{(L^2 - 1)} \frac{\sqrt{2}}{(\mathrm{EVM})^2 \log_2 M}} \right] \tag{2.74}$$

While the ASE noise can be treated as Gaussian noise, NLIN can be more difficult to tackle, as it is a phase noise. In the lack of a more refined method, it is possible to conveniently extract the BER by treating the NLIN as a circular AWGN process. The variance of the two noise contributions sum, as they are independent, but this may be not sufficient to characterize BER. This is a reasonable approach, however it lacks for taking into account properties of autocorrelation of NLIN, that may be leveraged to further reduce the impact of noise [115, 59]. The error performance is

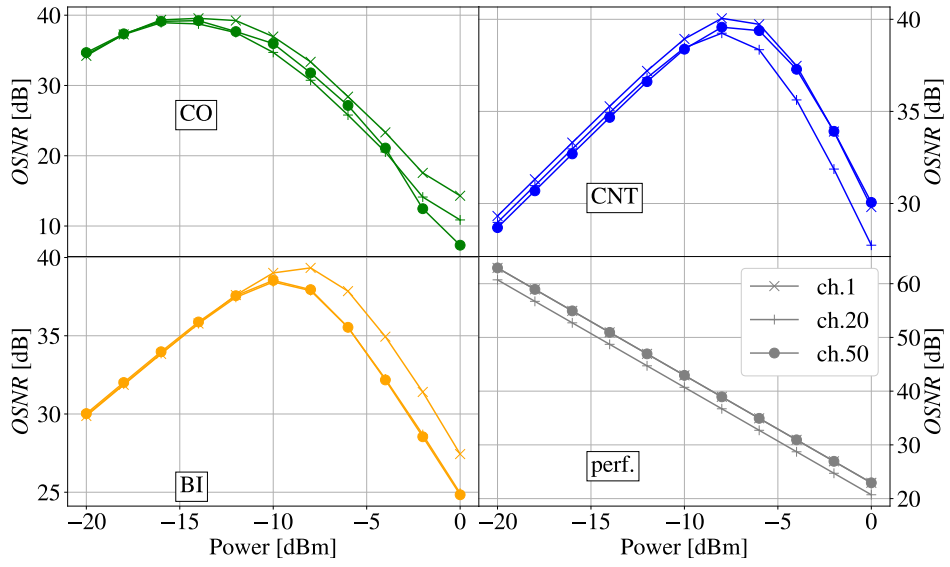

Figure 2.15: Total OSNR for 16-QAM constellation.

dependent from the input distribution of symbols, however this dependence can be disregarded, as using channel coding it is possible to modify the statistics of the input distribution. The computation of overall OSNR is shown in Fig. 2.15. In the bottom right part the highly-idealized perfect amplification scenario for NLIN is computed along a null ASE contribution. This is useful to comprehend the NLIN contribution to the overall performance. In Fig. 2.16, the BER is computed for a 16-QAM modulation format. The plot suggest that it may be possible to utilize higher modulation format for channels with intermediate power levels, as the error performance is excellent for nearly all launch power and pumping schemes. Instead, for the copropagating case, high launch power is shown to give more problematic error performance. Fig. 2.17 provide a detailed view of this region. As it can be seen, the performance for launch power of 0dBm is so degraded that BER is 10^{-1} for channel 50 and approximately 10^{-2} for channel 1. In order to compare the results with a higher modulation, Fig. 2.18 show the

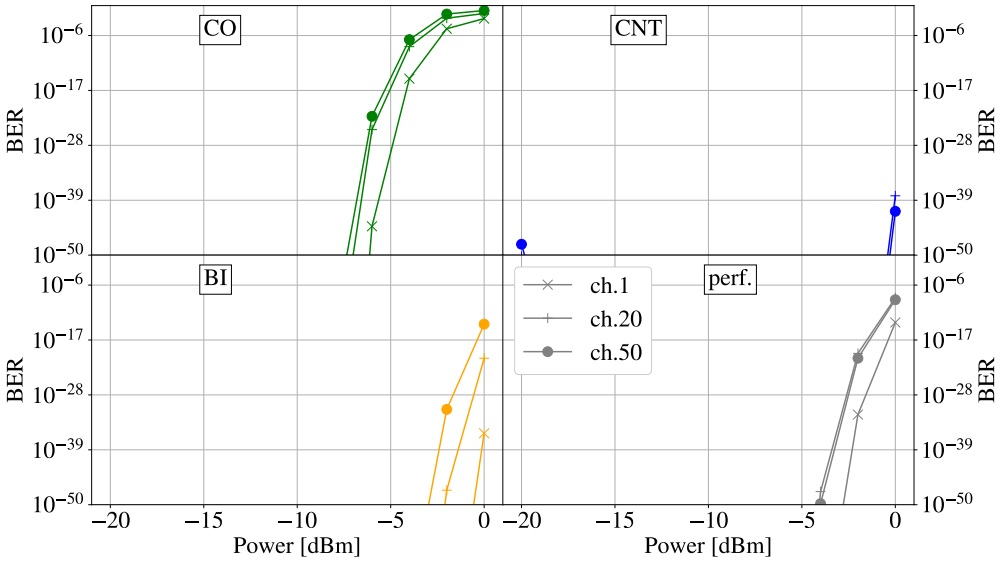

Figure 2.16: BER versus channel power, for 16-QAM constellation. The extremely low values of predicted BER in the approximation are reported for completeness.

effect on BER of the very high modulation format of 64-QAM. For such high modulation, even if the NLIN power changes only slightly (due to the factors in Fig. 2.1), the vicinity of the symbols in the constellation implies a strong increase in the error rate. In the zoomed version, Fig. 2.19, we see that, in the worst case scenario of channel 50 of the copropagating RAL, the error rate approaches 0.5, the error rate of a useless channel. As a final remark, we point out that, for error rates as high as the one represented in Fig. 2.19, the method utilizing EVM will underestimate the error in an experimental setting, due to the many received points whose nearest constellation symbol is not the transmitted symbol.

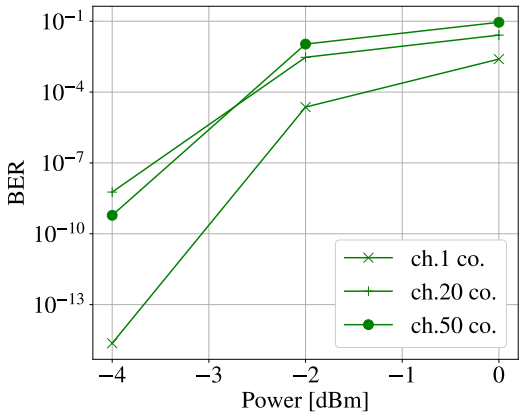

Figure 2.17: BER versus channel power, for 16-QAM constellation, copropagating case zoom.

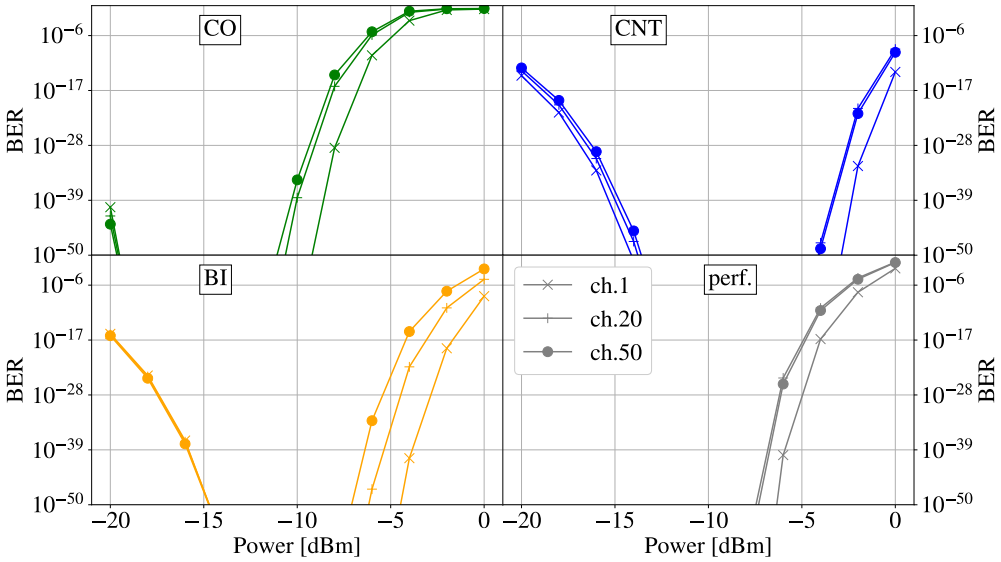

Figure 2.18: BER versus channel power, for 64-QAM constellation. The extremely low values of predicted BER in the approximation are reported for completeness.

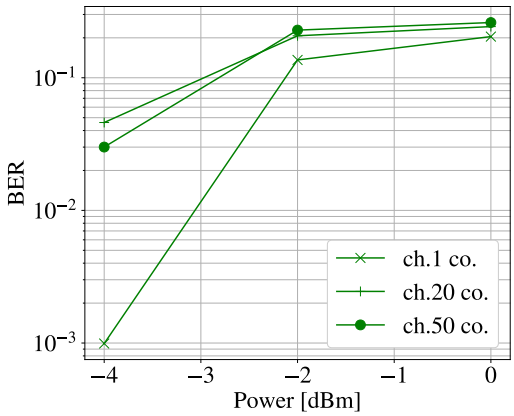

Figure 2.19: BER versus channel power, for 64-QAM constellation, copropagating case zoom.

3 QUANTUM PROPAGATION MODELS AND NLIN

Now nobody knows just where the boundary between the classical and quantum domain is situated

J.S. Bell [12]

The quantum nature of radiation, combined with the technological capability of detecting physical magnitudes which are close to the single-quanta level, opens up the possibility to interact with optical systems exibiting non-classical behaviors. This aspect has a strong impact also in optical communications, as also the interaction with disturbances, and so the generation of noise, is ultimately ruled by quantum mechanics. In fact, for optical and infrared frequencies, such as the one used in fiber-optical communications, the energy quanta $\hbar\omega$ is in the order of $\sim$ 1eV: materials used in photodetection have comparable bandgap energy and receiver electronics is thus technologically mature to detect single photons. This chapter will provide a review of results and methods in quantum optics, that may be utilized to address the technological problem of the *coexistence* between WDM and QKD channels, with particular attention with respect to NLIN.

3.1 INTRODUCTION TO QUANTUM NOISE

3.1.1 *From semiclassical to quantized fields models*

The usual theory of shot noise in classical optical communications is a semiclassical approach that uses Poisson statistics of arrival times to take into account the inherently quantum-mechanical distribution of photons.

In section 1.2.1, we described a simple consequence of this model for OOK, that is the so called "quantum limit": a minimum probability of error due to uncertainty in Poisson distributed photocount.

Such model, when used for computing systems performance, relies on classical field propagation inside the fiber, which in practice is often computed using

approximated methods such as Eq. (1.5). By deriving the average field power at the receiver over a certain bandwidth, the complete Poisson arrival statistics is derived. The receiver output signal is considered to be the average photodetector current in statistical sense, plus the shot noise. In many applications, under the assumption of sufficiently high average number of received photons, this noise can be approximated as Gaussian.

From fundamental physics, it is known that the electromagnetic fields can be described quantum-mechanically using the second quantization formalism, developed by Dirac in 1927 [32]. In this treatment, the electromagnetic field is decomposed in modes like in usual linear propagation theory, and a harmonic oscillator Hamiltonian is associated for each mode. By identifying canonical variables in the field, the promotion of the dynamical variables to observables is performed and the canonical commutation relation is established for the corresponding operator. This formalism allows to describe the system quantum-mechanically. As a matter of fact, this is the basis for the extremely rich branch of Quantum Field Theory (QFT) [108], whose object of interest are the *quantized field*, representing electromagnetic fields, but also the matter fields (Schrödinger fields). QFT has applications in nearly all modern physics. In particular, the physical scenario of electromagnetic field propagation inside an optical fiber, many interacting particles are described in principle by a many-body theory. In this scenario [120], the description of the interaction can be approximated with an averaged interaction potential, thus obtaining a mean-field description. It is possible to show that the classical NLSE is a mean field equation derived from the full quantum-field theoretical treatment.

The natural questions that one can make from the systems point of view are: how well does the semiclassical model of detection describe the actual detection, compared to the full quantum field detection? And also, what are the limitations of models based on a classical field propagation, for example the NLIN model described in this paper, in describing the quantum characteristics of detection? Finally, how does the quantized field model contribute in describing the telecommunication properties of channels specifically designed to convey quantum states, as QKD channels, and how is it difficult to set the computations? In this chapter we will not answer to the questions in a complete and comprehensive way, but we will provide tools for further investigation.

The framework of interest to address the interaction noise in quantum terms is the theory of open quantum systems. Within this theory, many tools have been developed for modeling the interaction of a quantum system with an environment. The main one is represented by a set of master equations tackling the evolution of density matrices. Those equations are called the Redfield and Gorini

– Kossakowski – Sudarshan – Lindblad (GKSL) equations [52, 109]. However, the model is valid only over a set of assumptions, that we may assess critically for the usage for the NLIN. For example, this approach utilizes the Markov property in computing the time evolution. Another related approach is the more general model with so-called semiclassical Langevin equations, that leverages the phase-space representation of the quantum state in order to obtain a c-values equation with stochastic terms. This approach have been developed for fiber optics by Drummond and Carter [38, 37], and was used for assessing noise due to gain, absorption and Raman processes. In addition, the quantum-mechanical description of the measurement process is of interest. The von Neumann projection interpretation describes the measurement process as the transformation that will provide an eigenvalue of the observable, and set the system, immediately after such measurement event, in the corresponding eigenstate. By further developing the measurement theory, it is possible to extend the realm of quantum description, without imposing such a strong characterization of classical measurement apparatus like in the von Neumann postulate. This can be done by assessing that coupling to external measurement apparatus consists in having the quantum state in the product Hilbert space of the system under test *and* the measurement apparatus, which can be *both* modeled as quantum systems. Taking statistical averages in the measurement apparatus, Hilbert space turns out to have a mathematical analogous in taking partial traces in the corresponding density matrix [79, 159].

Let us focus on the required characteristics of the desired model. In the previous chapter, the usage of metrics which are averaged over the constellation symbols, such as the OSNR, and the BER, allowed one to express the performance of a classical system. A more detailed representation of the channel would be the transition probability matrix for all the symbols in the constellation. A quantum channel is completely characterized by the conditional statistical description of the output state symbol, obtained via density matrices, given the input state [21]. So a complete model for the quantum channel is able to predict the density matrices at the receiver, taking into account the interaction with surrounding material and other fields. A direct modeling of all the interaction of the field mediated by the microscopical constituents of the fiber is extremely difficult to solve, so the utilized methods cited before follow the approach of deriving effective macroscopic fields. The theory of open quantum systems provides a set of tools to tackle this statistical problem. In fact, the interaction of a quantum system with its environment, which may eventually have many degrees of freedom, can be addressed taking into account the dynamics of the environment only in statistical sense, using stochastic equations. Quantum dynamics predicts unitary evolution

of the complete system. Often, the actual evolution of a system, when interacting with the environment, is not unitary, and the Hamiltonian treatment of the system, as it was isolated, is unsatisfactory. This is the case of optical signals occupying an electromagnetic mode in the fiber, in which noise is generated through interaction with the environment. Let us consider a total system state in the Hilbert space $\mathcal{H}_T$, which is the tensor product of the system Hilbert space, $\mathcal{H}$, and the environment Hilbert space $\mathcal{H}_E$. Let us denote by ρ_T the total system density matrix, composed by system density matrix ρ, and the environment one ρ_E. In a typical setting, ρ represents the matrix that will be ultimately interact with the photodetector. Assuming the total system is isolated, the evolution of the total density matrix is described by the von Neumann equation [134]:

$$i\hbar\frac{d}{dt}\rho_T = -[\rho_T, \hat{H}_T] \tag{3.1}$$

where $\hat{H}$ is the total Hamiltonian, and the operator $-[\rho, \hat{H}]$ is often called Liouvillian $\mathfrak{L}\rho := -[\rho, \hat{H}]$. In fact, the above equation is the quantum-mechanical equivalent of the Liouville equation for the density in phase-space [79]. In classical terms, equations regulating probability density functions are called *master equations*, and are solved using tools like the versatile Fokker-Planck equations[†]. In the generalized setting of quantum statistical mechanics, those equations correspond to equations on the density matrix. It can be shown that the set of all the density matrices constitute a Hilbert space [109], called Fock-Liouville space. However, an equation in the total space, such as Eq. (3.1) is extremely difficult to solve in practice, due to the huge number of degrees of freedom of a typical environment. Moreover, it is not even interesting, as we are only concerned about the evolution of ρ, in its interaction with the system, that will be the variable from which the symbol will be decoded. Like in the previous description in 1.2.5, average values of a operator $\hat{O}$ [79] are obtained through the trace operator

$$\langle\hat{O}\rangle = \mathrm{Tr}\left[\rho\hat{O}\right]. \tag{3.2}$$

In the case of a system interacting with an environment, the density matrix can be obtained using the partial trace over the environment, indicated by Tr_E. For clarity, if the system density matrix is

$$\rho = \sum_{i,j} |s_i\rangle \langle s_j|,$$

[†]In the setting of classical statistical mechanics, Fokker-Planck equation can be derived from the master equation, using Kramers-Moyal expansion and diffusive approximation, i.e. retention of drift and diffusion terms only [133].

and the environment one is

$$\rho_E = \sum_{i,j} |e_i\rangle \langle e_j| ,$$

then the total density matrix admits the representation

$$\rho_T = \sum_{i,j,k,l} |s_i\rangle \langle s_j| \otimes |e_k\rangle \langle e_l| , \tag{3.3}$$

where $\otimes$ denoted the tensor product. The partial trace operator is defined as

$$\rho = \mathrm{Tr}_E [\rho_T] = \sum_{i,j} |a_i\rangle \langle a_j| \, \mathrm{Tr} \left[\sum_{k,l} |b_k\rangle \langle b_l| \right] \tag{3.4}$$

A similar treatment holds for expected values. Notice that taking the trace has some similarity with the procedure of obtaining a total probability. With respect to the total system, ρ is called *reduced density matrix*.

The master equations used in quantum optics are master equations for the reduced density matrix [16, 27, 109, 56]. In order to assess the feasibility of our analysis using the GKSL or Redfield equations, we reproduce, following Gardiner and Zoller [52] some steps of their derivation, and identify all the approximations that are used. In the following, we will suppose to know the Hamiltonians. The actual model for the Hamiltonians will be addressed later following the quantization procedure of Drummond [38], based on the approach of Hillery and Mlodinov [77]. Let us start from the total master equation (3.1), and write the decomposition of the Hamiltonian in $\hat{H}_s$, the system part, $\hat{H}_E$, the environment one, and $\hat{H}_{int}$ the interaction. For convenience, let us transform the equation in the interaction picture. Let ρ_I be the total density matrix in the interaction picture. The transformation of Eq. (3.1) follows the standard rules for picture conversion [134]. We obtain

$$i\hbar \frac{d}{dt} \rho_I(t) = -[\hat{H}_{int}(t), \rho_I(t)], \tag{3.5}$$

where the time varying Hamiltonian of the interaction picture reads, with a slight abuse of notation

$$\hat{H}_{int}(t) = \exp\left[+i \frac{(\hat{H}_{sys} + \hat{H}_E)t}{\hbar} \right] \hat{H}_{int} \exp\left[-i \frac{(\hat{H}_{sys} + \hat{H}_E)t}{\hbar} \right]. \tag{3.6}$$

As for density matrices, observe that by taking the partial trace, remembering the inverse transform from the interaction picture:

$$\rho(t) = \mathrm{Tr}_E \left[\exp\left[-i\frac{(\hat{H}_{sys} + \hat{H}_E)t}{\hbar} \right] \rho_I(t) \exp\left[+i\frac{(\hat{H}_{sys} + \hat{H}_E)t}{\hbar} \right] \right]. \tag{3.7}$$

However, since $\hat{H}_E$ is a function of environment variables only, by using cyclic property of trace over the exponentials, the following is obtained:

$$\rho(t) = \exp\left[-i\frac{(\hat{H}_{sys})t}{\hbar} \right] \mathrm{Tr}_E[\rho_I(t)] \exp\left[+i\frac{(\hat{H}_{sys})t}{\hbar} \right] \tag{3.8}$$

In order to deduce the dynamics of the system, and solve Eq. (3.5), let us introduce reasonable initial conditions. Assume that the system and the environment are initially independent, so we have the factorization

$$\rho_T(0) = \rho(0) \otimes \rho_E = \rho_{int}(0) \tag{3.9}$$

and we assume that the environment, that models a reservoir, is not affected in its statistical properties by the weak coupling to the system. Using the initial condition, we can integrate the right side of Eq. (3.5). Notice that the integral will in principle contain the desired density matrix evolution. In order to circumvent the problem, let us integrate twice, obtaining

$$\rho_I(t) = \rho_I(0) - \frac{i}{\hbar}\int_0^t d\tau\, [\hat{H}_{int}(\tau), \rho_I(0)] + \tag{3.10}$$

$$+ \left(-\frac{1}{\hbar^2}\right) \int_0^t d\tau \int_0^\tau d\tau'\, \left[\hat{H}_{int}(\tau), [\hat{H}_{int}(\tau'), \rho_I(\tau')]\right]. \tag{3.11}$$

One could go on expanding the expression in a power series of the perturbation $\hat{H}_{int}(t)$. Instead, by time differentiating the expression (3.10), an integro-differential equation is obtained:

$$\frac{d}{dt}\rho_I(t) = -\frac{i}{\hbar}[\hat{H}_{int}(t), \rho_I(0)] - \frac{1}{\hbar^2}\int_0^t d\tau\, \left[\hat{H}_{int}(t)[\hat{H}_{int}(\tau), \rho_I(\tau)]\right]. \tag{3.12}$$

Let us reasonably assume that the partial trace $\mathrm{Tr}_E(\hat{H}_{int}\rho_I(0)) = 0$, which corresponds to assuming that the interaction has no diagonal elements in the representation that diagonalizes $\hat{H}_E$. By taking the partial trace in Eq. (3.12)

$$\frac{d}{dt}\rho = -\frac{1}{\hbar^2}\int_0^t d\tau\, \mathrm{Tr}_E\left(\left[\hat{H}_{int}(t)[\hat{H}_{int}(\tau), \rho_I(\tau)]\right]\right). \tag{3.13}$$

Still, the integral contains the total density matrix. In order to eliminate this dependency, let us assume weak coupling, so to have factorization $\rho_T(t) \approx \rho(t) \otimes \rho_E$ even in times different than zero. By applying the above assumption,

$$\frac{d}{dt}\rho = -\frac{1}{\hbar^2}\int_0^t d\tau \ \mathrm{Tr}_E\left(\left[\hat{H}_{int}(t)[\hat{H}_{int}(\tau), \rho(\tau)\otimes\rho_E]\right]\right). \tag{3.14}$$

Let us introduce a realistic physical assumption. Usually the environment system is in thermal equilibrium, so the fluctuation time of the environment density matrix is much shorter than the characteristic correlation time of the system density matrix. Recall that, at thermal equilibrium, the density matrix and its relative Hamiltonian commute, so in the von Neumann equation we have stationarity. Since ρ is approximately constant in the short time in which the integrand becomes zero, it is possible to utilize the so-called Markov approximation, i.e. $\rho(\tau) \approx \rho(t)$. Furthermore, the result undergoes a negligible change when the integration range is extended to $-\infty$. Thus, by defining $s = t - \tau$

$$\frac{d}{dt}\rho = -\frac{1}{\hbar^2}\int_0^{+\infty} ds \ \mathrm{Tr}_E\left(\left[\hat{H}_{int}(t)[\hat{H}_{int}(t-s), \rho(t)\otimes\rho_E]\right]\right). \tag{3.15}$$

This equation is often called the Redfield equation. To be a valid equation it must describe for every t a valid density matrix. Its validity is not ensured by its definition [52], and this is an issue fixed by the passages that lead to the GKSL equation [109]. Let us describe the main one, without developing further: consider now the operator acting on A given by the commutator $[H, A]$, often called the superoperator $\tilde{H}A = [H, A]$. The eigenvalues of this superoperator form a complete basis of the space of operators, and by diagonalizing the superoperator we transform the commutators in Eq. (3.15). This transformation allows one to express the requirement of validity explained before in a more concise manner, and the resulting equation, after some passages, is the GKSL one.

We point out that there exists an axiomatic ways to derive the GKSL equation, that uses the concept of complete positive trace-preserving maps, which are transformations that map density matrices into density matrices, with suitable properties [109]. This was the approach originally proposed by the authors of the model [60].

3.2 QUANTIZATION OF FIELDS IN NONLINEAR DISPERSIVE FIBER

So far the methods for quantum (noise) dynamics were illustrated. These methods require the knowledge of the Hamiltonian of the system, the environment and the coupling. Our task now is to review how previous models included physical

effects as dispersion and nonlinearity into the quantum theory. Theoretical treatment of quantization in realistic media and waveguides has been developed in the 1990s, by the pioneering work of Hillery, Mlodinov [77], Drummond [39, 37] Haus [67] and others [14, 135], with the main focus being on the description of the quantum dynamics of a soliton pulse. Many subleties arise when dealing with such theoretical framework, such as non-unique definition of the Lagrangian, that may lead to incorrect theories if not addressed. Without the pretence of completeness, we will list some of them in the following section, in which we will describe common methods and techniques to obtain a quantum field theory of propagating waves in realistic fibers. Following Drummond [39], we lay down the mathematical model for tackling quantization in guided propagation, taking into account full nonlinearity and dispersion. The desired model should include coupling to attenuation reservoirs (electronic and vibrational). Coupling to reservoirs is modeled in a way that the microscopic properties of the medium are not needed.

In order to explain in a clear way the procedure of quantization, let us reproduce the treatment in Drummond [39] from the most idealized scenario, the one of a nondispersive and linear medium, then introduce dispersion and finally take into account also nonlinearity.

3.2.1 *Linear case*

Let us start by expressing energy of a linearly polarized field in a fiber of length L, made by isotropic material. By writing the energy, we obtain a hint on which canonical variable to use in the procedure of second quantization. In particular, the choice of the electric displacement field $\mathbf{D}$ was used for the first time by Hillery and Mlodinow [77]. Assume that the fields are linearly polarized as $\mathbf{B} = B\mathbf{e}_B$, $\mathbf{E} = E\mathbf{e}_E$, $\mathbf{D} = D\mathbf{e}_E$ with suitable *transverse* versors. The approximation of transverse guided field, can be dropped by choosing to integrate in the full space [39]). If the propagation is along the z direction, the axis of the fiber, the total energy reads

$$W = \int_0^L \left[\frac{1}{2\mu_0} B^2(z) + \int_{-\infty}^{t} E(\tau, z) \frac{\partial D}{\partial \tau}(\tau, z) d\tau \right] A_{\text{eff}} dz \tag{3.16}$$

where μ_0 is the vacuum magnetic permeability. For a general nonlinear medium, the electrostatic energy density require the integration over all displacements to be carried out. This is needed in general, as nonlinear polarization lead to non-

constant contributions to the electric energy along the various displacements[‡]. In absence of free charges $\nabla \cdot \mathbf{D} = 0$, and it is possible to introduce a dual vector potential Λ,

$$\mu_0 \frac{\partial \Lambda}{\partial t} = B \tag{3.17}$$

$$\frac{\partial \Lambda}{\partial z} = D \tag{3.18}$$

A possible Lagrangian density function, whose Euler-Lagrange equations are Maxwell equations, is

$$\mathcal{L} = C \left[\frac{1}{2} \mu_0 \dot{\Lambda}^2(z) - U \left(\frac{\partial}{\partial z} \Lambda(z), z \right) \right] \tag{3.19}$$

where U is electrostatic energy density in Eq. (3.16), and C a constant. Recall the Euler-Lagrange equation for the Lagrangian density which is dependent on a field ψ are, in symbolic form:

$$\frac{\partial \mathcal{L}}{\partial \psi} - \frac{\partial}{\partial t} \frac{\partial \mathcal{L}}{\partial (\partial_t \psi)} - \nabla \cdot \frac{\partial \mathcal{L}}{\partial (\nabla \psi)} = 0 \tag{3.20}$$

where ∂_t and ∂_z are shorthand notation for $\frac{\partial}{\partial t}$ and $\frac{\partial}{\partial z}$. So the Euler-Lagrange corresponding to the proposed density in Eq. (3.19) is

$$\frac{\partial}{\partial t} \frac{\partial \mathcal{L}}{\partial (\partial_t \Lambda)} + \frac{\partial}{\partial z} \frac{\partial \mathcal{L}}{\partial (\partial_z \Lambda)} = 0. \tag{3.21}$$

That is equivalent to Maxwell equations, when completed with the definition of the potential Λ. By observing the Euler-Lagrange equation, it is clear that the conjugate momentum is B, as

$$\frac{\partial \mathcal{L}}{\partial (\partial_t \Lambda)} = \mu_0 \dot{\Lambda} = B \tag{3.22}$$

The corresponding Hamiltonian can be written with the choice of a scale factor, and by requiring the equivalence to total energy, it can be written as $H = W$:

$$H = \int_0^L dz \left[B(z) \frac{\partial \Lambda}{\partial t} - \mathcal{L} \right] \tag{3.23}$$

[‡]We simply use the common argument of elements of electric field energy $dW_E = E\, dD$

with the choice of $C = 1$. Now we are ready to impose quantization of the fields, promoting to observables the fields $\hat{\Lambda}$, $\hat{B}$, and establishing the canonical commutator relation [32]. The equal time commutation relation is

$$[\hat{\Lambda}(z), \hat{B}(z')] = i\hbar\delta(z - z'). \tag{3.24}$$

The eigenstates which diagonalize the Hamiltonian, which will be Fock states, since the Hamiltonian include polarization energy, must be understood as coupled matter-field excitations, called "dressed" photons or photon-polaritons. Now let us apply a modal decomposition to the potential operator $\hat{\Lambda}$:

$$\hat{\Lambda}(t, z) = \sqrt{2\pi}\int_{-\infty}^{+\infty} d\beta \ \left[\hat{a}(\beta)\lambda(\beta)e^{i\beta z} + \hat{a}(\beta)^{\dagger}\lambda(\beta)^{*}e^{-i\beta z}\right]. \tag{3.25}$$

The expansion for the displacement is analogous, and it is found to be

$$\hat{D}(t, z) = i\sqrt{2\pi}\sqrt{\frac{\hbar\nu\varepsilon}{2\beta V}}\int_{-\infty}^{+\infty} d\beta \ \beta \left[\hat{a}(\beta)e^{i\beta z} - \hat{a}(\beta)^{\dagger}e^{-i\beta z}\right]. \tag{3.26}$$

Choosing normal ordering of operators, we obtain the Hamiltonian

$$\hat{H} = 2\pi\int_{-\infty}^{+\infty} d\beta \ \hbar\omega(\beta)\hat{a}^{\dagger}(\beta)\hat{a}(\beta) \tag{3.27}$$

where $\omega(\beta) = \omega_0$ for the present description of field, and will be generalized in the following section. The above Hamiltonian have been obtained by fixing

$$\lambda(\beta) = \sqrt{\frac{\hbar\nu\varepsilon}{2\beta V}} \tag{3.28}$$

where V is the effective mode volume $V = LA_{eff}$, ν is the phase velocity of light, such that $\omega(\beta)/\beta = \nu$, in a compatible manner with respect to the total energy.

3.2.2 *Treatment of dispersion*

The inclusion of dispersion, and the concept of a "dressed" photon, is straightforward. It turns out that the total Hamiltonian (3.27), derived in a similar way from a candidate Lagrangian that reproduces the classical field equations, will account for the dispersion in the term $\omega(\beta)$ [40]. Observe that, if the usual classical treatment of dispersion expands the propagation constant versus the frequency, in this case it is more natural to do the opposite. Without deriving the dispersion Lagrangian, let us start from Eq. (3.27), and compute the expansion to the second

order of $\omega(\beta)$, as it is the case of interest for GVD. The details of the susceptibility model are the same as the classical treatment [2]. Consider the task of describing pulse propagation. The pulse spectrum is regarded as a narrowband spectrum around the optical frequency ω_0, or, in propagation constant terms, β_0. Let us expand the frequency as

$$\omega(\beta) = \omega(\beta_0) + \sum_{n=1}^{\infty} \frac{1}{n!} \frac{d^n \omega}{d\beta^n}(\beta_0)\delta\beta^n \tag{3.29}$$

where $\delta\beta = \beta - \beta_0$. The evaluation in β_0 symbol is dropped in the following for brevity. Now, by assuming vanishing contribution to the field by components of propagation constant less than $\beta_0 - \Delta$ and more than $\beta_0 + \Delta$, we can restrict the integral in Eq. (3.27) as

$$\hat{H} = 2\hbar \int_{\beta_0-\Delta}^{\beta_0+\Delta} d\beta\ \omega(\beta)\hat{a}^\dagger(\beta)\hat{a}(\beta) \tag{3.30}$$

$$= 2\hbar \int_{\beta_0-\Delta}^{\beta_0+\Delta} d\beta \left(\omega_0 + \sum_{n=1}^{\infty} \frac{1}{n!} \frac{d^n \omega}{d\beta^n}\delta\beta^n\right) \hat{a}^\dagger(\beta)\hat{a}(\beta). \tag{3.31}$$

Let us now introduce the Fourier transform of ladder operators:

$$\hat{a}(z) = \frac{1}{2\pi} \int_{-\infty}^{+\infty} d\beta\ \hat{a}(\beta) \exp[i\beta z] \tag{3.32}$$

$$\hat{a}^\dagger(z) = \frac{1}{2\pi} \int_{-\infty}^{+\infty} d\beta\ \hat{a}^\dagger(\beta) \exp[-i\beta z] \tag{3.33}$$

so, using the transform representation for Eq. (3.33).

$$\hat{H} = \frac{\hbar}{2\pi} \int_{-\Delta}^{\Delta} d\delta\beta \left(\omega_0 + \sum_{n=1}^{\infty} \frac{1}{n!} \frac{d^n \omega}{d\beta^n}\delta\beta^n\right) \times \tag{3.34}$$

$$\times \int dz\ \hat{a}^\dagger(z) \int dz'\ \hat{a}\left(z'\right) \exp\left[i\delta\beta\left(z' - z\right)\right]. \tag{3.35}$$

After some passages, the expression can be written as [70, p. 447]:

$$\hat{H} = \hbar\omega_0 \int dz\ \hat{a}^\dagger(z)\hat{a}(z) + \hbar \sum_{n=1}^{\infty} \frac{(-i)^n}{n!} \frac{d^n \omega}{d\beta^n} \int dz \hat{a}^\dagger(z) \frac{\partial^n}{\partial z^n} \hat{a}(z), \tag{3.36}$$

So far, this is the Hamiltonian with ladder operators defined for creation and annihilation at the optical frequency. If one compute the same Hamiltonian using

the substitution $\hat{a}(z) \longrightarrow \hat{a}(z)\exp[i\omega_0 t]$, and restrict the summation to the second (GVD) term, the Hamiltonian reduces to

$$\hat{H} = -\frac{\hbar}{2}\frac{d^2\omega}{d\beta^2}\hat{a}^\dagger(z)\frac{\partial^2}{\partial z^2}\hat{a}(z), \tag{3.37}$$

or, using integration by parts,

$$\hat{H} = \frac{\hbar}{2}\frac{d^2\omega}{d\beta^2}\frac{\partial}{\partial z}\hat{a}^\dagger(z)\frac{\partial}{\partial z}\hat{a}(z). \tag{3.38}$$

This is the Hamiltonian of a particle with mass, so here the concept of "dressed" photon is defined as the coupled light and matter excitation that propagates accordingly to a Hamiltonian like the one above. In fact, ladder operator are in direct correspondance with the complex amplitude. Let us compute the Heisemberg equation of motion from the Hamiltonian (3.38)

$$\frac{\partial}{\partial t}\hat{a}(z) = i\frac{1}{2}\frac{d^2\omega}{d\beta^2}\frac{\partial^2}{\partial z^2}\hat{a}(z) \tag{3.39}$$

This operator equation is very similar to the NLSE, but with exchanged time and space variables. Observe that these variables are actually linked by the group velocity $v_g = \beta_1^{-1} = \frac{d\beta}{d\omega}(\omega_0)$, so it is possible to interchange the variables as

$$\frac{\partial}{\partial z}\hat{a}(v_g t) = i\frac{1}{2}\left(\frac{d\beta}{d\omega}(\omega_0)\right)^3\frac{d^2\omega}{d\beta^2}\frac{\partial^2}{\partial t^2}\hat{a}(v_g t) \tag{3.40}$$

which after a simple passage becomes completely analogous to the NLSE

$$\frac{\partial}{\partial z}\hat{a}(v_g t) = -i\frac{1}{2}\frac{d^2\beta}{d\omega^2}(\omega_0)\frac{\partial^2}{\partial t^2}\hat{a}(v_g t). \tag{3.41}$$

Let us now discuss the inclusion of the Kerr effect into the model.

3.2.3 *Nonlinear dispersive case*

Kerr effect can be effectively modeled in the fiber's Hamiltonian using the result [39, 38].

$$\hat{H} = 2\pi\int d\beta\hbar\omega(\beta)\hat{a}^\dagger(\beta)\hat{a}(\beta) - \int d^3\mathbf{x}\left[\left(\frac{\chi^{(3)}(\mathbf{x})}{4\varepsilon^3(\omega_0)}\right) : |\hat{\mathbf{D}}|^4(\mathbf{x}) :\right] \tag{3.42}$$

where $\chi^{(3)}$ is the third order (Kerr) susceptibility and ε is the medium electric permittivity. For given operator $\hat{O}$, The notation $: \hat{O} :$ denotes operator normal (or

Wick) ordering, i.e. the disposition of all creation operators to the left side in the ladder operator expansion. By utilizing the rotating wave approximation [52], it is possible to write

$$-\int d^3\mathbf{x}\left[\left(\frac{\chi^{(3)}(\mathbf{x})}{4\varepsilon^3(\omega_0)}\right):|\hat{\mathbf{D}}|^4(\mathbf{x}):\right]\approx-\hbar\frac{K}{2}\int dz\hat{a}^\dagger(z)\hat{a}^\dagger(z)\hat{a}(z)\hat{a}(z) \tag{3.43}$$

where $K=\hbar\omega_0 v_g\gamma$. Recall $\gamma=\frac{n_2\omega_0}{cA_{eff}}$ where c is the speed of light in vacuum. Finally, the total Hamiltonian will be, utilizing the normalization that leads to the complex amplitude $\hat{a}(z)\longrightarrow\hat{a}(z)\exp[i\omega_0 t]$:

$$\hat{H}=\hbar\left[\frac{\omega_2}{2}\int dz\,\frac{\partial}{\partial z}\hat{a}^\dagger(z)\frac{\partial}{\partial z}\hat{a}(z)-\frac{K}{2}\int dz\,\hat{a}^\dagger(z)\hat{a}^\dagger(z)\hat{a}(z)\hat{a}(z)\right] \tag{3.44}$$

where $\omega_2=\frac{d^2\omega}{d\beta^2}$.

Notice that the previous formulation completely neglects attenuation. In fact, it is not trivial to include attenuation into the Hamiltonian formulation, as it is usually done in the phenomenological classical model. The role of attenuation on quantum system dynamics will be addressed later in section 3.3.5. The Kerr effect in the fiber induces light squeezing [71]. Nonlinear phenomena in quantum optics open up a plethora of experimental methods and technological tools, like squeezed light manipulation and quantum non-demolition measurements [94, 85].

3.2.4 *Hartree ansatz and mean-field equation*

There is a strong similarity between the classically-derived NLSE, and the mean-field equation in the many-body theory of interacting bosons with δ contact interaction potential. One can indeed argue that the NLSE *is* the mean field equation from the many-body Hamiltonian of the dispersive fiber with Kerr effect, as commented by Lai and Haus [99, 100]. Following their work, let us derive the equation using Hartree variational principle. This point of view is useful to strengthen the binding between many-body theory and fiber optics. Future perspective may open up as the usage of beyond mean-field correction terms in the treatment of quantum fields of photons inside the fiber, in a similar way to the treatment of Bose-Einstein condensate in atomic gases using Lee-Huang-Yang corrections.

Let us approach the problem of formulating the dynamics of the quantum field in the Schrödinger picture, instead of the previously used Heisemberg picture. Starting from the Hamiltonian (3.44), we recall that in Schrödinger

picture observables, differently from states, do not evolve with time, and the corresponding Schrödinger equation for the state $|\psi\rangle$ reads

$$i\hbar\frac{d|\psi\rangle}{dt} = \hat{H}|\psi\rangle \tag{3.45}$$

Any quantum state of the system can be expressed in the Fock basis as

$$|\psi\rangle = \sum_n a_n \int dz_1 ... dz_n \, \frac{1}{\sqrt{n!}} f_n(z_1, ..., z_n, t)\hat{a}^\dagger(z_1)...\hat{a}^\dagger(z_n)|0\rangle \tag{3.46}$$

this expression is justified as $|\psi\rangle$ is a generic superposition of the n particle states, which are generated by integrating the contribution of pure states regarding the creation of photons at given set of positions $(x_1, ..., x_n)$. In this case the vacuum state must be interpreted as the tensor product of n single particle vacuum states. The function f_n serves as the many-body wavefunction for a number state n associated with given positions. It is symmetric because of bosonic nature of photons, and we require it to satisfy

$$\int dz_1 ... dz_n \, |f_n(z_1, ..., z_n)|^2 = 1 \qquad \forall n, t. \tag{3.47}$$

Moreover, we impose the normalization of coefficients

$$\sum_n |a_n|^2 = 1. \tag{3.48}$$

By substituting Eq. (3.46) into Schrödinger equation (3.45), a condition for the wavefunction is derived:

$$i\hbar\frac{df_n}{dt}(z_1, ..., z_n, t) = \left[\frac{\omega_2}{2}\sum_{j=1}^{n}\frac{\partial^2}{\partial z_j^2} - K\sum_{1\leqslant i<j\leqslant n}\delta(z_j - z_i)\right] f_n(z_1, ..., z_n, t). \tag{3.49}$$

This is the Schrödinger equation for a system of bosons with point-contact interaction [79]. Assuming that f_n is an eigensolution of the operator on the right-hand side, it is possible to separate:

$$f_n(z_1, ..., z_n, t) = f_n(z_1, ..., z_n)\exp[-iE_n t] \tag{3.50}$$

where E_n is a separation variable, physically representing a frequency. We obtain the separated equation

$$\left[\frac{\omega_2}{2}\sum_{j=1}^{n}\frac{\partial^2}{\partial z_j^2} - K\sum_{1\leqslant i<j\leqslant n}\delta(z_j - z_i)\right] f_n(z_1,...,z_n) = E_n f_n(z_1,...,z_n) \tag{3.51}$$

Now it is possible to use the so-called *time independent Hartree approximation*, of which the solution ansatz is called $f^{(H)}$,

$$f_n^{(H)}(z_1,...,z_n,t) = \prod_{j=1}^{n}\Phi_n(z_j,t), \tag{3.52}$$

in which the single particle wave functions Φ_n are to be found by minimization of the following functional

$$\begin{aligned}\langle\psi|i\frac{\partial}{\partial t} - \hat{H}|\psi\rangle &= \int f_n^{(H)*}\left[i\frac{\partial}{\partial t} - \frac{\omega_2}{2}\sum_{j=1}^{n}\frac{\partial^2}{\partial z_j^2} + K\sum_{1\leqslant i<j\leqslant n}\delta(z_j - z_i)\right] f_n^{(H)} \\ &= n\int dz\ \Phi_n^*\left[i\frac{\partial}{\partial t} - (n-1)\Phi_n^*\Phi_n\right]\Phi_n\end{aligned} \tag{3.53}$$

The corresponding Euler-Lagrange equation is a NLSE

$$\frac{\partial}{\partial t}\Phi_n = -i\frac{\omega_2}{2}\frac{\partial^2}{\partial z^2}\Phi_n + iK(n-1)\Phi_n^*\Phi_n\Phi_n. \tag{3.54}$$

The mean-field approach consists in the fact that all the particles obey the same potential, which is not dependent on an expression like f_n, which involves all the particle positions, but only on the single-particle wavefunction itself. The Hartree method gives a direct relationship between photon wavefunction and complex amplitude of the field, as expected.

By using a transformation which is analogous to the one utilized in 3.2.2, the equation can be made to correspond exactly to the NLSE, with the exception of the factor $(n-1)$, which can be however normalized with different definitions [155].

3.3 APPLICATIONS OF QUANTIZED FIELD METHODS

3.3.1 *Quantization and fiber modes*

Following Haus [70], we want to connect the formalism of second quantization with usual field descriptions in an elementary setting, and describe the main

aspects of nondispersive linear fiber propagation, from the point of view of quantized fields. This will lead us to the quantum treatment of attenuation and the description of quantum noise in waveguides. We represent the modes of a ring resonator of length L as harmonic oscillators. Suppose the m mode is at a frequency ω_m: classical mode amplitude obeys the equation

$$\frac{dA_m}{dt} = -i\omega_m A_m, \tag{3.55}$$

were we have assumed $|A_m|^2$ normalized to be the mode energy. The electric field amplitude of the mode m is proportional to the in-phase component of the complex amplitude, called $A_m^{(1)}(t)$,

$$E_m(t) \propto A_m^{(1)}(t) := \frac{1}{2}[A_m(t) + A_m^*(t)], \tag{3.56}$$

vice versa, the quadrature component $A_m^{(2)}(t)$ is defined as

$$A_m^{(2)}(t) := \frac{1}{2i}[A_m(t) - A_m^*(t)]. \tag{3.57}$$

By comparison with harmonic oscillator variables [70, p. 198], we recognize the operator representing A_m as the m-th mode annihilation operator $\hat{A}_m$. The creation operator $\hat{A}_m^\dagger$ represents its conjugate A_m^*. Representing states in Fock basis, we have the usual relations

$$\hat{A}_m |n_m\rangle = \sqrt{n_m}\,|n_m - 1\rangle \tag{3.58}$$

$$\hat{A}_m^\dagger |n_m\rangle = \sqrt{n_m + 1}\,|n_m + 1\rangle \tag{3.59}$$

and the commutation relation

$$\left[\hat{A}_n, \hat{A}_m^\dagger\right] = \delta_{nm}. \tag{3.60}$$

We can now write the Hamiltonian of the system, composed by all modes, as

$$\hat{H} = \sum_m \hbar\omega_m \left(\hat{A}_m^\dagger \hat{A}_m + \frac{1}{2}\right), \tag{3.61}$$

where the vacuum energy is represented by the term $\frac{1}{2}$ inside the brackets. From the Hamiltonian, Heisemberg equation of motion are derivable as

$$\frac{d\hat{A}_m}{dt} = -\frac{i}{\hbar}[\hat{A}_m, \hat{H}] \tag{3.62}$$

So, by using equations (3.60), (3.61), we find a direct correspondence between classical equations of field evolution and Heisemberg equation on ladder operators, via direct correspondence with harmonic oscillator conjugate variables:

$$\frac{d\hat{A}_m}{dt} = -i\omega_m \hat{A}_m \tag{3.63}$$

Since the spatial integral of quantization extends to L, the observable $\hat{H}$ may be viewed as the energy per length L. The transmission of a quantum state in a telecommunication scenario is characterized by a specific length L corresponding to the symbol period T via $L = v_g T$, where v_g is the group velocity. By using laser fields, the transmitted states can be regarded as coherent states.

3.3.2 *Coherent states for laser radiation*

Let us suppose to concentrate in a single mode of the radiation field, and to adopt its annihilation and creation operators – defined above – with the notation $\hat{A}$ and $\hat{A}^\dagger$ without subscripts. Coherent states have been systematically studied for the first time by Glauber [57, 58], addressing the solution of coherence in quantum radiation, which, involving different ordering of operators, is different from classical theory. They are states which can be defined in Fock basis as

$$|\alpha\rangle = e^{-\frac{|\alpha|^2}{2}} \sum_{n=0}^{+\infty} \frac{\alpha^n}{\sqrt{n!}} |n\rangle \,, \tag{3.64}$$

where $\alpha \in \mathbb{C}$. A crucial property of the coherent states is that they are the eigenstates of the creation operator:

$$\hat{A}^\dagger |\alpha\rangle = \alpha |\alpha\rangle \,. \tag{3.65}$$

It is known that laser radiation can be represented using coherent states [5]. The coherence property of radiation is intimately connected to the quantum behaviour [107]. For example classical interferometry is able to measure field coherence up to the second order. Higher order correlations were measured for the first time in a radioastronomy experiment from Hambury, Brown and Twiss [142], and were later found to be related to quantum description of radiation. Now we are ready to derive the semiclassical model of optical receivers. Consider

the evaluation of the distribution of the photon number from the coherent state. Computing the M^{th} order moment gives, after some passages:

$$\langle\alpha|(\hat{A}^{\dagger}\hat{A})^{M}|\alpha\rangle = e^{-|\alpha|^2}\sum_{n}\frac{|\alpha|^{2n}}{n!}n^{M}, \tag{3.66}$$

in this formulation, we recognize the probability distribution

$$p(n) = e^{-|\alpha|^2}\frac{|\alpha|^{2n}}{n!}, \tag{3.67}$$

so the number distribution of a coherent state is Poisson's of parameter $|\alpha|^2$. This is the result used in the semiclassical treatment of shot noise.

By using coherent states, we are able to encode in the quantum domain the properties of a classical coherent radiation field, for example from a infrared laser device. Consider now the role of detection. We will show how the detection performance will be affected by the quantum properties of the fields.

3.3.3 *Quantum theory of detection*

The creation and annihilation operators are not Hermitian, hence they cannot represent an observable. Nonetheless, the in-phase and quadrature operators are. In fact they represent conjugate variable analogous to the position and momentum ones in a harmonic oscillator. From a practical point of view, they are the variables which are ultimately measured in detection. Let us only consider theoretical limitations on the amplitude fluctuations, without including a full theory of detection. We may take into account the commutator relations for the quadrature components, that plays the role of a noise term as will be described. The ultimate noise limit on the product of the uncertainties is determined by the commutator, via the Heisemberg uncertainty relation. Heisemberg uncertainty relation is a simple algebraic result on Hilbert spaces. In order to illustrate that, consider two non-commuting observables $\hat{X}$, $\hat{Y}$, whose commutator is

$$[\hat{X},\hat{Y}] = iC \tag{3.68}$$

we are interested in computing a bound on the uncertainty product

$$\left\langle\Delta\hat{X}^2\right\rangle\left\langle\Delta\hat{Y}^2\right\rangle = \left(\left\langle\hat{X}^2\right\rangle - \langle\hat{X}\rangle^2\right)\left(\left\langle\hat{Y}^2\right\rangle - \langle\hat{Y}\rangle^2\right)$$

In fact, for an arbitrary state $|\psi\rangle$, the expectation of the quadratic errors can be written as the inner product between transformed states in the form $\Delta\hat{X}|\psi\rangle$:

$$\langle\psi|\Delta\hat{X}^2|\psi\rangle = \langle\psi|\,\Delta\hat{X}\Delta\hat{X}\,|\psi\rangle\,, \tag{3.69}$$

and similarly for Y. Let us define the auxiliary operators $\hat{x} = \Delta\hat{X}$ and $\hat{y} = \Delta\hat{Y}$. Such inner product obey the Schwarz inequality in the Hilbert space, which reads

$$\langle\psi|\hat{x}^2|\psi\rangle\ \langle\psi|\hat{y}^2|\psi\rangle \geqslant |\,\langle\psi|\hat{x}\hat{y}|\psi\rangle\,|^2 \tag{3.70}$$

By expressing the operator product $\hat{x}\hat{y}$ in commutative and anticommutative terms, and by using the commutator, already fixed before, we obtain

$$\hat{x}\hat{y} = \frac{1}{2}(\hat{x}\hat{y} + \hat{y}\hat{x}) + \frac{1}{2}iC \tag{3.71}$$

so by substitution we get the uncertainty relation

$$\left\langle\Delta\hat{X}^2\right\rangle\left\langle\Delta\hat{Y}^2\right\rangle \geqslant \frac{1}{4}C^2. \tag{3.72}$$

From a practical point of view, detection of both quadrature components is of interest in the case of coherent detection: coherent modulations encode information in both quadratures. Instead, for IM/DD systems, we are interested in detecting only the energy, that is associated with the photon number, which is a combination of the quadrature components, and it is possible to reduce the uncertainty for that particular combination, as there is no Heisemberg limit. This technique is often called "photon antibunching", and it is achieved via light squeezing [116, 52, 104]. The origins of this idea trace back to the first studies on vacuum electron devices in the microwave domain, such as travelling wave tubes and amplifiers [71].

Let us describe a simplified detection process in some detail, and compute the fluctuations for two detection methods, direct detection and homodyne detection, as described in section 1.2. First of all, for direct detection, we define the photoelectron (or electron-hole pair) number operator for a symbol time T, corresponding to a length $L = v_g T$, using the creation and annihilation operators of the modes inside this fiber length. Supposing an ideal photodetector with quantum efficiency equal to 1,

$$\hat{Q} = q\hat{A}^\dagger\hat{A}. \tag{3.73}$$

where q is the elementary charge. Considering the detection of a coherent state $|\alpha\rangle$ assigned to the time slot of interest, it is possible to simply compute the moments of the photoelectron operator, and obtain the noise, expressed as the variance.

$$\langle\alpha|\hat{Q}^2|\alpha\rangle - \langle\alpha|\hat{Q}|\alpha\rangle^2 = q^2\langle\alpha|n|\alpha\rangle = q^2|\alpha|^2 \tag{3.74}$$

this result corresponds to the variance of the corresponding Poisson random variable multiplied by the charge q. So, for direct detection, the full quantum theoretical treatment does not add more information power with respect to the semiclassical Poisson model. However, the physical origin of this noise term is due to the non-zero commutator of ladder operators. Indeed, it holds

$$\left\langle\hat{Q}^2\right\rangle = \left\langle\hat{A}^\dagger\hat{A}\hat{A}^\dagger\hat{A}\right\rangle; \tag{3.75}$$

in general, operator ordering plays a major role in the description of quantum noise.

Let us consider now the description of balanced homodyne detection. Referring to a simple setup as the one in Fig. 1.5a, we express the field operators at the output branches of the coupler with the observables $\hat{B}_1$, $\hat{B}_2$. By using known phase properties of the coupler, from its scattering matrix, and indicating the local oscillator field with $\hat{A}_L$, it holds

$$\hat{B}_1 = \frac{1}{\sqrt{2}}(\hat{A}_L - i\hat{A}) \tag{3.76}$$

$$\hat{B}_2 = \frac{1}{\sqrt{2}}(-i\hat{A}_L + \hat{A}) \tag{3.77}$$

The outcoming charge after the difference detector is, after some simple algebra

$$\hat{Q} = q(\hat{B}_1^\dagger\hat{B}_1 - \hat{B}_2^\dagger\hat{B}_2) \tag{3.78}$$

$$= q(\hat{A}_L^\dagger\hat{A} + \hat{A}^\dagger\hat{A}_L). \tag{3.79}$$

Consider the reception of a coherent state $|\alpha\rangle$, with the local oscillator in the coherent state $|\alpha_L\rangle$, some passages lead to

$$\left\langle\hat{Q}^2\right\rangle - \langle\hat{Q}\rangle^2 = q^2(|\alpha|^2 + |\alpha_L|^2) \tag{3.80}$$

This detector correspond to one of the pair of detector needed to receive a coherent modulated signal. In particular, it is the measure of the in-phase component of the field, as it is clearly seen by multiplying the in-phase component of the

received field. The noise due to measurement of both in-phase and quadrature components is subjected to the Heisemberg uncertainty relation. This is the maximum performance of a receiver such as the one in the case of the phase-diversity receiver shown in Fig. 1.5b.

3.3.4 *Classical treatment of thermal noise*

A simple and instructive quantum model is the treatment of noise in a waveguide with losses [70]. We discuss the thermal noise case as it illustrates some useful techniques, and highlight the parallelism between quantum and classical models. First of all, we will consider a ring resonator of length L, which support modes that will be equally spaced from the spectral point of view. This will be done without loss of generality, as, taking the limit $L \to \infty$, the modes will be represented in a continuum of possible frequencies. Consider a mode of amplitude A_n and propagation constant β_n in a single mode waveguide. For example, this could be the case of one polarization inside a single mode fiber. Let A_n be normalized such that $|A_n|^2$ represents the mode energy. Let the system be at thermal equilibrium. Since there are two degrees of freedom associated to every mode, by the equipartition theorem [79] of classical statistical mechanics, the statistical average of the mode energy is

$$\left\langle |A_n|^2 \right\rangle = k_B \theta \tag{3.81}$$

where k_B is the Boltzmann constant and θ is the absolute temperature. Furthermore, by the requirement that the propagation is stationary, the modes must be uncorrelated. If $n \neq m$:

$$\langle A_n A_m^* \rangle = 0 \tag{3.82}$$

Now consider the computation of the average energy per unit length, and introduce another definition of the mode amplitude. Let β be the propagation constant, and $\Delta\beta$ the mode spacing in reciprocal space. By taking the limit of small spacing $\Delta\beta$

$$\sum_{n,m} \left\langle \frac{A_n^* A_m}{L} \right\rangle = \sum_{n,m} \frac{1}{L} \left(\frac{\Delta\beta L}{2\pi} \right)^2 \langle A_n^* A_m \rangle \approx \int d\beta \int d\beta' \left\langle a^*(\beta) a\left(\beta'\right) \right\rangle, \tag{3.83}$$

this is done introducing the new mode amplitude definition

$$a(\beta) = \frac{\sqrt{L}}{2\pi} A_n. \tag{3.84}$$

In this way the requirements on the correlation between modes translate into

$$\langle a(\beta)a(\beta')\rangle = \frac{1}{2\pi}k_B\theta\delta(\beta-\beta') \tag{3.85}$$

Finally, it is possible to derive the Nyquist formula for the thermal power spectral density propagating in each mode in a bandwidth B.

$$\mathcal{P} = k\theta \tag{3.86}$$

The typical "ultraviolet catastrophe" for white noise is evident: integrating the power spectral density for all the propagation constants, we obtain divergence. Utilizing the Bose statistics for energy distribution at finite temperature we are able to correct the result as in Planck black body radiation analysis [134].

Suppose now to include losses in the waveguide. For each mode amplitude in the continuum of propagation constants β, supposing constant attenuation rate α, it holds

$$\frac{d}{dz}a(\beta) = (i\beta-\alpha)a(\beta)+s(\beta,z) \tag{3.87}$$

while the introduction of s, which is a random variable, the so-called *Langevin* source, seems arbitrary, it is needed for the conservation of noise spectrum. In fact, since the waveguide is at thermal equilibrium, the noise spectrum must be constant with respect to the position z. By imposing this property, we are able to characterize in a stochastic manner the term s:

$$\frac{d}{dz}\left[\langle a(\beta)a^*(\beta')\rangle\right] = -2\alpha\left\langle a(\beta)a^*\left(\beta'\right)\right\rangle + \left\langle s(\beta,z)a^*\left(\beta'\right)+a(\beta)s^*\left(\beta',z\right)\right\rangle = 0 \tag{3.88}$$

Now notice that loss is physically due to coupling to charges which will be different from point to point. This means that noise source correlation is local

$$\langle s(\beta,z)s(\beta,z')\rangle) = \delta(z-z') \tag{3.89}$$

The only relevant term in the expectation value of cross a and s terms is the contribution of the noise source s to the mode amplitude. Over a length Δz, the average contribution is $\Delta z/2s(z)$. So the requirement (3.88) translates into

$$-2\alpha\left\langle a(\beta)a^*\left(\beta'\right)\right\rangle + \frac{\Delta z}{2}\left\langle s(\beta,z)s^*(\beta',z)+s(\beta,z)s^*(\beta',z)\right\rangle = 0 \tag{3.90}$$

taking the limit $\Delta z \to 0$ we are finally able to characterize the noise source

$$\left\langle s(\beta, z), s^*(\beta', z') \right\rangle = \frac{1}{2\pi} 2\alpha k \theta \delta(z - z') \delta(\beta - \beta') \tag{3.91}$$

The generalization to frequency dependent attenuation is straightforward. Notice that, being the noise approximately Gaussian distributed by the Central Limit theorem, the second-moment characterization of the process specify in a unique way the noise. We have seen that the conservation of noise correlation require some statistical properties of Langevin sources. In the quantum domain, the same role is played by the commutator operator.

3.3.5 *Quantum treatment of loss and fluctuations*

By using the formalism developed in section 3.3.1, ladder operators in the continuum of propagation constants inside the optical fiber can be introduced. Observing the structure of the ladder operator in the ring resonator case of Eq. (3.61), it can be noticed that the term $\left\langle \hat{A}_m^\dagger \hat{A}_m \right\rangle$ represents the average number of photons in the mode m. By considering the normalization of the annihilation operator as the section before, we obtain

$$\hat{a}(\beta) = \frac{\sqrt{L}}{2\pi} \hat{A}_m \tag{3.92}$$

and similarly for the creation operator. It is possible to obtain the commutation relation also for continuous ladder operators as

$$[\hat{a}(\beta), \hat{a}^\dagger(\beta')] = \frac{1}{2\pi} \delta(\beta - \beta') \tag{3.93}$$

By omitting zero-point energy, which does not influence the actual Heisemberg equations of motions, the Hamiltonian is

$$\hat{H} = 2\pi\hbar \int d\beta \omega(\beta) \hat{a}^\dagger(\beta) \hat{a}(\beta) \tag{3.94}$$

Now, consider propagation in presence of losses. In an equivalent way as the classical treatment, let us write the equation of motion which includes decay of the mode amplitude. In order to do that, assume to normalize the field amplitude operator replacing $\hat{a}(\beta)$ with $\hat{a}(\beta) \exp[-i\omega t]$ and remove so the usual phase

progression term $\exp[-i\omega t]$ in the dynamical description. Adding the additional, still uncharacterized, noise term [68], the equation reads

$$\frac{d}{dt}\hat{a}(\beta) = -\sigma(\beta)\hat{a}(\beta) + \hat{s}(\beta). \tag{3.95}$$

where σ represent a classical decay, and $\hat{s}$ is the noise source. The interpretation of the noise term operator is the coupling to loss reservoirs, and actually the new operator calls for a renewed Hilbert space of the system. The concept of a *reservoir* is a statistical mechanics tool useful to represent a subsystem in thermal equilibrium with which coupling of the subsystem of interest occurs. Since a full microscopic model of the loss would be complicated, the concept of reservoir is paramount for calculating mean effect of coupling. In this case, in order to model noise, it is not even required to obtain an detailed expression for coupling to loss reservoir. In fact, the commutator bracket must be preserved [52, 70], as it is an intrinsic property of the ladder operators. Expressing this requirement in the previous evolution equation, yields

$$\begin{aligned}\frac{d}{dt}\left[\hat{a}(\beta), \hat{a}^{\dagger}\left(\beta'\right)\right] =& -\left[\sigma(\beta) + \sigma\left(\beta'\right)\right]\left[\hat{a}(\beta), \hat{a}^{\dagger}\left(\beta'\right)\right] \\ &+ \left[\hat{s}(\beta), \hat{a}^{\dagger}\left(\beta'\right)\right] + \left[\hat{a}(\beta), \hat{s}^{\dagger}\left(\beta'\right)\right] \\ =&0.\end{aligned} \tag{3.96}$$

By considering the influence of the noise term into the mode amplitude, the commutator encodes the suppression of mode photons. Its averaged effect over a time Δt is

$$\left[\hat{s}(\beta), \hat{a}^{\dagger}(\beta')\right] = \frac{1}{2}\left[\hat{s}(\beta), \hat{s}^{\dagger}(\beta')\right]\Delta t, \tag{3.97}$$

and by using the commutator of the ladder operators,

$$\left[\hat{s}(\beta), \hat{s}^{\dagger}(\beta')\right] = \frac{1}{2\pi}2\sigma(\beta)\delta(t - t')\delta(\beta - \beta'). \tag{3.98}$$

Since the equation of motion is linear in the operators, integration can be formally done like with c-numbers. Supposing to propagate the field until time T:

$$\hat{a}(\beta, T) = \exp\left[-\sigma T\right]\left(\hat{a}(\beta, 0) + \int_0^T dt\ \exp[\sigma t]\hat{s}(\beta)\right). \tag{3.99}$$

The above equation and its Hermitian conjugate allow for the computation of the propagated field. Finally, if one carries out the calculation for a mode field in coherent state and ground state for reservoirs, an interesting result will be

obtained. Suppose that the coupled system is in the product state $|\alpha(\beta)\rangle|0\rangle := |\alpha(\beta)\rangle \otimes |0\rangle$. It is interesting to compute the average fluctuations of the in-phase and quadrature component of the field. First of all, let us compute the average photon number, averaging over all possible modes

$$\left\langle 2\pi \int d\beta\ \hat{a}^{\dagger}(\beta, T)\hat{a}(\beta, T) \right\rangle = \exp(-2\sigma T)|\alpha(\beta)|^2 \tag{3.100}$$

notice the reduction due to the absorption rate. Computing the in-phase fluctuations, using the definition of this operator, and properties of coherent states

$$\begin{aligned} &\left\langle \hat{a}^{(1)}(\beta, T)\hat{a}^{(1)}(\beta', T) \right\rangle - \left\langle \hat{a}^{(1)}(\beta, T) \right\rangle \left\langle \hat{a}^{(1)}(\beta', T) \right\rangle = \\ &= \frac{1}{4}\frac{1}{2\pi}\delta(\beta - \beta') \end{aligned} \tag{3.101}$$

the result for the quadrature fluctuation is identical.

In conclusion, we have seen that the argument of conservation of commutator brackets implies characterization of noise sources, in an analogous way as Langevin sources. There is an important duality in the principles: conservation of noise energy at thermal equilibrium and conservation of commutator brackets. Moreover, by computing the quantum fluctuations with the loss reservoir at the ground state, it was possible to acknowledge the resemblance of quantum fluctuations and thermal noise.

3.4 PHASE-SPACE METHODS

Working with operator equations in field theory is often impractical. As we have described before, the most common way to operate in practical computations is by using density matrices. In order to obtain representations for those matrices, a particular basis of states must be selected. This corresponds to the choice of a particular representation in phase-space, called also phase-space of harmonic oscillator density operator. Since the dynamics will be described using the density matrix, which depends on the choice of the basis, by specializing the basis on a coherent state variables, the density matrix equations can be converted in c-number equations. In fact, dynamics in the phase-space representation can be readily described using Itô or Stratonovich integrals in stochastic differential equations, under reasonable assumptions [22, 23, 107].

Let us introduce the topic by comparing the general theory of random variable characteristic functions with the one in a quantum framework. When dealing with continuous random variables a particularly useful tool is the so-called

"characteristic function", which corresponds to the Fourier transform of the probability density function (p.d.f.). If the variable is X, then the characteristic function is defined as:

$$C(\xi) = \langle \exp[i\xi X] \rangle , \tag{3.102}$$

where $\langle \cdot \rangle$ indicates the expectation operator.

In a similar way, a quantum version of the characteristic function can be defined. If $\hat{X}$ is an observable, its characteristic function is:

$$C(\xi) = \left\langle \exp\left[i\xi \hat{X}\right] \right\rangle , \tag{3.103}$$

where $\langle \cdot \rangle$ indicates the expected value with respect to a state. However, since the observables are typically expressed as sums of ladder operators, the exponentiation becomes inconvenient, as it may contain different orders. A useful identity, called Baker-Hausdorff identity, relate the exponentiation procedure with simpler steps:

$$\exp\left[i\xi(\hat{X} + \hat{Y})\right] = \exp\left[i\xi\hat{X}\right] \exp\left[i\xi\hat{Y}\right] \exp\left[\frac{\xi^2}{2}[\hat{X}, \hat{Y}]\right] . \tag{3.104}$$

Let us consider a coherent state $|\alpha\rangle$. For such a state, the in-phase component is

$$\langle \alpha | \hat{A}^{(1)} | \alpha \rangle = \frac{1}{2}(a + a^*). \tag{3.105}$$

By calculating the Baker-Hausdorff expansion related to $\hat{A}^{(1)}$, we are able to find not only the expected value of the in-phase component, but the whole statistics. The computation gives

$$C(\xi) = \exp\left[-\frac{\xi^2}{8} + i\xi\frac{\alpha + \alpha^*}{2}\right] . \tag{3.106}$$

This expression resembles the characteristic function of a Gaussian random variable with mean $(\alpha + \alpha^*)/2$ and variance 1/4. Indeed, since the interpretation of probability density is valid in this case, we found that the corresponding in-phase component is Gaussian distributed. An analogous argument holds for the quadrature component, for which the result is identical. A similar argument can be carried out for the thermal state, which is

$$|\theta\rangle = \sum_n c_n |n\rangle \tag{3.107}$$

where $|n\rangle$ is the number state and c_n obeys the Bose-Einstein distribution p_{B-E} as

$$\langle c_n c_m^* \rangle = \delta_{nm} p_{B-E}(n). \tag{3.108}$$

Computing the characteristic function of the in-phase component expressed in terms of ladder operators, it is found to correspond to a Gaussian distribution

$$C(\xi) = \exp\left[-\frac{\xi^2(1+2\langle n\rangle)}{8}\right], \tag{3.109}$$

that have zero mean and $(1+2\langle n\rangle)/4$ variance. The same holds for the quadrature component.

Now the interesting question to be asked is how this technique generalizes to multiple observables, like for example in the case of joint in-phase and quadrature observables. In the case of random variables, the generalization is straightforward: given X_1, and X_2 jointly distributed random variables, their characteristic function is defined as:

$$C(\xi_1, \xi_2) = \langle \exp[i(\xi_1 X_1 + \xi_2 X_2)] \rangle . \tag{3.110}$$

The Fourier transform of the characteristic function is the joint distribution function. In the case of observables, however, the order of the operators introduce novel aspects that are to be considered.

3.4.1 *Wigner distribution*

Let us consider two non-commuting observables, $\hat{X}_1$ and $\hat{X}_2$. Let the characteristic function be defined as:

$$C(\xi_1, \xi_2) = \left\langle \exp\left[i(\xi_1 \hat{X}_1 + \xi_2 \hat{X}_2)\right] \right\rangle . \tag{3.111}$$

The Wigner function is defined as the inverse Fourier transform of the characteristic function expressed with observables [3].

$$W(x_1, x_2) = \left(\frac{1}{2\pi}\right)^2 \int d\xi_1 \int d\xi_2 C(\xi_1, \xi_2) \exp(-i\xi_1 x_1 - i\xi_2 x_2) \tag{3.112}$$

[3] In probability theory it is often the case that the convention of the "reciprocal" domain is changed of sign with respect to the usual Fourier transform. When referring to characteristic functions, the conventional probabilistic definition is used [46].

The "marginal", which is the integral of the Wigner function with respect to one of the two variables, can be interpreted as a probability, whereas the Wigner function itself cannot – it can even become negative. It turns out that, for a coherent state $|\alpha\rangle$, if we define the variables corresponding to the observables as A_1 and A_2, for the in-phase and quadrature components, respectively, the the Wigner function is

$$W(A_1, A_2) = \frac{1}{2\pi} \exp\left[-2\left[A_1 - \mathrm{Re}(\alpha)\right]^2\right] \exp\left[-2\left[A_2 - \mathrm{Im}(\alpha)\right]^2\right] \tag{3.113}$$

which is represented by a bivariate Gaussian function.

When the Wigner function is computed with respect to the density operator, we obtain a phase-space representation for the state [22]. In order to generalize the theory of the characteristic function, we introduce the concept of *quantum characteristic function*, which leverages the description in terms of ladder operators. Given a state with density matrix ρ, it is defined as [52]:

$$\chi(\lambda, \lambda^*) = \mathrm{Tr}\left[\rho \exp\left[\lambda \hat{a}^\dagger - \lambda^* \hat{a}\right]\right] \tag{3.114}$$

This is analogous to the previous definition, but *specialized* to the case of ladder operators. The quantum characteristic function has the property of generating all the normally-ordered moments [52, p. 121]. So the a straightforward representation for the density matrix is represented by the Wigner function

$$W(\alpha, \alpha^*) = \frac{1}{\pi^2} \int \mathrm{d}^2\lambda \, \chi(\lambda, \lambda^*) \exp\left(\lambda\alpha^* + \lambda^*\alpha\right) \tag{3.115}$$

The Wigner representation is a symmetrically-ordered operator representation, and it is suited for applications in which the field behaves almost classically [54].

3.4.2 *Glauber-Sudarshan P representation*

Since the coherent stated have many useful properties, a decomposition of the density operator in terms of those states is particularly useful. This approach, developed by Glauber and Sudarshan [57] is called P-representation, and the P function is defined as:

$$\rho = \int \mathrm{d}^2\alpha \, P(\alpha, \alpha^*) \, |\alpha\rangle \langle\alpha| \tag{3.116}$$

Recall that

$$\int d^2\alpha \ |\alpha\rangle \langle\alpha| = \pi \sum_n |n\rangle \langle n| = \pi \tag{3.117}$$

and, due to the definition,

$$\mathrm{Tr}[\rho] = \int d^2\alpha \ P(\alpha, \alpha^*) = 1 \tag{3.118}$$

Moments are generated by

$$\left\langle \hat{a}^{\dagger r} \hat{a}^s \right\rangle = \int d^2\alpha \ \alpha^{*r} \alpha^s P(\alpha, \alpha^*) \tag{3.119}$$

The Glauber-Sudarshan representation is a normally-ordered operator representation, and it is suited for applications in which the field behaves almost classically [54].

3.4.3 *Positive definite P representation (+P)*

The previous functions cannot in general be interpreted as positive definite probability distributions, however, at the cost of doubling the number of phase-space variables, an approach from Drummond and Gardiner [35] gives the wanted property. Because of this property, it is possble to derive a Fokker-Planck equation with a positive definite diffusion matrix for this representation [52, p. 195]. The definition of the positive P function can be given implicitly using the characteristic function

$$\chi(\lambda, \lambda^*) = \int\int d^2\alpha d^2\beta \ P(\alpha, \beta) \exp[\lambda\beta - \lambda^*\alpha] \tag{3.120}$$

This is the approach of choice for the development of stochastic differential equations in the form of Itô or Stratonovich, as illustrated by Carter [22]. Finally, we remark that existence properties are a to be assessed for all those implicitly-defined functions, but are out of the scope of this thesis. It turns out [52] that Wigner function always exists, whereas other functions exist for a wide class of states.

Thermal states and coherent states density operators

As an example, let us consider the quantum treatment of thermal radiation in detection. This was a main problem addressed in seminal work by Helstrom [76] and Glauber [57]. For the moment, let us restrict to the case in which strong

assumptions are made for propagation, and the shape of the density matrix at the receiver is not to be derived using master equations. Considering thermal excitation of a single mode, the resulting quantum state can be written as the maximum entropy distribution, which is geometric [21]

$$p(n) = \left(\frac{N}{1+N}\right)^n \frac{1}{1+N}. \tag{3.121}$$

Since the average number of bosons obey the Bose-Einstein statistics,

$$N = \frac{1}{\exp[\hbar\omega/k\theta] - 1}, \tag{3.122}$$

then the density operator ρ_θ has a representation in the Fock basis

$$\rho_\theta = \sum_{n=0}^{\infty} \left(\frac{N}{1+N}\right)^n |n\rangle \langle n|. \tag{3.123}$$

Let us consider a coherent state $|\alpha_0\rangle$, with density matrix ρ. In the Glauber-Sudarshan P representation it is trivially represented as

$$\rho = \int d^2\alpha \, \delta(\alpha - \alpha_0) \, |\alpha\rangle \langle\alpha| \tag{3.124}$$

whereas a thermal state have the representation

$$\rho_\theta = \frac{1}{\pi N} \int d^2\alpha \, \exp\left[-\frac{|\alpha|^2}{N}\right] |\alpha\rangle \langle\alpha| \tag{3.125}$$

so it has a Gaussian components in the phase-space of coherent states. Glauber [57] showed how the coherent state, when added to the thermal one, gives a representation in P space as

$$\rho_{\text{perturbed}} = \frac{1}{\pi N} \int d^2\alpha \, \exp\left[-\frac{|\alpha - \alpha_0|^2}{N}\right] |\alpha\rangle \langle\alpha| \tag{3.126}$$

The detection of such state is a problem pertaining quantum receiver optimization, however this representation can be generalized and used to compute field evolution along the fiber.

3.5 CONCLUDING REMARKS

The detection problem in the case of the transmission of a QKD channel which is disturbed by a set of WDM channels can be cast into a problem of quantum

telecommunications in the presence of noise. However, this is not the only way to tackle the problem. A classical and simplified model have been developed [25], but it neglects the role of loss of coherence; the results shown suggest that NLIN is not particularly impactful with respect to other impairments for QKD channels, and can be neglected, at least from the point of view of its noise power level. In fact, most experimental work concentrates on the impact of in-band ASE, Raman scattering (both spontaneous and stimulated), and FWM. It is also true that most experimental work focus on short to medium distance communications, which are of interest today for QKD systems. From the technological point of view, further numerical studies should be carried out in order to assess the impact of NLIN in this case, and compare it with different noise sources. The study on RALs may become in this respect particularly interesting, due to the variety and number of copropagating waves that may couple with the QKD channels and represent disturbances. In this scenario, many of the disturbances do already have models, like attenuation and Raman processes [22]. From the theoretical point of view, we have reviewed the usual methods to tackle noise using the formalism of quantized fields: by using some assumptions on the interaction between the system and the environment, master equations like Eq. (3.15) have been illustrated. In the literature, the equations have been applied to various disturbance problems [52]. However, the case of NLIN presents some difficulties. First of all, the state of the environment field is not thermal, so taking traces over the reservoir may not be simple. As we have seen in the case of classical telecommunications, NLIN is much influenced by modulation format, so the statistics of the constellation must be included into the model.

Further study may involve the development of suitable approaches similar to Redfield or GKSL equations. An assessment of the impact and comparison of diverse noise sources should be carried out using a numerical simulations, and tested using both DV-QKD and CV-QKD, but concentrating especially on the latter, which is gaining attention in recent times, and may perform better in terms of coexistence. As for the development of NLIN coupling may require the usage of non Markovian models. Furthermore, it would be interesting to explore the impact of phase-matched FWM on quantum channels, a phenomenon that may be driven by the coexistence of many signal and pump wave in a RAL.

4 CONCLUSIONS

Current optical communications systems utilize technologies that are based on the sharing of the same propagation medium by waves that are differentiated from the functional point of view. In fact, one of the most important breakthroughs in optical communications is WDM, with which up to hundreds of channels can be conveyed into the same optical fiber. Moreover, much effort has been put into the development of Raman amplified links, that may supersede EDFAs in the task of mitigating the effect of losses. These two technologies are implemented together in systems: the Raman amplification scheme, consisting in propagating CW pumps in the same direction of the signal and/or in the opposite direction, can be finely tuned in order to amplify the channels of a WDM system in a equalized way, and this is usually accomplished using various pump wavelength/power allocation algorithms, the most efficient exploiting machine learning. In a typical Raman amplified WDM link, some tens to hundreds of channel are sharing the same physical medium with Raman pumps. In this scenario it is particularly interesting to obtain noise performance metrics for the channels, as many non-idealities of the fiber give rise to impairments. Even if many models have already been developed, not all the aspects are completely understood.

In this thesis, the problem of modeling the XPM-induced phase perturbations in Raman amplified links has been addressed. This is a inter-channel disturbance phenomenon in WDM systems, and it is influenced by the Raman amplification along the fiber, which is channel-dependent. The resulting model is a generalization of the model proposed by Dar and Mecozzi [30], and consists in a system of coupled NLSEs, with which the perturbative analysis for the received symbol has been reproduced. Using this model, numerical simulations have been realized in order to obtain realistic estimates of the noise, which is called NLIN. In the simulations, the focus has been given on NLIN and ASE noise. SPM phase shifts have been neglected, since noise suppression techniques are very efficient for this kind of disturbance. In the numerical simulations, particular highlight has been given to the characteristics of NLIN, its dependence on channel position, the influence of the choice of the Raman amplification scheme. It turns out that the choice of the Raman amplification scheme entails a *tradeoff* between NLIN and ASE noise performance. More specifically, considering an equalized amplification, NLIN performance is enhanced by counterpropagating schemes, as the signal

pulses are attenuated along all the fiber, whereas in copropagating schemes, they are amplified at the input and stay at higher power along the whole fiber. The behavior of ASE is opposite. The numerical simulations open up the possibility of studying in detail NLIN, and may be useful to formulate and solve optimization problems on performance of Raman amplified WDM system. Future work may involve the study of the impact of the link length on the NLIN and ASE tradeoff, and the study of how bidirectional pumping can implement an optimal scheme with respect to noises, considering also noise mitigation techniques at the receiver.

The second topic of this thesis regards quantum telecommunications, that is a field undergoing very fast development. In recent years, increasing effort had been given to the problem of the coexistence of QKD channels with WDM channels, in the same physical medium. In this thesis we reviewed present literature on this topic, in order to understand the impact of NLIN, which might be of some relevance even in this scenario. In a second moment, by approaching the problem in a top-down fashion, we explored methodology for describing interaction of radiation and matter in a quantum-mechanical setting. We argued that, for this kind of interaction in communication systems, the formalism of quantized fields is extremely useful, both as a conceptual tool, and as a modeling tool. The framework of open quantum systems is particularly useful as it provides master equations for the density matrix, and introduces major simplifications in the treatment of disturbances. Furthermore, phase-space representation has been shown to be the main tool for the writing of stochastic equations for the quantum variables of interest. Future work may involve the direct modeling of NLIN utilizing master equations, keeping into account the fact that, due to the non-thermal nature of the interacting radiation, some of the approximations typically used in master equations are no longer valid. By using numerical simulations of master equations or Langevin equations, it may be possible to obtain a ultimate bound on overall system performance, for example in terms of quantum BER. This analysis may be done in conjunction with the calculation of the impact of FWM, Raman processes, and ASE noise, for which some models in phase-space are already available.

APPENDICES

A - FIBER OPTIC COMMUNICATIONS STANDARDS

The used frequency band designation in optical communication technologies are summarized in Table 4.1.

Code	Description	Wavelength range [nm]
O	Original	1260 - 1360
E	Extended	1360 - 1460
S	Short	1460 - 1530
C	Conventional	1530 - 1565
L	Long	1565 - 1625
U	Ultra-long	1625 - 1675

Table 4.1: Frequency band designation for standards for fiber optics communications.

As for WDM, technology, the standardization details include specific grid placements for both technologies [81, 82]. As for the aspects of interest in this thesis, we only remark the spectral spacing, that influence walkoff and pulse collision. In the case of *Coarse*-WDM (CWDM) [82], the standard spectral spacing is 20nm, which in C band corresponds to about 2.5THz. In the case of *Dense*-WDM (DWDM) [81], the spacing ranges from 12.5GHz to 100GHz and above, in steps of 12.5GHz.

B - SECOND ORDER CORRECTION FOR DISPERSED GAUSSIAN PULSES

As shown, local interaction approximation is useful when $D(z) \approx D_m := D(z_m)$, with $z_m = -\frac{mT}{\beta_2 \Omega}$. In this case, the time integral is a simple Gaussian integral, and it can be evaluated as

$$X^{(0)}_{0,m,m} = \frac{f_B(z_m)}{\beta_2 \Omega}. \tag{4.1}$$

this may be viewed as a zero order approximation in D. A slight improvement of this result is available for Gaussian pulses.

By expanding the dependence on D to the second order, around D_m, we obtain a correction which accounts for the dispersion phenomenon *within* the integration range of the collision. It turns out that the first order term is null, and

$$X_{0,m,m} \approx X^{(0)}_{0,m,m} + \Delta X^{(2)}_{0,m,m} \tag{4.2}$$

where

$$\Delta X^{(2)}_{0,m,m} = \frac{1}{\beta_2 \Omega} \frac{1}{\Omega^2 T_0^2} \tag{4.3}$$

the corrected coefficient may be written as

$$X_{0,m,m} \approx \frac{1}{\beta_2 \Omega} \left(1 + \frac{1}{\Omega^2 T_0^2} \right) \tag{4.4}$$

this correction give an excellent improvement with respect to numerical computation of the integral, when compared to the 0^{th} order approximation.

Let us derive this result. In order to simplify the computation we introduce an auxiliary variable, adopting $\sigma = \sqrt{1 + D^2}$.

$$\frac{d\sigma}{dD}(D_m) = \left(-T_0 \frac{D_m}{\sqrt{1 + D_m^2}} \right) \tag{4.5}$$

Let us compute the first order correction:

$$\begin{aligned} \Delta X^{(1)}_{0,mm} &= \frac{\sqrt{\pi} U_0^4 T_0^2}{\beta_2 \Omega} \int_{\mathbb{R}} d\zeta \frac{\partial C}{\partial D}(D_m, \zeta) \cdot (D - D_m) = \\ &= \frac{\sqrt{\pi} U_0^4 T_0^2}{p_2 \Omega} \int_{\mathbb{R}} d\zeta \frac{1}{\sqrt{2}\sigma_m} \cdot \exp\left[-\frac{(\zeta + mT)^2}{2\sigma_m^2} \right] \left[-\frac{1}{\sigma_m} + \frac{(\zeta + mT)^2}{\sigma_m^3} \right] \times \\ &\times \left[-T_0 \frac{D_m}{\sqrt{1 + D_m^2}} \right] \cdot \left(\frac{\zeta + mT}{\Omega T_0^2} \right) = 0 \end{aligned} \tag{4.6}$$

where C =, and ζ =by using properties of Gaussian moments, we notice that the only moments occuring are mean and kurtosis. So the first order approximation is null.

To compute the second order correction, let us use the chain rule twice

$$\frac{\partial^2 C}{\partial D^2} = \frac{d^2\sigma}{dD^2} \cdot \frac{\partial C}{\partial \sigma} + \left(\frac{d\sigma}{dD} \right)^2 \frac{\partial^2 C}{\partial \sigma^2} \tag{4.7}$$

By integrating the first term of the sum in eq (4.7) we obtain

$$\Delta X^{(1)}_{0,mm} = \frac{\sqrt{\pi} U_0^4 T_0^2}{\beta_2 \Omega} \int_{\mathbb{R}} d\zeta \frac{1}{\sqrt{2}\sigma_m} \exp\left[-\frac{(\zeta + mT)^2}{2\sigma_m^2}\right] \left[-\frac{1}{\sigma_m} + \frac{(\zeta + mT)^2}{\sigma_m^3}\right] \times \tag{4.8}$$

$$\times \left[\frac{T_0}{(1 + D_m^2)^{3/2}}\right] \frac{1}{2} \frac{(\zeta + mT)^2}{\Omega^2 T_0^4}$$

so we have a variance, and a central moment of order 4.
As for the second term in 4.7 the integral reads

$$= \frac{\sqrt{\pi} U_0^4 T_0^2}{\beta_2 \Omega} \int_{\mathbb{R}} d\zeta \frac{1}{\sqrt{2}\sigma_m} \exp\left[-\frac{(\zeta + mT)^2}{2\sigma_m^2}\right] \left[\left(-\frac{1}{\sigma_m} + \frac{(\zeta + mT)^2}{\sigma_m^3}\right)^2 + \right. \tag{4.9}$$

$$\left. + \left(\frac{1}{\sigma_m^2} - \frac{3(\zeta + mT)^2}{\sigma_m^4}\right)\right] \left(-T_0 \frac{D_m}{\sqrt{1 + D_m^2}}\right)^2 \frac{1}{2} \frac{(\zeta + mT)^2}{\Omega^2 T_0^4}$$

so we have a variance, and central moments of order 4 and 6. Computation of higher order central moments is obtained by

$$\mathbb{E}[(X - \mu)^n] = (n - 1)!! \sigma^n \tag{4.10}$$

Summing the two contribution the dependence on D_m vanishes, and we are left with eq. (4.3).

C - SELECTION OF RELEVANT COLLISIONS

In order to setup the integration technique, it is possible to notice that only some indexes m are to be considered as valid collision in a short fiber such as the one of interest for the amplifier. By using a threshold on the pulse collision energy (normalized to 1), it is possible to select only the desired m, and to filter out all the m that give place to weak interaction. Let $0 < \xi < 1$ be such threshold. Let M be the set of the m values to be considered. The computation of M is complicated, because of the very definition of ξ, which involves the actual computation of the integral

$$M = \left\{ m \;\middle|\; \sqrt{\frac{\pi}{2}} \frac{U_0^4 T_0 \beta_2 \Omega}{(1 + D^2(z_m))^{\frac{1}{2}}} \int_0^L dz f_B(z) \exp\left[-\frac{(mT + \beta_2 \Omega z)^2}{2T_0^2(1 + D^2(z_m))}\right] \geqslant \xi \right\} \tag{4.11}$$

Since we are only concerned about the selection of the m, one possible approximation is to discard the contribution of $f_B(z)$. This assumption is acceptable if inter-collision spacing is sufficiently small. By normalizing the Gaussian and computing the upper and lower extreme of integration with respect to the Gaussian peak, and considering a new normalized threshold, which is related to the pulse energy by

$$\epsilon = \sqrt{\frac{2}{\pi}} \frac{(1 + D^2(z_m))^{\frac{1}{2}}}{U_0^4 T_0 \beta_2 \Omega} \xi \tag{4.12}$$

it is possible to obtain a trascendental condition on m to be solved simply using some solver or by table lookup. The alternative, simplified condition is

$$\frac{1}{2}\left[\Phi\left(\frac{mT + \beta_2 \Omega L}{\sqrt{2}T_0(1 + D^2(z_m))^{\frac{1}{2}}}\right) - \Phi\left(\frac{mT}{\sqrt{2}T_0(1 + D^2(z_m))^{\frac{1}{2}}}\right)\right] > \epsilon \tag{4.13}$$

where Φ is the Gaussian error function. This approximation must be validated, but it is a good starting point to understand the behavior of the interactions.

D - COMMENTS ON OVERALL NLIN COMPUTATION

The procedure followed to calculate the overall NLIN consisted in obtaining one time integral of every m, and then to integrate its contribution in space and obtain the corresponding m. Referring to notation in Eq. (2.62), every computation of $I_{\Omega,m}(z)$ has a computational cost proportional to the product of the space samples and the time samples. The overall tens to hundreds of pulses are then inserted in the overall noise computation from a single interfering channel in the following form

$$\sum_m X^2_{0,m,m} = \sum_m \int_0^L \int_0^L dz dz' f_B(z) f_B(z') \int_{-\infty}^{+\infty} \int_{-\infty}^{+\infty} dt dt' |g^{(0)}(z,t)|^2 |g^{(0)}(z',t')|^2 \times \tag{4.14}$$

$$\times |g^{(0)}(z, t - mT - \beta_2 \Omega z)|^2 |g^{(0)}(z', t' - mT - \beta_2 \Omega z)|^2 \tag{4.15}$$

By exchanging the summation symbol with each of the integration ones (it is possible because finite summation is a continuous functional), one obtains

$$\sum_{m} X^2_{0,m,m} = \int_0^L \int_0^L dz dz' fB(z) fB(z') \int_{-\infty}^{+\infty} \int_{-\infty}^{+\infty} dt dt' |g^{(0)}(z,t)|^2 |g^{(0)}(z',t')|^2 \times \tag{4.16}$$

$$\times \sum_{m} |g^{(0)}(z, t - mT - \beta_2 \Omega z)|^2 |g^{(0)}(z', t' - mT - \beta_2 \Omega z)|^2 \tag{4.17}$$

so this simple algebraic passage suggest a novel method for computing the overall noise, without necessarily compute the single $X_{0,m,m}$ for each m. The complexity of this method is increased with respect to the previous one, however, starting from the last expression, some approximation may be developed in order to obtain fast estimates of the overall NLIN.

BIBLIOGRAPHY

[1] Govind P. Agrawal. *Fiber-Optic Communication Systems*. John Wiley & Sons, Feb. 23, 2012. 627 pp. ISBN: 978-0-470-92282-8.

[2] Govind P. Agrawal. *Nonlinear fiber optics*. Academic Press, 2013.

[3] O. Alia et al. "1.6 Tbps Classical Channel Coexistence With DV-QKD Over Hollow Core Nested Antiresonant Nodeless Fibre (HC-NANF)." In: *2021 European Conference on Optical Communication (ECOC)*. 2021 European Conference on Optical Communication (ECOC). Sept. 2021, pp. 1–4. DOI: 10.1109/ECOC52684.2021.9605918.

[4] Obada Alia et al. "DV-QKD Coexistence With 1.6 Tbps Classical Channels Over Hollow Core Fibre." In: *Journal of Lightwave Technology* (2022). Conference Name: Journal of Lightwave Technology, pp. 1–1. ISSN: 1558-2213. DOI: 10.1109/JLT.2022.3180232.

[5] F. T. Arecchi. "Measurement of the Statistical Distribution of Gaussian and Laser Sources." In: *Physical Review Letters* 15.24 (Dec. 13, 1965). Publisher: American Physical Society, pp. 912–916. DOI: 10.1103/PhysRevLett.15.912.

[6] A. Arnold, F. Fagnola, and L. Neumann. "Quantum fokker-planck models: the lindblad and wigner approaches." In: *Quantum Probability and Related Topics*. Vol. Volume 23. QP-PQ: Quantum Probability and White Noise Analysis Volume 23. WORLD SCIENTIFIC, Oct. 2008, pp. 23–48. ISBN: 978-981-283-526-0. DOI: 10.1142/9789812835277_0003.

[7] E. Arthurs and J. L. Kelly Jr. "On the Simultaneous Measurement of a Pair of Conjugate Observables." In: *Bell System Technical Journal* 44.4 (1965), pp. 725–729. ISSN: 1538-7305. DOI: 10.1002/j.1538-7305.1965.tb01684.x.

[8] Marco Avesani et al. "Deployment-ready quantum key distribution over a classical network infrastructure in Padua." In: *Journal of Lightwave Technology* 40.6 (2022). Publisher: IEEE, pp. 1658–1663.

[9] Marco Avesani et al. "Resource-effective quantum key distribution: a field trial in Padua city center." In: *Optics Letters* 46.12 (June 2021). Publisher: The Optical Society, p. 2848. DOI: 10.1364/ol.422890.

[10] Arash Bahrami, Andrew Lord, and Timothy Spiller. "Quantum key distribution integration with optical dense wavelength division multiplexing: a review." In: *IET Quantum Communication* 1.1 (2020). _eprint: https://onlinelibrary.wiley.com/doi/pdf/10.1049/iet-qtc.2019.0005, pp. 9–15. ISSN: 2632-8925. DOI: 10.1049/iet-qtc.2019.0005.

[11] F. E. Becerra et al. "Experimental demonstration of a receiver beating the standard quantum limit for multiple nonorthogonal state discrimination." In: *Nature Photonics* 7.2 (Feb. 2013). Number: 2 Publisher: Nature Publishing Group, pp. 147–152. ISSN: 1749-4893. DOI: 10.1038/nphoton.2012.316.

[12] J. S. Bell. *Speakable and unspeakable in quantum mechanics: collected papers on quantum philosophy*. Cambridge [Cambridgeshire] ; New York: Cambridge University Press, 1987. 212 pp. ISBN: 978-0-521-33495-2.

[13] Nevio Benvenuto and Michele Zorzi. *Principles of Communications Networks and Systems*. John Wiley & Sons, Sept. 19, 2011. 718 pp. ISBN: 978-1-119-97982-1.

[14] K. J. Blow et al. "Continuum fields in quantum optics." In: *Physical Review A* 42.7 (Oct. 1, 1990). Publisher: American Physical Society, pp. 4102–4114. DOI: 10.1103/PhysRevA.42.4102.

[15] Alberto Boaron et al. "Secure quantum key distribution over 421 km of optical fiber." In: *Physical review letters* 121.19 (2018). Publisher: APS, p. 190502.

[16] J. Bonetti et al. *A simple approach to the quantum theory of nonlinear fiber optics*. Number: arXiv:1902.00561. Feb. 1, 2019.

[17] Alberto Bononi et al. "Cross-Phase Modulation Induced by OOK Channels on Higher-Rate DQPSK and Coherent QPSK Channels." In: *Journal of Lightwave Technology* 27.18 (Sept. 2009). Conference Name: Journal of Lightwave Technology, pp. 3974–3983. ISSN: 1558-2213. DOI: 10.1109/JLT.2009.2021537.

[18] Max Born and Emil Wolf. *Principles of Optics: Electromagnetic Theory of Propagation, Interference and Diffraction of Light*. Elsevier, June 1, 2013. 871 pp. ISBN: 978-1-4831-0320-4.

[19] Jake Bromage. "Raman amplification for fiber communications systems." In: *journal of lightwave technology* 22.1 (2004). Publisher: IEEE, pp. 79–93.

[20] Yuan Cao et al. "Time-scheduled quantum key distribution (QKD) over WDM networks." In: *Journal of Lightwave Technology* 36.16 (2018). Publisher: IEEE, pp. 3382–3395.

[21] Gianfranco Cariolaro. *Quantum Communications*. Signals and Communication Technology. Cham: Springer International Publishing, 2015. ISBN: 978-3-319-15599-9 978-3-319-15600-2. DOI: 10.1007/978-3-319-15600-2.

[22] S. J. Carter. "Quantum theory of nonlinear fiber optics: Phase-space representations." In: *Physical Review A* 51.4 (Apr. 1, 1995). Publisher: American Physical Society, pp. 3274–3301. DOI: 10.1103/PhysRevA.51.3274.

[23] S. J. Carter and P. D. Drummond. "Squeezed quantum solitons and Raman noise." In: *Physical Review Letters* 67.27 (Dec. 30, 1991). Publisher: American Physical Society, pp. 3757–3760. DOI: 10.1103/PhysRevLett.67.3757.

[24] S. J. Carter et al. "Squeezing of quantum solitons." In: *Physical Review Letters* 58.18 (May 4, 1987). Publisher: American Physical Society, pp. 1841–1844. DOI: 10.1103/PhysRevLett.58.1841.

[25] Yan Chen et al. "Impact of Cross-Phase Modulation Induced by Classical Channels on the CV-QKD in a Hybrid System." In: *Chinese Physics Letters* 30.11 (Nov. 2013). Publisher: IOP Publishing, p. 110302. ISSN: 0256-307X. DOI: 10.1088/0256-307X/30/11/110302.

[26] Iris Choi, Robert J Young, and Paul D Townsend. "Quantum key distribution on a 10Gb/s WDM-PON." In: *Optics express* 18.9 (2010). Publisher: Optical Society of America, pp. 9600–9612.

[27] Dariusz Chruściński and Saverio Pascazio. "A Brief History of the GKLS Equation." In: *Open Systems & Information Dynamics* 24.3 (Sept. 2017), p. 1740001. ISSN: 1230-1612, 1793-7191. DOI: 10.1142/S1230161217400017.

[28] Ronen Dar et al. "Accumulation of nonlinear interference noise in fiber-optic systems." In: *Optics Express* 22.12 (June 16, 2014). Publisher: Optica Publishing Group, pp. 14199–14211. ISSN: 1094-4087. DOI: 10.1364/OE.22.014199.

[29] Ronen Dar et al. "Inter-Channel Nonlinear Interference Noise in WDM Systems: Modeling and Mitigation." In: *Journal of Lightwave Technology* 33.5 (Mar. 2015). Conference Name: Journal of Lightwave Technology, pp. 1044–1053. ISSN: 1558-2213. DOI: 10.1109/JLT.2014.2384998.

[30] Ronen Dar et al. "Properties of nonlinear noise in long, dispersion-uncompensated fiber links." In: *Optics Express* 21.22 (Oct. 2013). Publisher: The Optical Society, p. 25685. DOI: 10.1364/oe.21.025685.

[31] Ronen Dar et al. "Time varying ISI model for nonlinear interference noise." In: *Optical Fiber Communication Conference (2014), paper W2A.62*. Optical Fiber Communication Conference. Optica Publishing Group, Mar. 9, 2014, W2A.62. DOI: 10.1364/OFC.2014.W2A.62.

[32] Paul Adrien Maurice Dirac. *The Principles of Quantum Mechanics*. Clarendon Press, 1981. 340 pp. ISBN: 978-0-19-852011-5.

[33] S.J. Dolinar. "An optimum receiver for the binary coherent state quantum channel." In: *Research Laboratory of Electronics, MIT, Quarterly Progress Report* 11 (1973), pp. 115–120.

[34] Justin Dove, Christopher Chudzicki, and J. Shapiro. "Phase-Noise Limitations on Nonlinear-Optical Quantum Computing." In: *undefined* (2015).

[35] P. D. Drummond and C. W. Gardiner. "Generalised P-representations in quantum optics." In: *Journal of Physics A: Mathematical and General* 13.7 (July 1980). Publisher: IOP Publishing, pp. 2353–2368. ISSN: 0305-4470. DOI: 10.1088/0305-4470/13/7/018.

[36] P. D. Drummond and A. D. Hardman. "Simulation of Quantum Effects in Raman-Active Waveguides." In: *Europhysics Letters (EPL)* 21.3 (Jan. 1993). Publisher: IOP Publishing, pp. 279–284. ISSN: 0295-5075. DOI: 10.1209/0295-5075/21/3/005.

[37] Peter D Drummond and Steve J Carter. "Quantum-field theory of squeezing in solitons." In: *JOSA B* 4.10 (1987). Publisher: Optical Society of America, pp. 1565–1573.

[38] Peter D Drummond and Joel Frederick Corney. "Quantum noise in optical fibers. I. Stochastic equations." In: *JOSA B* 18.2 (2001). Publisher: Optical Society of America, pp. 139–152.

[39] Peter D. Drummond. "Electromagnetic quantization in dispersive inhomogeneous nonlinear dielectrics." In: *Physical Review A* 42.11 (Dec. 1, 1990). Publisher: American Physical Society, pp. 6845–6857. DOI: 10.1103/PhysRevA.42.6845.

[40] Peter D. Drummond and Mark Hillery. *The Quantum Theory of Nonlinear Optics*. Cambridge University Press, Mar. 27, 2014. 385 pp. ISBN: 978-1-139-91583-0.

[41] Mikhail Elezov et al. "Towards the fiber-optic Kennedy quantum receiver." In: *EPJ Web of Conferences* 220 (2019). Publisher: EDP Sciences, p. 03011. ISSN: 2100-014X. DOI: 10.1051/epjconf/201922003011.

[42] Tobias A. Eriksson et al. "Coexistence of Continuous Variable Quantum Key Distribution and 7×12.5 Gbit/s Classical Channels." In: *2018 IEEE Photonics Society Summer Topical Meeting Series (SUM)*. 2018 IEEE Photonics Society Summer Topical Meeting Series (SUM). ISSN: 2376-8614. July 2018, pp. 71–72. DOI: 10.1109/PHOSST.2018.8456709.

[43] Tobias A. Eriksson et al. "Joint Propagation of Continuous Variable Quantum Key Distribution and 18x24.5 Gbaud PM-16QAM Channels." In: *2018 European Conference on Optical Communication (ECOC)*. 2018 European Conference on Optical Communication (ECOC). Sept. 2018, pp. 1–3. DOI: 10.1109/ECOC.2018.8535421.

[44] René-Jean Essiambre et al. "Capacity Limits of Optical Fiber Networks." In: *Journal of Lightwave Technology* 28.4 (Feb. 2010). Conference Name: Journal of Lightwave Technology, pp. 662–701. ISSN: 1558-2213. DOI: 10.1109/JLT.2009.2039464.

[45] U. Fano. "Description of States in Quantum Mechanics by Density Matrix and Operator Techniques." In: *Reviews of Modern Physics* 29.1 (Jan. 1, 1957). Publisher: American Physical Society, pp. 74–93. DOI: 10.1103/RevModPhys.29.74.

[46] Willliam Feller. *An introduction to probability theory and its applications, vol 2*. John Wiley & Sons, 2008.

[47] A. C. Ferreira et al. "Analysis of the nonlinear optical switching in a Sagnac interferometer with non-instantaneous Kerr effect." In: *Optics Communications* 285.6 (Mar. 15, 2012), pp. 1408–1417. ISSN: 0030-4018. DOI: 10.1016/j.optcom.2011.10.026.

[48] J. M. Fini, P. L. Hagelstein, and H. A. Haus. "Agreement of stochastic soliton formalism with second-quantized and configuration-space models." In: *Physical Review A* 57.6 (June 1, 1998). Publisher: American Physical Society, pp. 4842–4853. DOI: 10.1103/PhysRevA.57.4842.

[49] Sebastian Fortin and Olimpia Lombardi. "Partial Traces in Decoherence and in Interpretation: What Do Reduced States Refer to?" In: *Foundations of Physics* 44.4 (Apr. 1, 2014), pp. 426–446. ISSN: 1572-9516. DOI: 10.1007/s10701-014-9791-3.

[50] Wolfgang Freude et al. "Quality metrics for optical signals: Eye diagram, Q-factor, OSNR, EVM and BER." In: *2012 14th International Conference on Transparent Optical Networks (ICTON)*. 2012 14th International Conference on Transparent Optical Networks (ICTON). ISSN: 2161-2064. July 2012, pp. 1–4. DOI: 10.1109/ICTON.2012.6254380.

[51] Andrea Galtarossa and Curtis R. Menyuk. *Polarization Mode Dispersion*. Springer Science & Business Media, July 27, 2005. 320 pp. ISBN: 978-0-387-23193-8.

[52] Crispin Gardiner, P. Zoller, and Peter Zoller. *Quantum Noise: A Handbook of Markovian and Non-Markovian Quantum Stochastic Methods with Applications to Quantum Optics*. Springer Science & Business Media, Aug. 27, 2004. 476 pp. ISBN: 978-3-540-22301-6.

[53] A. Georgiadis. "Gain, phase imbalance, and phase noise effects on error vector magnitude." In: *IEEE Transactions on Vehicular Technology* 53.2 (Mar. 2004). Conference Name: IEEE Transactions on Vehicular Technology, pp. 443–449. ISSN: 1939-9359. DOI: 10.1109/TVT.2004.823477.

[54] A. Gilchrist, C. W. Gardiner, and P. D. Drummond. "Positive P representation: Application and validity." In: *Physical Review A* 55.4 (Apr. 1, 1997). Publisher: American Physical Society, pp. 3014–3032. DOI: 10.1103/PhysRevA.55.3014.

[55] C.R. Giles and E. Desurvire. "Modeling erbium-doped fiber amplifiers." In: *Journal of Lightwave Technology* 9.2 (Feb. 1991). Conference Name: Journal of Lightwave Technology, pp. 271–283. ISSN: 1558-2213. DOI: 10.1109/50.65886.

[56] V. Giovannetti and G. M. Palma. "Master Equations for Correlated Quantum Channels." In: *Physical Review Letters* 108.4 (Jan. 24, 2012). Publisher: American Physical Society, p. 040401. DOI: 10.1103/PhysRevLett.108.040401.

[57] Roy J. Glauber. "Coherent and Incoherent States of the Radiation Field." In: *Physical Review* 131.6 (Sept. 15, 1963). Publisher: American Physical Society, pp. 2766–2788. DOI: 10.1103/PhysRev.131.2766.

[58] Roy J. Glauber. "The Quantum Theory of Optical Coherence." In: *Physical Review* 130.6 (June 15, 1963). Publisher: American Physical Society, pp. 2529–2539. DOI: 10.1103/PhysRev.130.2529.

[59] Ori Golani et al. "Modeling the Bit-Error-Rate Performance of Nonlinear Fiber-Optic Systems." In: *Journal of Lightwave Technology* 34.15 (Aug. 2016). Conference Name: Journal of Lightwave Technology, pp. 3482–3489. ISSN: 1558-2213. DOI: 10.1109/JLT.2016.2578983.

[60] Vittorio Gorini, Andrzej Kossakowski, and E. C. G. Sudarshan. "Completely positive dynamical semigroups of N-level systems." In: *Journal of Mathematical Physics* 17.5 (May 1976). Publisher: American Institute of Physics, pp. 821–825. ISSN: 0022-2488. DOI: 10.1063/1.522979.

[61] Philippe Grangier, Juan Ariel Levenson, and Jean-Philippe Poizat. "Quantum non-demolition measurements in optics." In: *Nature* 396.6711 (Dec. 1998), pp. 537–542. ISSN: 0028-0836, 1476-4687. DOI: 10.1038/25059.

[62] Edouard Grellier and Alberto Bononi. "Quality parameter for coherent transmissions with Gaussian-distributed nonlinear noise." In: *Optics Express* 19.13 (June 20, 2011). Publisher: Optica Publishing Group, pp. 12781–12788. ISSN: 1094-4087. DOI: 10.1364/OE.19.012781.

[63] Frédéric Grosshans and Philippe Grangier. "Continuous Variable Quantum Cryptography Using Coherent States." In: *Physical Review Letters* 88.5 (Jan. 16, 2002). Publisher: American Physical Society, p. 057902. DOI: 10.1103/PhysRevLett.88.057902.

[64] Frédéric Grosshans and Philippe Grangier. "Quantum cloning and teleportation criteria for continuous quantum variables." In: *Physical Review A* 64.1 (June 12, 2001). Publisher: American Physical Society, p. 010301. DOI: 10.1103/PhysRevA.64.010301.

[65] Frédéric Grosshans et al. "Quantum key distribution using gaussian-modulated coherent states." In: *Nature* 421.6920 (Jan. 2003). Number: 6920 Publisher: Nature Publishing Group, pp. 238–241. ISSN: 1476-4687. DOI: 10.1038/nature01289.

[66] Frédéric Grosshans et al. "Quantum key distribution using gaussian-modulated coherent states." In: *Nature* 421.6920 (Jan. 2003). Number: 6920 Publisher: Nature Publishing Group, pp. 238–241. ISSN: 1476-4687. DOI: 10.1038/nature01289.

[67] H. A. Haus and F. X. Kärtner. "Quantization of the nonlinear Schr\"odinger equation." In: *Physical Review A* 46.3 (Aug. 1, 1992). Publisher: American Physical Society, R1175–R1176. DOI: 10.1103/PhysRevA.46.R1175.

[68] H. A. Haus and J. A. Mullen. "Quantum Noise in Linear Amplifiers." In: *Physical Review* 128.5 (Dec. 1, 1962). Publisher: American Physical Society, pp. 2407–2413. DOI: 10.1103/PhysRev.128.2407.

[69] H.A. Haus. "The noise figure of optical amplifiers." In: *IEEE Photonics Technology Letters* 10.11 (Nov. 1998). Conference Name: IEEE Photonics Technology Letters, pp. 1602–1604. ISSN: 1941-0174. DOI: 10.1109/68.726763.

[70] Hermann A Haus. *Electromagnetic noise and quantum optical measurements*. Springer Science & Business Media, 2000.

[71] Hermann A Haus. "From classical to quantum noise." In: *JOSA B* 12.11 (1995). Publisher: Optical Society of America, pp. 2019–2036.

[72] Bing He, Qing Lin, and Christoph Simon. "Cross-Kerr nonlinearity between continuous-mode coherent states and single photons." In: *Physical Review A* 83.5 (May 18, 2011). Publisher: American Physical Society, p. 053826. DOI: 10.1103/PhysRevA.83.053826.

[73] J.J. Healy, Alper Kutay, and Haldun Ozaktas. *Linear Canonical Transforms*. Springer, 2016.

[74] R. W. Hellwarth. "Theory of Stimulated Raman Scattering." In: *Physical Review* 130.5 (June 1, 1963). Publisher: American Physical Society, pp. 1850–1852. DOI: 10.1103/PhysRev.130.1850.

[75] C.W. Helstrom, J.W.S. Liu, and J.P. Gordon. "Quantum-mechanical communication theory." In: *Proceedings of the IEEE* 58.10 (Oct. 1970). Conference Name: Proceedings of the IEEE, pp. 1578–1598. ISSN: 1558-2256. DOI: 10.1109/PROC.1970.7983.

[76] Carl W. Helstrom. "Quantum detection and estimation theory." In: *Journal of Statistical Physics* 1.2 (June 1, 1969), pp. 231–252. ISSN: 1572-9613. DOI: 10.1007/BF01007479.

[77] Mark Hillery and Leonard D. Mlodinow. "Quantization of electrodynamics in nonlinear dielectric media." In: *Physical Review A* 30.4 (Oct. 1, 1984). Publisher: American Physical Society, pp. 1860–1865. DOI: 10.1103/PhysRevA.30.1860.

[78] J. J. Hopfield. "Theory of the Contribution of Excitons to the Complex Dielectric Constant of Crystals." In: *Physical Review* 112.5 (Dec. 1, 1958). Publisher: American Physical Society, pp. 1555–1567. DOI: 10.1103/PhysRev.112.1555.

[79] Kerson Huang. *Statistical mechanics*. John Wiley & Sons, 2008.

[80] Kyo Inoue. "Quantum noise of Raman amplification in a fiber transmission line." In: *JOSA B* 35.7 (July 1, 2018). Publisher: Optica Publishing Group, pp. 1698–1707. ISSN: 1520-8540. DOI: 10.1364/JOSAB.35.001698.

[81] ITU-T. *Recommendation database - G.694.1*. ITU. URL: https://www.itu.int/itu-t/recommendations/rec.aspx?rec=11482 (visited on 08/29/2022).

[82] ITU-T. *Recommendation database - G.694.2*. ITU. URL: https://www.itu.int/ITU-T/recommendations/rec.aspx?rec=7057 (visited on 08/29/2022).

[83] Pontus Johannisson and Magnus Karlsson. "Perturbation analysis of nonlinear propagation in a strongly dispersive optical communication system." In: *Journal of Lightwave Technology* 31.8 (2013). Publisher: IEEE, pp. 1273–1282.

[84] Fotini Karinou et al. "Experimental evaluation of the impairments on a QKD system in a 20-channel WDM co-existence scheme." In: *2017 IEEE Photonics Society Summer Topical Meeting Series (SUM)*. 2017, pp. 145–146. DOI: 10.1109/PHOSST.2017.8012692.

[85] F. X. Kärtner and H. A. Haus. "Quantum-nondemolition measurements and the "collapse of the wave function"." In: *Physical Review A* 47.6 (June 1, 1993). Publisher: American Physical Society, pp. 4585–4592. DOI: 10.1103/PhysRevA.47.4585.

[86] D. J. Kaup and B. A. Malomed. "Soliton trapping and daughter waves in the Manakov model." In: *Physical Review A* 48.1 (July 1, 1993). Publisher: American Physical Society, pp. 599–604. DOI: 10.1103/PhysRevA.48.599.

[87] R.S. Kennedy. "A near-optimum receiver for the binary coherent state quantum channel." In: *Quarterly Progress Report* 108 (1973). Publisher: Research Laboratory of Electronics, M.I.T, pp. 219–225.

[88] T. A. B. Kennedy. "Quantum theory of cross-phase-modulational instability: Twin-beam correlations in a X3 process." In: *Physical Review A* 44.3 (Aug. 1, 1991). Publisher: American Physical Society, pp. 2113–2123. DOI: 10.1103/PhysRevA.44.2113.

[89] T. A. B. Kennedy and P. D. Drummond. "Quantum-field superpositions via self-phase modulation of coherent wave packets." In: *Physical Review A* 38.3 (Aug. 1, 1988). Publisher: American Physical Society, pp. 1319–1326. DOI: 10.1103/PhysRevA.38.1319.

[90] Kazuro Kikuchi. "Coherent Optical Communications: Historical Perspectives and Future Directions." In: *High Spectral Density Optical Communication Technologies*. Ed. by Masataka Nakazawa, Kazuro Kikuchi, and Tetsuya Miyazaki. Optical and Fiber Communications Reports. Berlin, Heidelberg: Springer, 2010, pp. 11–49. ISBN: 978-3-642-10419-0. DOI: 10.1007/978-3-642-10419-0_2.

[91] Kazuro Kikuchi. "Digital coherent optical communication systems: fundamentals and future prospects." In: *IEICE Electronics Express* 8.20 (2011), pp. 1642–1662. DOI: 10.1587/elex.8.1642.

[92] Kazuro Kikuchi. "Fundamentals of Coherent Optical Fiber Communications." In: *Journal of Lightwave Technology* 34.1 (Jan. 2016). Conference Name: Journal of Lightwave Technology, pp. 157–179. ISSN: 1558-2213. DOI: 10.1109/JLT.2015.2463719.

[93] Pius Kirrmann, Guido Schneider, and Alexander Mielke. "The validity of modulation equations for extended systems with cubic nonlinearities." In: *Proceedings of the Royal Society of Edinburgh Section A: Mathematics* 122.1 (1992). Publisher: Royal Society of Edinburgh Scotland Foundation, pp. 85–91. ISSN: 1473-7124, 0308-2105. DOI: 10.1017/S0308210500020989.

[94] A. V. Kozlovskiĭ. "Decoherence of the field in quantum nondemolition photon number measurement using the Kerr nonlinearity." In: *Optics and Spectroscopy* 97.5 (Nov. 1, 2004), pp. 755–763. ISSN: 1562-6911. DOI: 10.1134/1.1828626.

[95] Anton Kozubov, Andrei Gaidash, and George Miroshnichenko. "Quantum model of decoherence in the polarization domain for the fiber channel." In: *Physical Review A* 99.5 (May 28, 2019). Publisher: American Physical Society, p. 053842. DOI: 10.1103/PhysRevA.99.053842.

[96] Dimitar Ivanov Kroushkov et al. "Simple Estimation of the XPM-Induced Phase Error Variance in Hybrid OOK-PSK Systems." In: *IEEE Photonics Technology Letters* 24.9 (May 2012). Conference Name: IEEE Photonics Technology Letters, pp. 733–735. ISSN: 1941-0174. DOI: 10.1109/LPT.2012.2187332.

[97] Rupesh Kumar, Hao Qin, and Romain Alléaume. "Coexistence of continuous variable QKD with intense DWDM classical channels." In: *New Journal of Physics* 17.4 (Apr. 2015). Publisher: IOP Publishing, p. 043027. ISSN: 1367-2630. DOI: 10.1088/1367-2630/17/4/043027.

[98] Shiva Kumar and M. Jamal Deen. *Fiber Optic Communications: Fundamentals and Applications*. John Wiley & Sons, May 12, 2014. 573 pp. ISBN: 978-0-470-51867-0.

[99] Y. Lai and H. A. Haus. "Quantum theory of solitons in optical fibers. I. Time-dependent Hartree approximation." In: *Physical Review A* 40.2 (July 1, 1989). Publisher: American Physical Society, pp. 844–853. DOI: 10.1103/PhysRevA.40.844.

[100] Y. Lai and H. A. Haus. "Quantum theory of solitons in optical fibers. II. Exact solution." In: *Physical Review A* 40.2 (July 1, 1989). Publisher: American Physical Society, pp. 854–866. DOI: 10.1103/PhysRevA.40.854.

[101] Chi-Wung Lau et al. "Binary quantum receiver concept demonstration." In: *Free-Space Laser Communication Technologies XVIII*. Free-Space Laser Communication Technologies XVIII. Vol. 6105. SPIE, Mar. 1, 2006, pp. 144–150. DOI: 10.1117/12.660268.

[102] Xiang Liu et al. "Phase-conjugated twin waves for communication beyond the Kerr nonlinearity limit." In: *Nature Photonics* 7.7 (2013). Publisher: Nature Publishing Group, pp. 560–568.

[103] Xue Liu, Joseph W. Haus, and S. M. Shahriar. "Modulation instability for a relaxational Kerr medium." In: *Optics Communications* 281.10 (May 15, 2008), pp. 2907–2912. ISSN: 0030-4018. DOI: 10.1016/j.optcom.2008.01.026.

[104] Antonín Luks and Vlasta Perinová. *Quantum Aspects of Light Propagation*. Boston, MA: Springer US, 2009. ISBN: 978-0-387-85589-9 978-0-387-85590-5. DOI: 10.1007/b101766.

[105] Norbert Lütkenhaus. "Security against individual attacks for realistic quantum key distribution." In: *Physical Review A* 61.5 (Apr. 6, 2000). Publisher: American Physical Society, p. 052304. DOI: 10.1103/PhysRevA.61.052304.

[106] Hisham A. Mahmoud and Huseyin Arslan. "Error vector magnitude to SNR conversion for nondata-aided receivers." In: *IEEE Transactions on Wireless Communications* 8.5 (May 2009). Conference Name: IEEE Transactions on Wireless Communications, pp. 2694–2704. ISSN: 1558-2248. DOI: 10.1109/TWC.2009.080862.

[107] Leonard Mandel and Emil Wolf. *Optical Coherence and Quantum Optics*. Cambridge University Press, Sept. 29, 1995. 1200 pp. ISBN: 978-0-521-41711-2.

[108] Franz Mandl and Graham Shaw. *Quantum Field Theory*. John Wiley & Sons, May 17, 2010. 497 pp. ISBN: 978-0-471-49683-0.

[109] Daniel Manzano. "A short introduction to the Lindblad Master Equation." In: *AIP Advances* 10.2 (Feb. 1, 2020), p. 025106. ISSN: 2158-3226. DOI: 10.1063/1.5115323.

[110] Gianluca Marcon and Francesco Lorenzi. *PyNLIN: a Python package and scripts for the evaluation of nonlinear interference noise in single mode fiber transmissions.* https://github.com/geeanlooca/PyNLIN.

[111] Gianluca Marcon et al. "Model-Aware Deep Learning Method for Raman Amplification in Few-Mode Fibers." In: *Journal of Lightwave Technology* 39.5 (Mar. 2021). Publisher: Institute of Electrical and Electronics Engineers (IEEE), pp. 1371–1380. DOI: 10.1109/jlt.2020.3034692.

[112] D. Marcuse. "Derivation of analytical expressions for the bit-error probability in lightwave systems with optical amplifiers." In: *Journal of Lightwave Technology* 8.12 (Dec. 1990). Conference Name: Journal of Lightwave Technology, pp. 1816–1823. ISSN: 1558-2213. DOI: 10.1109/50.62876.

[113] M. Margalit et al. "Cross phase modulation squeezing in optical fibers." In: *Optics Express* 2.3 (Feb. 2, 1998). Publisher: Optica Publishing Group, pp. 72–76. ISSN: 1094-4087. DOI: 10.1364/OE.2.000072.

[114] C. J. McKinstrie et al. "Translation of quantum states by four-wave mixing in fibers." In: *Optics Express* 13.22 (Oct. 31, 2005). Publisher: Optica Publishing Group, pp. 9131–9142. ISSN: 1094-4087. DOI: 10.1364/OPEX.13.009131.

[115] Antonio Mecozzi and René-Jean Essiambre. "Nonlinear Shannon Limit in Pseudolinear Coherent Systems." In: *Journal of Lightwave Technology* 30.12 (June 2012). Publisher: Institute of Electrical and Electronics Engineers (IEEE), pp. 2011–2024. DOI: 10.1109/jlt.2012.2190582.

[116] Pierre Meystre and Murray Sargent. *Elements of Quantum Optics*. Springer Science & Business Media, Sept. 4, 2007. 507 pp. ISBN: 978-3-540-74211-1.

[117] R Momose et al. "On a Relation Between Quantum Interference and Standard Quantum Limit." In: *NASA conference publication.* 3322 (1996). Place: Washington Publisher: National Aeronautics and Space Administration, Scientific and Technical Information Office : [for sale by the National Technical Information Service OCLC: 106687250, p. 307. ISSN: 0191-7811.

[118] R. Momose, M. Sasaki, and O. Hirota. "Physical Interpretation of Optimum Quantum Detection Operators." In: *Quantum Communication, Computing, and Measurement*. Ed. by O. Hirota, A. S. Holevo, and C. M. Caves. Boston, MA: Springer US, 1997, pp. 289–297. ISBN: 978-1-4615-5923-8. DOI: 10.1007/978-1-4615-5923-8_31.

[119] Christopher Monroe. "Demolishing quantum nondemolition." In: *Physics Today* 64.1 (2011), p. 8. ISSN: 00319228. DOI: 10.1063/1.3541926.

[120] John W. Negele and Henri Orland. *Quantum Many-Particle Systems*. Boca Raton: CRC Press, May 23, 2019. 476 pp. ISBN: 978-0-429-49792-6. DOI: 10.1201/9780429497926.

[121] Geoffrey New. *Introduction to Nonlinear Optics*. Cambridge University Press, Apr. 7, 2011. 275 pp. ISBN: 978-1-139-50076-0.

[122] Michele N. Notarnicola, Matteo G. A. Paris, and Stefano Olivares. *Hybrid near-optimum binary receiver with realistic photon-number-resolving detectors*. Number: arXiv:2207.07518. July 15, 2022. DOI: 10.48550/arXiv.2207.07518.

[123] Samuel L. I. Olsson, Magnus Karlsson, and Peter A. Andrekson. "Nonlinear phase noise mitigation in phase-sensitive amplified transmission systems." In: *Optics Express* 23.9 (May 4, 2015), pp. 11724–11740. ISSN: 1094-4087. DOI: 10.1364/OE.23.011724.

[124] Athanasios Papoulis. "Pulse compression, fiber communications, and diffraction: a unified approach." In: *Journal of the Optical Society of America A* 11.1 (Jan. 1994). Publisher: The Optical Society, p. 3. DOI: 10.1364/josaa.11.000003.

[125] Matteo Paris and Jaroslav Rehacek. *Quantum State Estimation*. Springer Science & Business Media, Aug. 11, 2004. 548 pp. ISBN: 978-3-540-22329-0.

[126] K. A. Patel et al. "Coexistence of High-Bit-Rate Quantum Key Distribution and Data on Optical Fiber." In: *Physical Review X* 2.4 (Nov. 20, 2012). Publisher: American Physical Society, p. 041010. DOI: 10.1103/PhysRevX.2.041010.

[127] Philip Pearle. "Simple derivation of the Lindblad equation." In: *European Journal of Physics* 33.4 (Apr. 2012). Publisher: IOP Publishing, pp. 805–822. ISSN: 0143-0807. DOI: 10.1088/0143-0807/33/4/805.

[128] Victor E. Perlin and Herbert G. Winful. "On trade-off between noise and nonlinearity in WDM systems with distributed Raman amplification." In: *Optical Fiber Communications Conference (2002), paper WB1*. Optical Fiber Communication Conference. Optica Publishing Group, Mar. 17, 2002, WB1.

[129] P. Poggiolini et al. "The GN-Model of Fiber Non-Linear Propagation and its Applications." In: *Journal of Lightwave Technology* 32.4 (Feb. 2014). Conference Name: Journal of Lightwave Technology, pp. 694–721. ISSN: 1558-2213. DOI: 10.1109/JLT.2013.2295208.

[130] Pierluigi Poggiolini et al. "Analytical modeling of nonlinear propagation in uncompensated optical transmission links." In: *IEEE Photonics technology letters* 23.11 (2011). Publisher: IEEE, pp. 742–744.

[131] David M. Pozar. *Microwave Engineering*. John Wiley & Sons, Nov. 22, 2011. 752 pp. ISBN: 978-0-470-63155-3.

[132] Gabriele Riccardi et al. "Reproducing the most general quantum channel in the lab: is it possible?" In: *2020 IEEE Photonics Conference (IPC)*. 2020 IEEE Photonics Conference (IPC). ISSN: 2575-274X. Sept. 2020, pp. 1–2. DOI: 10.1109/IPC47351.2020.9252533.

[133] Hannes Risken. "Fokker-Planck Equation." In: *The Fokker-Planck Equation: Methods of Solution and Applications*. Ed. by Hannes Risken. Springer Series in Synergetics. Berlin, Heidelberg: Springer, 1996, pp. 63–95. ISBN: 978-3-642-61544-3. DOI: 10.1007/978-3-642-61544-3_4.

[134] J. J. Sakurai and Eugene D. Commins. "Modern Quantum Mechanics, Revised Edition." In: *American Journal of Physics* 63.1 (Jan. 1995). Publisher: American Association of Physics Teachers, pp. 93–95. ISSN: 0002-9505. DOI: 10.1119/1.17781.

[135] Eduard Schmidt et al. "Quantum theory of light in nonlinear media with dispersion and absorption." In: *Journal of Modern Optics* 45.2 (Feb. 1, 1998). Publisher: Taylor & Francis _eprint: https://doi.org/10.1080/09500349808231696, pp. 377–401. ISSN: 0950-0340. DOI: 10.1080/09500349808231696.

[136] Rene Schmogrow et al. "Error Vector Magnitude as a Performance Measure for Advanced Modulation Formats." In: *IEEE Photonics Technology Letters* 24.1 (Jan. 2012). Conference Name: IEEE Photonics Technology Letters, pp. 61–63. ISSN: 1941-0174. DOI: 10.1109/LPT.2011.2172405.

[137] W. Schottky. "Über spontane Stromschwankungen in verschiedenen Elektrizitätsleitern." In: *Annalen der Physik* 362.23 (1918), pp. 541–567. ISSN: 00033804, 15213889. DOI: 10.1002/andp.19183622304.

[138] Rishad Ahmed Shafik, Md. Shahriar Rahman, and AHM Razibul Islam. "On the Extended Relationships Among EVM, BER and SNR as Performance Metrics." In: *2006 International Conference on Electrical and Computer Engineering*. 2006 International Conference on Electrical and Computer Engineering. Dec. 2006, pp. 408–411. DOI: 10.1109/ICECE.2006.355657.

[139] Jiushu Shao, Mo-Lin Ge, and Hu Cheng. "Decoherence of quantum-nondemolition systems." In: *Physical Review E* 53.1 (Jan. 1, 1996). Publisher: American Physical Society, pp. 1243–1245. DOI: 10.1103/PhysRevE.53.1243.

[140] Wies aw Leo ski and Adam Miranowicz. "Kerr nonlinear coupler and entanglement." In: *Journal of Optics B: Quantum and Semiclassical Optics* 6.3 (Mar. 2004). Publisher: IOP Publishing, S37–S42. ISSN: 1464-4266. DOI: 10.1088/1464-4266/6/3/007.

[141] Carlo G Someda and George I Stegeman. *Anisotropic and nonlinear optical waveguides*. Elsevier, 2012.

[142] Carlo Giacomo Someda. *Electromagnetic waves*. CRC press, 2006.

[143] A. Serdar Tan et al. "An ML-Based Detector for Optical Communication in the Presence of Nonlinear Phase Noise." In: *2011 IEEE International Conference on Communications (ICC)*. 2011 IEEE International Conference on Communications (ICC). ISSN: 1938-1883. June 2011, pp. 1–5. DOI: 10.1109/icc.2011.5962741.

[144] Luc Thevenaz. *Advanced fiber optics: concepts and technology*. EPFL press, 2011.

[145] Satoshi Tsukamoto et al. "Coherent Demodulation of 40-Gbit/s Polarization-Multiplexed QPSK Signals with 16-GHz Spacing after 200-km Transmission." In: *Optical Fiber Communication Conference and Exposition and The National Fiber Optic Engineers Conference (2005), paper PDP29*. Optical Fiber Communication Conference. Optica Publishing Group, Mar. 6, 2005, PDP29.

[146] Jin Wang and J.M. Kahn. "Accurate bit-error-ratio computation in nonlinear CRZ-OOK and CRZ-DPSK systems." In: *IEEE Photonics Technology Letters* 16.9 (Sept. 2004). Conference Name: IEEE Photonics Technology Letters, pp. 2165–2167. ISSN: 1941-0174. DOI: 10.1109/LPT.2004.833033.

[147] Liu-Jun Wang et al. "Long-distance copropagation of quantum key distribution and terabit classical optical data channels." In: *Physical Review A* 95.1 (Jan. 3, 2017). Publisher: American Physical Society, p. 012301. DOI: 10.1103/PhysRevA.95.012301.

[148] Wei Wang et al. "Amplified Spontaneous Emission and Rayleigh Scattering in Few-Mode Fiber Raman Amplifiers." In: *IEEE Photonics Technology Letters* 29.14 (July 2017). Conference Name: IEEE Photonics Technology Letters, pp. 1159–1162. ISSN: 1941-0174. DOI: 10.1109/LPT.2017.2707062.

[149] Norbert Wiener. "The operational calculus." In: *Mathematische Annalen* 95.1 (Dec. 1, 1926), pp. 557–584. ISSN: 1432-1807. DOI: 10.1007/BF01206627.

[150] Ewan M. Wright. "Quantum theory of soliton propagation in an optical fiber using the Hartree approximation." In: *Physical Review A* 43.7 (Apr. 1, 1991). Publisher: American Physical Society, pp. 3836–3844. DOI: 10.1103/PhysRevA.43.3836.

[151] Lian-Ao Wu and Daniel A. Lidar. "Overcoming quantum noise in optical fibers." In: *Physical Review A* 70.6 (Dec. 10, 2004). Publisher: American Physical Society, p. 062310. DOI: 10.1103/PhysRevA.70.062310.

[152] Tiejun J Xia et al. "In-band quantum key distribution (QKD) on fiber populated by high-speed classical data channels." In: *Optical Fiber Communication Conference*. Optical Society of America, 2006, OTuJ7.

[153] Xin Lu Ye and Qing Lin. "Efficient and flexible generation of entangled qudits with cross-phase modulation." In: *JOSA B* 29.7 (July 1, 2012). Publisher: Optica Publishing Group, pp. 1810–1814. ISSN: 1520-8540. DOI: 10.1364/JOSAB.29.001810.

[154] Esra Unal Yilmaz et al. "Manakov model of coupled NLS equation and its optical soliton solutions." In: *Journal of Ocean Engineering and Science* (Mar. 17, 2022). ISSN: 2468-0133. DOI: 10.1016/j.joes.2022.03.005.

[155] B. Yoon and J. W. Negele. "Time-dependent Hartree approximation for a one-dimensional system of bosons with attractive delta-function interactions." In: *Physical Review A* 16.4 (Oct. 1, 1977). Publisher: American Physical Society, pp. 1451–1457. DOI: 10.1103/PhysRevA.16.1451.

[156] Dimitris Zavitsanos et al. "Coexistence of Discrete-Variable QKD with WDM classical signals in the C-band for fiber access environments." In: *2019 21st International Conference on Transparent Optical Networks (ICTON)*. IEEE, 2019, pp. 1–5.

[157] Wolfgang Zeiler et al. "Modeling of four-wave mixing and gain peaking in amplified WDM optical communication systems and networks." In: *Journal of Lightwave Technology* 14.9 (1996). Publisher: IEEE, pp. 1933–1942.

[158] Wojciech Hubert Zurek. "Decoherence and the Transition from Quantum to Classical — Revisited." In: *Quantum Decoherence: Poincaré Seminar 2005*. Ed. by Bertrand Duplantier, Jean-Michel Raimond, and Vincent Rivasseau. Progress in Mathematical Physics. Basel: Birkhäuser, 2007, pp. 1–31. ISBN: 978-3-7643-7808-0. DOI: 10.1007/978-3-7643-7808-0_1.

[159] Wojciech Hubert Zurek. "Decoherence, einselection, and the quantum origins of the classical." In: *Reviews of Modern Physics* 75.3 (May 22, 2003). Publisher: American Physical Society, pp. 715–775. DOI: 10.1103/RevModPhys.75.715.

COLOPHON

This document was typeset using the typographical look-and-feel `classicthesis` developed by André Miede and Ivo Pletikosić. The style was inspired by Robert Bringhurst's seminal book on typography *"The Elements of Typographic Style"*. `classicthesis` is available for both LaTeX and LyX:

https://bitbucket.org/amiede/classicthesis/

Happy users of `classicthesis` usually send a real postcard to the author, a collection of postcards received so far is featured here:

http://postcards.miede.de/

Thank you very much for your feedback and contribution.